Mechanisms for CO_2 Sequestration in Geological Formations and Enhanced Gas Recovery

Roozbeh Khosrokhavar

Mechanisms for CO_2 Sequestration in Geological Formations and Enhanced Gas Recovery

Proefschrift

ter verkrijging van de graad van doctor
aan de Technische Universiteit Delft,
op gezag van de Rector Magnificus prof. ir. K.C.A.M. Luyben,
voorzitter van het College voor Promoties,
in het openbaar te verdedigen op vrijdag 17 december 2014 om 12:30 uur

door

Roozbeh KHOSROKHAVAR

Master of Science in Chemical Engineering,
Tehran Polytechnic
geboren te Tehran, Iran.

Dit proefschrift is goedgekeurd door de promotoren:
Prof.dr. Hans Bruining

Copromotor Dr. Karl-Heinz Wolf

Samenstelling promotiecommissie:

Rector Magnificus,	voorzitter
Prof. dr. Hans Bruining,	Technische Universiteit Delft, promotor
Dr. Karl-Heinz Wolf,	Technische Universiteit Delft, copromotor
Prof. dr. ir. Pacelli Zitha,	Technische Universiteit Delft,
Prof. dr. Chris Spiers,	Universiteit Utrecht,
Prof. Rien Herber,	Rijksuniversiteit Groningen,
Dr. Rouhi Farajzadeh,	Technische Universiteit Delft,
Dr. Andreas Busch,	Shell International, Rijswijk
Prof. dr. Ir. Jan Dirk Jansen	Technische Universiteit Delft, reservelid

The research was carried out within the context of the $CATO_2$ program (CO_2 capture, transport and storage in the Netherlands). Their financial support is acknowledged. The author is also thankful GRASP program, founded by the European Commission, for awarded research fellowship through "Marie Curie Actions Program".

Cover design by R. Khosrokhavar, Scanning electron microscope (SEM) image of the black shale.

Printed by CPI-Wöhrmann Print Service- Zutphen

ISBN: 978-94-6203-737-3

بنام خالق زیبایی ها

هیچ صیادی در جوی حقیری که به گودالی می ریزد، مرواریدی صید نخواهد کرد! (فروغ فرخزاد)

To Negar

To my mother and my father

Table of Contents

Chapter 1

Introduction

The growing concern about global warming has increased interest in the geological storage of carbon dioxide (CO_2) [1]. Global and national energy outlooks to 2030 and beyond indicate growing global energy demand, particularly in non-OECD countries, and a continued dominant role for fossil fuels in the world's energy mix, even as utilization of renewable energy sources grows faster than utilization of fossil fuels [2-4]. Regarding to the United Nations (UN) report in 2007, human activities and so-called greenhouse effects are very likely to be the source of global warming [5, 6]. Indeed, the increasing amount of greenhouse gases (e.g., CH_4, CO_2, H_2O, etc.) in the atmosphere could be the reason for the temperature rise measured over the last hundred years [7]. Compared to other greenhouse gases CO_2 is the most important one as it is responsible for about 64% of the enhanced greenhouse effects as inferred from its radiative forcing [8]. Fossil fuels provide about 80% of the current global energy demand and account for 75% of current CO_2 emissions [9]. One way to decrease CO_2 emission will be to switch from high carbon to low carbon fuels. However, a rapid move away from oil, natural gas and coal is unlikely to be achievable without serious disruption to the global economy. To conclude, an achievable option is to reduce CO_2 emissions. The IPCC report suggests the following present or future options [5]: 1) - improve energy efficiency by decreasing the fossil fuel consumption, 2) - switching from high carbon to low carbon fuels, 3) - increased use of fuels with low or near zero carbon footprint, 4) - Storing CO_2 through the enhancement of natural, biological sinks, 5) - CO_2 capture and storage (CCS). To choose a mitigation option the potential and capacity of the option, social acceptance, side effect and more importantly the associated costs [10] and innovation [11, 12] are key parameters. In a transition period from a fossil fuel based society to a sustainable energy society it is predicted that CO_2 capture and subsequent sequestration (CCS) in geological formations can be developed to play a role in reducing greenhouse gas emissions [13]. However, for current state of the art technology, carbon dioxide sequestration is still energetically demanding due to high separation costs [14]. Geological sequestration means "the capture of CO_2 directly from anthropogenic

sources and disposing of it deep into the ground for geologically significant periods of time" [15]. These geological formations are: (a) deep saline aquifers, (b) depleted oil and gas reservoir, (c) CO_2 driven enhanced oil recovery, (d) deep unmineable coal seams, (e) CO_2 driven enhanced coal bed methane (ECBM) recovery and (f) enhanced gas recovery, e.g., in shale formations. The following mechanisms may contribute to the sequestration of CO_2 in geological formations [8]: hydrodynamic trapping, dissolution trapping, mineralization-based trapping and physical and chemical sorption in coals and shales.

Global CO_2 emissions from the energy sector are about 30 billion tons per year with this number possibly doubling by 2050 [16]. It is expected [15] that this annual amount must be reduced significantly to decrease the potential from global warming. It is stated that in order to keep CO_2 levels in stabilized condition in the atmosphere, a reduction of approximately 20 billion tons of CO_2 is needed per year [17]. Carbon sequestration has the potential to decrease emissions by as much as 5 to 10 billion tons per year by taking advantage of a global CO_2 storage capacity of 2,000 Gt in geological formations [18]. In various studies the total CO_2 storage capacity of unmineable coalbeds is estimated to range between 100 and 300 Gt CO_2 [19] and the total storage capacity of deep saline aquifers is estimated to range between 1000 and 10,000 Gt CO_2 [19].

Saline aquifers are the most abundant subsurface formations with large storage capacities. A saline aquifer is a geological formation with a sufficiently high porosity and permeability that contains water with large amounts of dissolved solids [20, 21]. For CO_2 storage in aquifers the following aspects are relevant [22]: storage capacity, mass transfer rate of CO_2, low permeable cap rock, geological characterization of the aquifer formations and cap rock structures, leakages from the reservoir and from wells and the sensitivity to corrosion in the wells. Efficient storage of carbon dioxide (CO_2) in aquifers is favored by its dissolution in the aqueous phase [23]. Firstly, the volume available for gaseous CO_2 is far less than for the CO_2 that can be dissolved in the water initially present in the aquifer. Secondly, the partial molar volume of CO_2 in the gas phase is about twice as large as the partial molar volume of CO_2 in water [24], meaning that storage in the water phase leads to less pressure increase per amount of sequestered CO_2. Transfer of CO_2 from the gas phase to the aqueous phase would be slow if it were only driven by diffusion. However, dissolution of CO_2 in water forms a mixture that is denser than the original water or brine [25]. This causes a local density increase, which induces natural convection currents accelerating the rate of CO_2 dissolution [1]. The occurrence of natural convection enhances the total storage rate in the aquifer since convection currents bring the carbon dioxide lean brine to the top and the contaminated brine to the bottom. Natural convection will eventually become less important as the brine becomes fully saturated with CO_2 (see Chapters 2 and 3).

The potential for the geologic storage of CO_2 in shale formations that have undergone hydraulic fracturing for extraction is being explored for several reasons [26]: (a) shales are widely distributed, (b) existing infrastructure of wells, pipelines, etc. is or will be available and (c) pore pressures in the shale formations prior to CO_2 injection are reduced by gas production. Development of shale resources may create capacity for CO_2 storage because the innovations developed are directly transferable, particularly those that relate to well completion, such as new approaches to cementing, more mature horizontal drilling methods, and development of field treatment techniques for saline water [27]. Thus, understanding the behavior of CO_2 in shale is an important part of advancing the opportunity for the geologic storage of CO_2, particularly because of the fact that the geological characteristics of a particular storage site often influences the design of the related CO_2 capture and transportation infrastructure [28]. The studies reviewed illustrate that the opportunity for geologic storage of CO_2 in shales can be significant, but knowledge of the characteristics of the different types of gas shales found globally is needed. The potential for CO_2 sorption as part of geologic storage in depleted shale gas reservoirs must be assessed with respect to the individual geology of each formation [29].

This thesis confines its interest to investigate the sequestration capacity of CO_2 in saline aquifers and more specifically on the mass transfer between CO_2 and the brine, show the effect of salinity and visualize the fingering of CO_2 in bulk phase in the absence of porous media by applying Schlieren technique. In addition, we also illustrate the importance of shale formations in the world and apply an experimental method to measure the sorption capacity with regards to enhanced gas recovery- EGR prospect. To achieve our goals we designed, constructed and improved three different setups that form the main core of this thesis.

The main research objectives addressed in this thesis are:

1. To qualify, experimentally and numerically, the mass transfer rate of CO_2 to water (brine), oil and Visualization of Natural Convection Flow of CO_2 in Aqueous and Oleic Systems.
2. To investigate the effect of salinity on the transfer rate of CO_2 in bulk and porous media.
3. To model natural convection instability of CO_2 in bulk aqueous and oleic phase.
4. To measure the sorption capacity of shale experimentally by applying the Manometric method based on Monte-Carlo simulation.
5. To review shale gas formations and their potential for carbon storage.

This thesis is based on a number of articles published (or submitted). The thesis consists of 6 chapters. Chapter 2 addresses research objectives (1, 2, and 3). This is accomplished by comparison of numerical model results with a set of high pressure visual experiments, based on the Schlieren technique, in which we observe the effect of gravity-induced fingers when sub- and super-critical CO_2 at in situ pressures and temperatures is brought above the liquid, i.e., water, brine or oil. A short but comprehensive description of the Schlieren set-up and the transparent pressure cell is presented. The Schlieren set-up is capable of visualizing instabilities in natural convection flows in the absence of a porous medium. The experiments show that the prevailing features that occur in a porous medium also occur in bulk, e.g., unstable gravity fingering and pressure decline. The work presented in this chapter was selected and awarded in 2012 in yearly scientific meeting at TU Delft. The experiments show that natural convection currents are weakest in highly concentrated brine and strongest in oil, due to the higher and lower density contrasts respectively. Therefore, the set-up can screen aqueous salt solutions or oil for the relative importance of natural convection flows. The experimental results are compared to numerical results. It is shown that natural convection effects are stronger in cases of high density differences. The set-up can screen any fluid for its relative importance of natural convection flows. To our knowledge there is no visual data in the literature for natural convection flow of super critical CO_2 in aqueous and oleic phase. There is no available experiment for CO_2-oil. There is no data in the literature which has shown the diffusive layer in the way that our experiments reveal it. There is the first time that we showed the continuity of fingers. We can safely say that no theory can predict this continuous fingering behavior.

In chapter 3 we experimentally studied the effect of salinity and pressure on the rate of mass transfer in aquifer storage of carbon dioxide in porous media and thus we address parts of the objectives (1, 2). There is a large body of literature that numerically and analytically address the storage capacity and the rate of transfer between the overlying CO_2-gas layer and the aquifer below. There is a lack of experimental work at field conditions that study the transfer rate into water saturated porous medium at in-situ conditions using carbon dioxide and brine at elevated pressures. Such an experiment requires relatively large volumes and sub and supercritical pressures. We emphasize that the experiment is not based on a pressure decay configuration, but uses a constant gas pressure and measures the dissolution rate using a high pressure ISCO pump. It is confirmed that the transfer rate is much faster than the predicted by Fick's law in the absence of natural convection currents.

Chapter 4 addresses objective (4). Here we investigated sorption of CH_4 and CO_2 on Belgium Carboniferous shale Using a Manometric Set-up. Some studies indicate that, in shale, five

molecules of CO_2 can be stored for every molecule of CH_4 produced. The technical feasibility of Enhanced Gas Recovery (EGR) needs to be investigated in more detail. Globally, the amount of extracted natural gas from shale has increased rapidly over the past decade. A typical shale gas reservoir combines an organic-rich deposition with extremely low matrix permeability. One important parameter in assessing the technical viability of (enhanced) production of shale gas is the sorption capacity. Our focus is on the sorption of CH_4 and CO_2. Therefore we have chosen to use the manometric method to measure the excess sorption isotherms of CO_2 at 318 K and of CH_4 at 308, 318 and 336 K and at pressures up to 105 bar. Only a few measurements have been reported in the literature for high-pressure gas sorption on shales. The experiments on CH_4 show, as expected, a decreasing sorption for increasing temperature. We apply an error analysis based on Monte-Carlo simulation of our experiments. This chapter was selected as the best research proposal in the NUPUS yearly meeting in 2013 and allowed a student from Stuttgart to accomplish her master thesis in Delft.

Chapter 5 addresses objective (5). In chapter 5 we review global shale gas resources and consider both the opportunities and challenges for their development. It then provides a review of the literature on opportunities to store CO_2 in shale, thus possibly helping to mitigate the impact of CO_2 emissions from the power and industrial sectors. The studies reviewed illustrate that the opportunity for geologic storage of CO_2 in shales might be significant, but knowledge of the characteristics of the different types of gas shales found globally is required. The potential for CO_2 sorption as part of geologic storage in depleted shale gas reservoirs must be assessed with respect to the individual geology of each formation. Likewise, the introduction of CO_2 into shale for enhanced gas recovery (EGR) operations may significantly improve both reservoir performance and economics.

In chapter 6 the main conclusions of the thesis are summarized.

REFERENCES:

1. Khosrokhavar, R., G. Elsinga, A. Mojaddam, R. Farajzadeh, and J. Bruining. *Visualization of Natural Convection Flow of Super Critical CO_2 in Water by Applying Schlieren Method*. in *SPE EUROPEC/EAGE Annual Conference and Exhibition*. 2011.
2. British Petroleum, *BP Energy Outlook 2030*, 2013.
3. Exxon Mobil, *The Outlook for Energy: A View to 2040*, 2013.
4. Shell, *New Lens Scenarios: A Shift in Perspective for a World in Transition*, 2013.
5. Metz, B., O. Davidson, H. De Coninck, M. Loos, and L. Meyer, *Carbon dioxide capture and storage*. 2005.
6. Healy, J.K. and J.M. Tapick, *Climate Change: It's Not Just a Policy Issue for Corporate Counsel-It's a Legal Problem*. Colum. J. Envtl. L., 2004. **29**: p. 89.
7. IPCC, *IPCC, 2014: Summary for Policymakers, in Climate Change 2014, Mitigation of Climate Change, O. Edenhofer, et al., Editors. 2014, Contribution of Working Group III to the Fifth Assessment Report of the Intergovernmental Panel on Climate Change: Cambridge, United Kingdom and New York, NY, USA*. 2014.

8. Farajzadeh, R., P.L. Zitha, and J. Bruining, *Enhanced mass transfer of CO_2 into water: experiment and modeling*. Industrial & Engineering Chemistry Research, 2009. **48**(13): p. 6423-6431.
9. Metz, B., *Climate Change 2007-Mitigation of climate change: Working Group III Contribution to the fourth assessment report of the IPCC*. Vol. 4. 2007: Cambridge University Press.
10. Wilson, E.J., M.G. Morgan, J. Apt, M. Bonner, C. Bunting, J. Gode, R.S. Haszeldine, C.C. Jaeger, D.W. Keith, and S.T. McCoy, *Regulating the geological sequestration of CO_2*. Environmental Science & Technology, 2008. **42**(8): p. 2718-2722.
11. Schumpeter, J.A., *Capitalism, socialism and democracy*2013: Routledge.
12. Piketty, T., *Capital in the 21st Century*, 2014, Harvard University Press Cambridge.
13. Khosrokhavar, R., C. Schoemaker, E. Battistutta, K.-H.A. Wolf, and J. Bruining. *Sorption of CO_2 in Shales Using the Manometric Set-up*. in *SPE Europec/EAGE Annual Conference*. 2012. Society of Petroleum Engineers.
14. Eftekhari, A.A., H. Van Der Kooi, and H. Bruining, *Exergy analysis of underground coal gasification with simultaneous storage of carbon dioxide*. Energy, 2012. **45**(1): p. 729-745.
15. Bachu, S., *Sequestration of CO_2 in geological media in response to climate change: road map for site selection using the transform of the geological space into the CO_2 phase space*. Energy Conversion and Management, 2002. **43**(1): p. 87-102.
16. Mosher, K., J. He, Y. Liu, E. Rupp, and J. Wilcox, *Molecular simulation of methane adsorption in micro-and mesoporous carbons with applications to coal and gas shale systems*. International Journal of Coal Geology, 2013. **109**: p. 36-44.
17. Davis, S.J., K. Caldeira, and H.D. Matthews, *Future CO_2 emissions and climate change from existing energy infrastructure*. Science, 2010. **329**(5997): p. 1330-1333.
18. Benson, S.M. and F.M. Orr, *Carbon dioxide capture and storage*. Mrs Bulletin, 2008. **33**(04): p. 303-305.
19. Wilcox, J., *Carbon capture* 2012: Springer.
20. Bachu, S., D. Bonijoly, J. Bradshaw, R. Burruss, S. Holloway, N.P. Christensen, and O.M. Mathiassen, *CO_2 storage capacity estimation: Methodology and gaps*. International Journal of Greenhouse Gas Control, 2007. **1**(4): p. 430-443.
21. Xu, T., J.A. Apps, and K. Pruess, *Numerical simulation of CO_2 disposal by mineral trapping in deep aquifers*. Applied geochemistry, 2004. **19**(6): p. 917-936.
22. Pruess, K. and J. Garcia, *Multiphase flow dynamics during CO_2 disposal into saline aquifers*. Environmental Geology, 2002. **42**(2-3): p. 282-295.
23. Khosrokhavar, R., G. Elsinga, R. Farajzadeh, and H. Bruining, *Visualization and investigation of natural convection flow of CO_2 in aqueous and oleic systems*. Journal of Petroleum Science and Engineering, 2014(0).
24. Gmelin, L., *Gmelin Handbuch der anorganischen Chemie, 8. Auflage. Kohlenstoff, Teil C3, Verbindungen*, 1973, ISBN 3-527-81419-1.
25. Parkhurst, D.L. and C. Appelo, *Description of input and examples for PHREEQC version 3- A computer program for speciation, batch-reaction, one-dimensional transport, and inverse geochemical calculations*. US Geological Survey Techniques and Methods, Book 6, Modeling Techniques, 2013.
26. Rodosta, T., J. Hull, and M. Zoback, *Interdisciplinary Investigation of CO_2 Sequestration in Depleted Shale Gas Formations*, 2013, U.S. Department of Energy,.
27. Nicot, J.-P. and I.J. Duncan, *Common attributes of hydraulically fractured oil and gas production and CO_2 geological sequestration*. Greenhouse Gases: Science and Technology, 2012. **2**(5): p. 352-368.
28. International Energy Agency, *CO_2 Emissions From Fuel Combustion: Highlights (2013 Edition), International Energy Agency: France* 2013.
29. Khosrokhavar, R., K.-H. Wolf, and H. Bruining, *Sorption of CH_4 and CO_2 on a carboniferous shale from Belgium using a manometric setup*. International Journal of Coal Geology, 2014. **128**: p. 153-161.

Chapter 2

Visualization and Numerical Investigation of Natural Convection Flow of CO_2 in Aqueous and Oleic Systems

ABSTRACT

Optimal storage of carbon dioxide (CO_2) in aquifers requires dissolution in the aqueous phase. Nevertheless, transfer of CO_2 from the gas phase to the aqueous phase would be slow if it were only driven by diffusion. Dissolution of CO_2 in water forms a mixture that is denser than the original water or brine. This causes a local density increase, which induces natural convection currents accelerating the rate of CO_2 dissolution. The same mechanism also applies to carbon dioxide enhanced oil recovery.

This study compares numerical models with a set of high pressure visual experiments, based on the Schlieren technique, in which we observe the effect of gravity-induced fingers when sub- and super-critical CO_2 at in situ pressures and temperatures is brought above the liquid, i.e., water, brine or oil. A short but comprehensive description of the Schlieren set-up and the transparent pressure cell is presented. The Schlieren set-up is capable of visualizing instabilities in natural convection flows; a drawback is that it can only be practically applied in bulk flow, i.e., in the absence of a porous medium. All the same many features that occur in a porous medium also occur in bulk, e.g., unstable gravity fingering.

The experiments show that natural convection currents are weakest in highly concentrated brine and strongest in oil, due to the higher and lower density contrasts respectively. Therefore, the set-up can screen aqueous salt solutions or oil for the relative importance of natural

convection flows. The Schlieren pattern consists of a dark region near the equator and a lighter region below it. The dark region indicates a region where the refractive index increases downward, either due to the presence of a gas liquid interface, or due to the thin diffusion layer, which also appears in numerical simulations. The experiments demonstrate the initiation and development of the gravity induced fingers.

The experimental results are compared to numerical results. It is shown that natural convection effects are stronger in cases of high density differences. However, due to numerical limitations, the simulations are characterized by much larger fingers.

KEYWORDS: *CO_2 sequestration; dissolution trapping; natural convection; fluid; visualization; schlieren technique*

Published in: Petroleum Science and Engineering volume 122, October 2014, pages 230–239 and COMSOL 2012.

2.1. INTRODUCTION

The Optimal storage [1] of carbon dioxide (CO_2) in aquifers requires dissolution of CO_2 in formation brine because the virtual density of dissolved CO_2 in water (1333 kg/m^3) is more favorable than its density in the supercritical gas-phase. Without dissolution of CO_2 in the aqueous phase the storage volume of CO_2 in aquifers would be of the order of 2% of the reservoir volume [2]. It is expected that, due to buoyancy forces, injected CO_2 rises to the top of the reservoir forming a gas layer. Transfer from the gas layer to the aquifer below would be slow if it were only driven by molecular diffusion. However, CO_2 mixes with the water (or brine) to form a denser aqueous phase (e.g., in pure water $\Delta\rho \sim 8$ kg/m^3 at 30 bar, see, [3]). This initiates convective currents and increases the dissolution rate, and thus dissolution of larger amounts of CO_2 in a shorter period of time.

Underground storage of CO_2 involves costly processes. First, the flue gas should be captured; its CO_2 fraction should be separated, transported to the injection site, and finally compressed and stored in the geological formation. A cost-effective approach may then be to use carbon dioxide enhanced oil recovery, which at the same time also stores part of the injected CO_2. Moreover, one of the challenges in the application of CO_2-based enhanced oil recovery techniques for naturally fractured reservoirs is the slow mass transfer between the carbon dioxide in the fracture and the crude oil in the matrix. As carbon dioxide is miscible with oil and causes a density increase of oil, natural convection phenomena could promote the transfer rates, increase the mixing between the carbon dioxide and the oil, and accelerate the oil production. Therefore, understanding the CO_2-oil interaction during these processes is of great interest for the petroleum industry. The initial stage of natural convection in a saturated porous layer with a denser fluid on top of a lighter fluid has been extensively studied by means of linear stability analysis, numerical simulations and the energy method ([4-17]). These analyses provide the criteria under which the boundary layer saturated with CO_2 becomes unstable. The results are usually expressed in terms of the Rayleigh number, which is dependent on the fluid and porous media properties and is defined as

$$Ra = \frac{k\Delta\rho g H}{\varphi \mu D} \qquad (2.1)$$

where k [m^2] is the permeability of the porous medium, $\Delta\rho$ [kg/m^3] is the characteristic density difference between the mixture and the fresh water, g [m/s^2] is the acceleration due to gravity, H [m] is the characteristic length of the system, φ [-] is the porosity, μ [Pa.s] is the viscosity of the mixture, and D [m^2/s] is the molecular diffusion coefficient of CO_2 in water. It has been shown that the critical time required for the onset of the convective currents is inversely related to the square of Ra, i.e., $t_c \propto Ra^{-2}$ [13, 16]. The critical wavelength of the fastest growing finger scales

with the inverse of Rayleigh number, i.e., $\lambda_c \propto Ra^{-1}$. Lapwood [18] showed that the interface will be unstable for Rayleigh numbers above $4\pi^2 \approx 40$ in porous media. In the absence of a porous medium (for bulk solutions), k in Equation (2. 1) is replaced by H_2 and natural convection occurs when Ra > 2100. It can be expected that the effect will be more pronounced for bulk solutions; however, for the time scales relevant for geological storage of CO_2 the effect will be also significant in porous media. There are many papers devoted to the theoretical description of convection currents during storage of CO_2 in aquifers; the effect was first mentioned by [19]. Mass transfer of CO_2 into water has been evaluated experimentally and analytically at different conditions. References [20-23] investigate the occurrence of natural convection by recording the pressure change in a cylindrical PVT-cell, where a fixed volume of CO_2 gas was brought into contact with a column of distilled water. The experimental results show that initially the mass-transfer rate is much faster than predicted by Fick's Law (diffusion-based model) indicating that another mechanism apart from molecular diffusion plays a role. It was conjectured that density-driven natural convection enhances the mass-transfer rate. This conjecture could be validated by comparison of experimental data with a numerical model that couples mass- and momentum conservation equations [22, 24]. Figure 2-1 compares the extent of natural convection in the presence and absence of a porous medium in a glass tube with a radius of 3.5 mm by measuring the pressure history. In one experiment the glass tube is filled with only water, and in the other one the tube is filled with a porous medium of the same height and saturated with water. The figure shows that, although natural convection enhances the transfer rate in water-saturated porous media, its enhancement is less than in a bulk liquid.

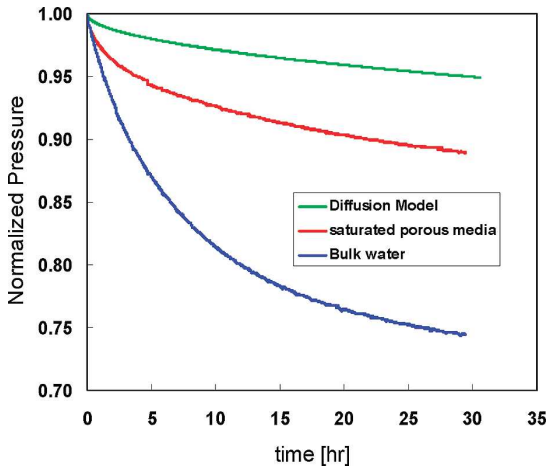

Figure 2-1: Comparison of the pressure history of the experiments with (red) and without porous media (blue). The green curve is based on a diffusion model in the absence of convection. The experiments were done in a glass tube with radius of 3.5 mm at 11 bar [21].

Okhotsimskiis et al [25] visualized the convective currents in a binary CO_2-water system and qualitatively evaluated the experimental results, based on Marangoni and free (or natural) convection effects, in bulk modules of gas and liquid. More recently, Kneafsey and Pruess [26] visualized the occurrence of fingers in the CO_2-water system at low pressures.

The objective of this chapter is to design and construct an experimental set-up, by which the development and growth of fingers of CO_2 in the aqueous and oleic phases at high pressure can be visualized. Because the density gradient plays the main role in occurrence of the convective currents, the Schlieren method has been used to visualize the phenomenon. By applying COMSOL Multiphysics the numeric results are compared with the experiment.

The structure of the chapter is as follows: first we describe our experimental Schlieren set-up and briefly explain the procedure. Then we illustrate the theoretical model that describes the natural convection flow in our experimental configuration. Later we provide a derivation to connect the refractive index gradient $\partial_z n$ to the concentration gradient $\partial_z c$, which can be used in the interpretation of the experiments. Afterwards, we present our experimental and numerical results. Finally we end the chapter with some concluding remarks.

2.2. EXPERIMENTAL SETUP

The main aim of the chapter is to visualize the induced convection currents when carbon dioxide is brought above a layer of liquid water, brine or oil. These currents originate because the density of the CO_2-liquid mixtures is higher than the pure liquid. It results in gravitationally-unstable flows in the CO_2-water (water and brine) or CO_2-oil mixtures. Our method of choice is the Schlieren method, because it is relatively simple to implement, it can be applied at high pressures and under favorable circumstances can be compared to numerical simulation data.

The Schlieren method (for more details see [27]) is an optical technique that can be applied to detect density gradients during fluid flow. The schematic of the Schlieren set-up is shown in Figure 2-2. To create a point source a 200 W light source is used behind an aperture diaphragm with an opening of 0.5 mm. The parallel light beam is created by locating the point source at a focal point of the first achromatic lens. This lens has a focal length of 1500 mm and a diameter of 110 mm. Because an achromatic lens (optical properties more or less independent of the wavelength of the light) is used, the chromatic aberration effect is minimized. In our Schlieren set-up, the distance between the light source and the Schlieren object, i.e., the high pressure cell (see Figure 2-2 and Figure 2-3) is about 1.6 m. In the high pressure cell the light rays will be deflected due to the gradients in refractive index caused by the variations in CO_2 concentration. Then the partially

deflected light beam converges in the focal plane of the second achromatic lens. This lens is identical to the first achromatic lens. A metal piece with a fine thickness is used as a knife edge on the focal plane of the second lens. The effect of the knife edge can be understood as follows. The light deflected by the inhomogeneity in CO_2 concentration will not be focused in the focal point, but rather will be displaced in the focal plane of the second lens. This means the deflected light rays are shifted with respect to the knife edge, which causes a change in the light transmission by the knife edge and consequently the recorded image intensity. In the present implementation the knife edge is placed horizontally, which results in the system to be sensitive to light deflections in the vertical directions, hence vertical gradients in CO_2 concentration. To record the Schlieren images, one black and white, CCD camera (Lavision- Imager intense**)** is used. The exposure time for the camera was set to 1 second to record the images with a resolution of 1000 × 1000 pixels.

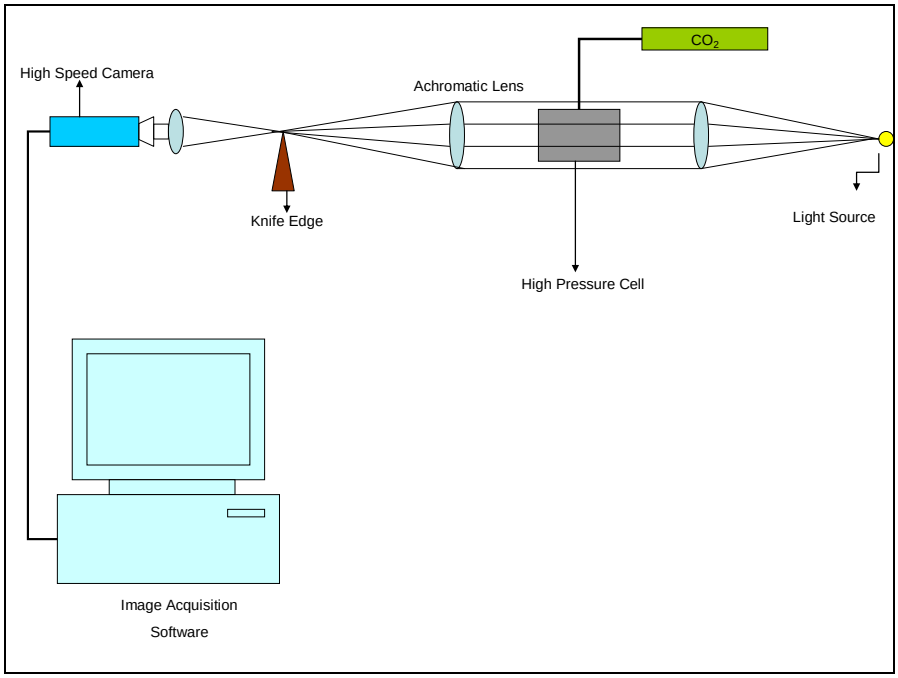

Figure 2-2: Schematic drawing of Schlieren set up on a vibration suppressing table. A horizontal knife edge is applied from the side. The high speed camera captures the intensity image. The deviation of the intensity is a measure of the concentration gradient in the z-direction perpendicular to the table (see Eq. (2.13)).

Figure 2-3 shows a schematic representation of the high pressure cell that can sustain 150 bar. The cell consists of a stainless steel frame with a cylindrical hole. Inside the hole there is a stainless steel cylinder bounded by two flanges. The cylinder has an outer diameter of 72 mm and a length of 122 mm. The two flanges on each side have the same inner and outer diameter as the cell. The length of the flanges is 22 mm. Between the flanges there are two glass windows with a diameter of 51 mm and a length of 25.4 mm. Between the two windows there is a gap of 11.6 mm and diameter of 25 mm that can contain the fluids. The gap has four connections, of which two are visible in

Figure 2-3. The other two connections are at the bottom and symmetrically at the other side. The bottom connector is used to bring water inside the high pressure cell; the top connector for filling the cell with CO_2. One side connector is used to record the pressure with a pressure transducer (PTX611, DRUCK, ±0.08% of span) and simultaneously to insert a thermocouple that measures the temperature in the upper half of the cell. The thermocouple and pressure transducer stick half a centimeter in the cell one centimeter above the equator. Another thermocouple is inserted in the other side connector and also measures the temperature in the upper half of the cell, in the exact mirror position of the other thermocouple. A heating wire was mounted around the cell to keep the cell at a constant temperature of 39°C.

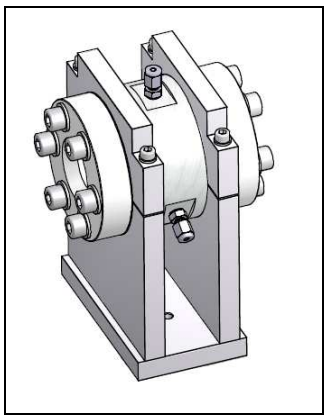

Figure 2-3: Cylindrical high pressure cell, in a holder, with two windows of thickness 25.4 mm.

Before usage, the windows are rinsed to make them as clean as possible. Initially the bottom half of the cell is filled with the aqueous or oleic phase. Subsequently gas is admitted from the top until the required pressures of 64 and 84 bar are reached. The gas in the container used to carry out the experiments consists of 99.98% pure carbon dioxide. There is one computer for recording the pressure history and one for recording the images with the high speed camera.

2.3. NUMERICAL MODELING

For the modeling we consider a 3-D model for natural convection flow of CO_2 in the aqueous or oleic phase (see Figure 2-4). The flow cell is a horizontal cylinder, of which the lower half is filled with brine or oil. The diameter of the fluid containing part of the cell is 25 mm and the length is 11.6 mm as in the experiment. The cell is filled with liquid until the equator. The CO_2 gas is brought on top of the liquid, after which natural convection starts. We applied the conventional equations for buoyant density flow and the Boussinesq approximation. This approximation uses constant

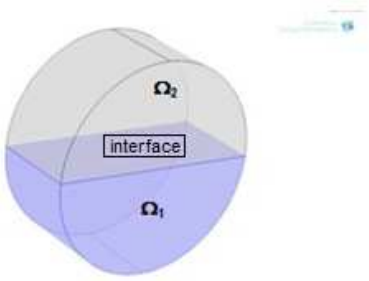

Figure 2-4: Geometry of the model.

densities except in the gravity term in the Navier Stokes equation. Due to the density heterogeneity the fresh (CO_2-free) liquid moves to the interface and CO_2 containing liquid moves downwards, accelerating the mass transfer rate. The boundary conditions are no flow conditions at the vessel boundary.

2.4. GOVERNING EQUATIONS

We consider a three-dimensional configuration of the horizontal cylinder (Figure 2-4). The vertical coordinate is the z-direction, whereas the horizontal coordinate is the x-direction. The coordinate perpendicular to the paper is the y-direction. The thickness of the interface is 11.6 mm in the y-direction. More details are given in this paper in the section where we explain the experimental set up. For the ease of reference, a brief description is written here. There are two parts in our cylindrical model. The upper part (Ω_2) is filled with the gas phase and the lower part (Ω_1) is filled with liquid. The governing equations in both domains of the cell are given below.

Liquid Phase Equations in Ω_1:

(a) Continuity Equation:

$$\text{div } \mathbf{v} = 0 \qquad (2.2)$$

(b) Conservation of Momentum, disregarding inertia effects:

$$\frac{\partial \mathbf{v}}{\partial t} = -\frac{1}{\rho}\mathbf{grad}p + \nu\ \Delta\mathbf{v} - \beta_c g \Delta c \qquad (2.3)$$

(c) Concentration Equation:

$$\frac{\partial c}{\partial t} + \mathbf{v} \cdot \mathbf{grad}\ c = D\Delta c \qquad (2.4)$$

Gas Phase Equations in Ω2:

$$\frac{\partial c_g}{\partial t} = D_g \Delta c_g \qquad (2.5)$$

Boundary and initial conditions for the liquid phase:

Initially, there is no CO_2 dissolved in the liquid, i.e. for t=0, and (x,y,z)$\in \Re^3$

$$w = v = u = c = 0$$

The boundary conditions of the model are:We use zero velocity and zero flux conditions at all boundaries except for the interface between gas and liquid. At this boundary we use Henry's law to relate the gas pressure to the carbon dioxide concentration in the liquid, i.e.,

$$K_{w-g}^{H} = a_{w,CO_2} / a_{g,CO_2} = m_{w,CO_2} \gamma_{w,CO_2} / f_{g,CO_2}\ , \qquad (2.6)$$

where $m_{w,\,CO2}$ is the molality of carbon dioxide in the water phase, $\gamma_{w,CO2}$ the activity coefficient, and $f_{g,\,CO2(g)}$ is the fugacity of carbon dioxide in the gas phase. We use PHREEQC [28] for the computations. The procedure to get activities in neutral molecules is given [29].

Boundary and initial conditions for the gas phase:

Initially at *t=0*,

$$C_g = \frac{f_{g,CO_2}}{R_B T}\ , \qquad (2.7)$$

Figure 2-5 and Figure 2-6 present results obtained by PHREEQC [28] for pure water, n-decane, brine with 25w/w% salt and 10w/w%.

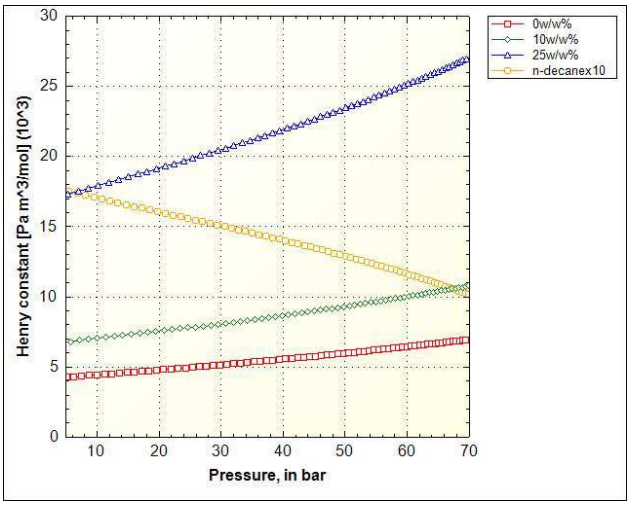

Figure 2-5: Henry's constant for a 25 w/w% and a 10 w/w% NaCl solution, fresh water and oil versus pressure. For n-Decane, the displayed Henry constant should be divided by 10.

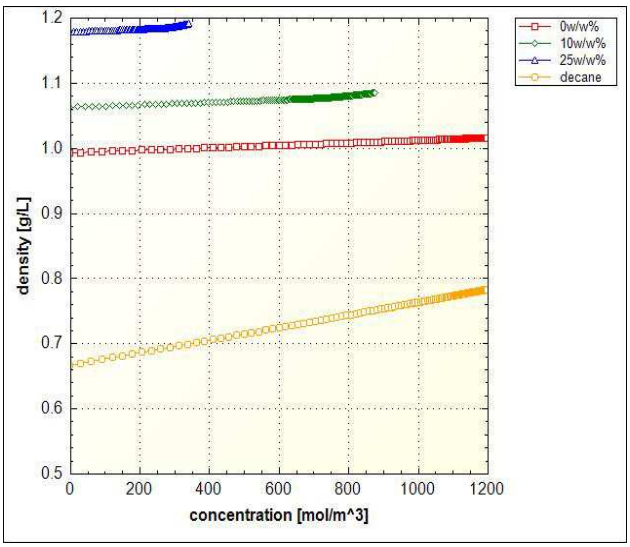

Figure 2-6: The density [g/L] of a 25 w/w%, a 10 w/w% NaCl solution, fresh water and oil versus dissolved C(4) concentration at T=312k. By C (4) we mean the sum of the CO_2, CO_3^{2-}, HCO_3^- at elevated level). For n-Decane the dissolved concentration on the horizontal axis should be multiplied to 10.

2.5 THEORY

Here, we follow [30, 31] to obtain a relation between the refractive index gradient and concentration gradient. By way of example we give here the derivation for pure water. We start with an equation that relates the refractive index of the solution to the refractive indexes of the components, i.e.,

$$\frac{n^2-1}{n^2+2}=\upsilon_w\frac{n_w^2-1}{n_w^2+2}+(1-\upsilon_w)\frac{n_{CO_2}^2-1}{n_{CO_2}^2+2}\ , \qquad (2.\ 8)$$

where n is the refractive index of the mixture, n_w is the refractive index of pure water, and n_{CO2} is the refractive index of "pure CO_2" if it were existing as a single pure component. We use $\upsilon_w=\rho_w/\rho_w^{(0)}$ to denote the volume fraction of water in the mixture. Therefore, Eq. (2. 8) can be converted to:

$$\frac{n^2-1}{n^2+2}=\frac{\rho_w}{\rho_w^{(0)}}\frac{n_w^2-1}{n_w^2+2}+\frac{\rho_{CO_2}}{\rho_{CO_2}^{(0)}}\frac{n_{CO_2}^2-1}{n_{CO_2}^2+2}\ , \qquad (2.\ 9)$$

Where $\rho_w^{(0)}$, is the density of pure water at the reference temperature and $\rho_{CO_2}^{(0)}/M_{CO_2}$ is the inverse partial molar volume of CO_2 at the relevant pressure and temperatures. We use ρ_w and ρ_{CO_2} to denote the concentrations of water and carbon dioxide. The data for the pure water and CO_2 can be found in [3] , page 72, to be $\rho_{CO_2}^{(0)}$ = $1/V_{CO2}$ =30.3 mol / liter, whereas $\rho_w^{(0)}$ = $1/V_{H2O}$ = 55.1 mol / liter at 39°C.

For ideal solutions the densities $\rho_w^{(0)}$ and $\rho_{CO_2}^{(0)}$ are constant at a given temperature, i.e., independent of the concentrations and pressure. As the sum of the volume fractions is unity we can write the relation:

$$\frac{\rho_w}{\rho_w^{(0)}}+\frac{\rho_{CO_2}}{\rho_{CO_2}^{(0)}}=1\ , \qquad (2.\ 10)$$

The Clausius-Mossotti relation reads in electrostatic units,

$$\frac{n^2-1}{n^2+2}=\frac{1}{3}\rho L\alpha\ , \qquad (2.\ 11)$$

where α is the polarizability [m^3/molecule], L=6.0225×10^{23} is Avogadro's number [molecules/mole] and ρ [moles/m^3] is the molar concentration. The refractive index n of CO_2 at atmospheric pressure and at 273.15 *K* is n=1.000449. The density of CO_2 at atmospheric pressure and 273.15 K is $\rho_{CO_{2g}}$ = 44.942 [mol/m^3]. Therefore we find that Lα = 1.998× 10^{-5}. Consequently, the refractive index of "pure CO_2" can be found from $L\alpha$ = 1.998× 10^{-5} and the density $\rho_{CO_2}^{(0)}$ by using Eq. (2. 11); from which we obtain n_{CO2} = 1.326. From the literature [32] we obtain for water, the 10 w/w% and the 25 w/w% brine solutions at 390C that nw = 1.339 , n10w/w%=1.35 and n25w/w%=1.37 (see also the data base in PHREEQC [28] . For n-decane the refractive index is 1.405 [33]).

After differentiation of Eq. (2. 9) towards z and using (2. 10) we obtain:

$$\frac{\partial}{\partial z}\left(\frac{n^2-1}{n^2+2}\right)=\frac{\partial}{\partial z}\left(1-\frac{\rho_{CO_2}}{\rho_{CO_2}^{(0)}}\right)\frac{n_w^2-1}{n_w^2+2}+\frac{\partial}{\partial z}\left(\frac{\rho_{CO_2}}{\rho_{CO_2}^{(0)}}\right)\frac{n_{CO_2}^2-1}{n_{CO_2}^2+2}=\left(\frac{n_{CO_2}^2-1}{n_{CO_2}^2+2}-\frac{n_w^2-1}{n_w^2+2}\right)\frac{1}{\rho_{CO_2}^{(0)}}\frac{\partial\rho_{CO_2}}{\partial z}, \quad (2.12)$$

Therefore it follows that

$$\frac{\Delta I}{I}\propto\frac{1}{n}\frac{\partial n}{\partial z}=\frac{6}{(n^2+2)^2}\left(\frac{n_{CO_2}^2-1}{n_{CO_2}^2+2}-\frac{n_w^2-1}{n_w^2+2}\right)\frac{1}{\rho_{CO_2}^{(0)}}\frac{\partial\rho_{CO_2}}{\partial z}, \quad (2.13)$$

where we used reference [27] for the derivation that $1/n\ \partial n/\partial z$ is proportional to the relative intensity variation $\Delta I / I$ in the recorded Schlieren image when the knife edge is oriented horizontally. This equation shows that the intensity fluctuations depend on the concentration gradient ($\partial_z \rho_{CO2}$) and on the difference of $(n^2 -1)/ (n^2 + 2)$ between pure water and "pure" CO_2. It is to be noted that this difference is very small for fresh water. For the salt solutions the refractive index of fresh water n_w should be replaced by the refractive index of the salt solution. For the n-decane experiments we replace n_w by the refractive index of n-decane. In these cases the term between brackets in Eq. (2. 13) is much larger than for fresh water.

2.6. EXPERIMENTAL RESULTS AND INTERPRETATION

Figure 2-7 to Figure 2-11 show the experimental results. Figure 2-7 to Figure 2-9 show results at decreasing salt concentrations. Figure 2-10 shows the result for oil and Figure 2-11 presents a result at supercritical conditions for pure water. In all experiments, the z-direction is taken as pointing vertically downward and the knife cuts the beam horizontally from below. The refractive index of the carbon dioxide containing solutions is lower than for the solutions without dissolved CO_2 (see [34]). Initially there is constant refractive index; the beam is not deflected and the observed intensity in the lower region is constant (dark grey). At later times the region below the equator appears dark as this is a region of increasing refractive index as we move downward from the equator. Indeed the beam is deflected in the direction of higher refractive index. Consequently the beam is deflected towards the knife edge and hits the knife edge. This leads to a darker region, as is observed in the experiments. At the gas-liquid interface we also expect that on average the refractive index increases from above the equator that contains a gas phase to below the equator that contains a liquid phase. This would also lead to a dark region.

Further downward, there will be fingers protruding from above in a rather erratic manner. As the light beam, which traverses in the x-direction, encounters many gravity fingers it will be deflected in all directions and shows more a typical scattering pattern and the lower half, beyond the dark region, shows an increased intensity [35-39] . So even if the beam is deflected downwards the

scattered light goes around the focal point and we expect a lighter region. This is also observed in the early stages of most experiments. Still below the scattering region, diffusion of carbon dioxide occurs, leading again to an increasing refractive index (positive refractive index gradient) and thus to a dark region. After some time the entire region is filled with fingers. The refractive index is therefore changing erratically in the z-direction.

Figure 2-7 presents the Schlieren pattern for a 25 w/w% NaCl solution. At this high salt concentration there is only a small density contrast due to the high Henry coefficient (see Figure 2-5) and consequently the Rayleigh number is relatively low. Moreover, according to Eq. (2. 13), the refractive index contrast is larger than for pure water. The experiment starts after admitting carbon dioxide into the cell at the required pressure. Gravity fingering only initiates after 50 seconds. Fingers reach the bottom of the cell after about 200 seconds. In the early stages fingers grow much slower than in the pure water- CO_2 system (see Figure 2-9). For $700 < t < 1000$ seconds the instabilities are still clearly visible in the 25% brine case as opposed to the pure water-CO_2 system where the fingering becomes less pronounced after thousand seconds.

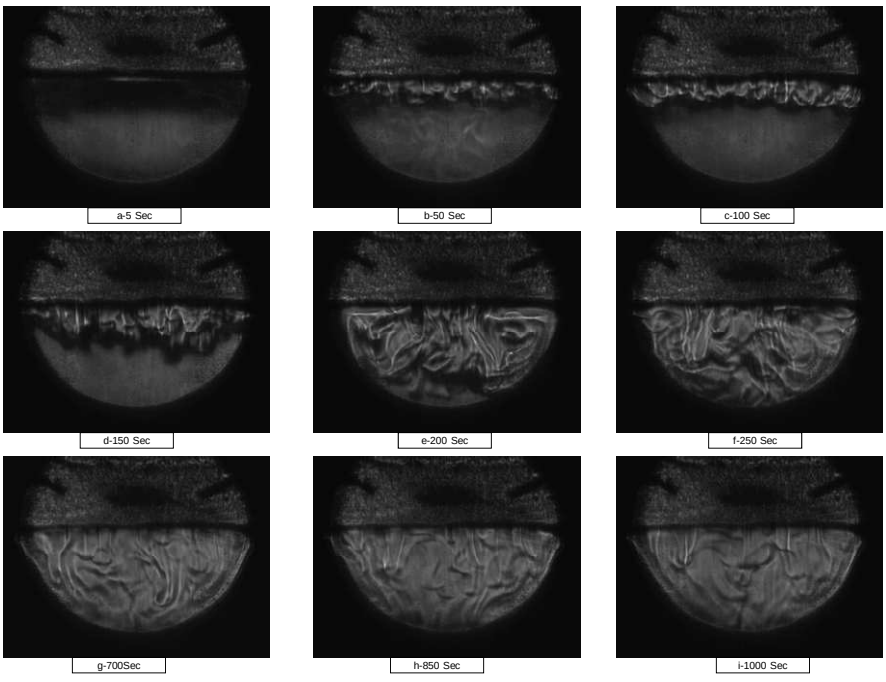

Figure 2-7: Schlieren pattern in CO_2-Brine (25w/w% salt) after different times. It shows fingers in the lower half of the circle. The upper half is filled with CO_2 at 64 bar.

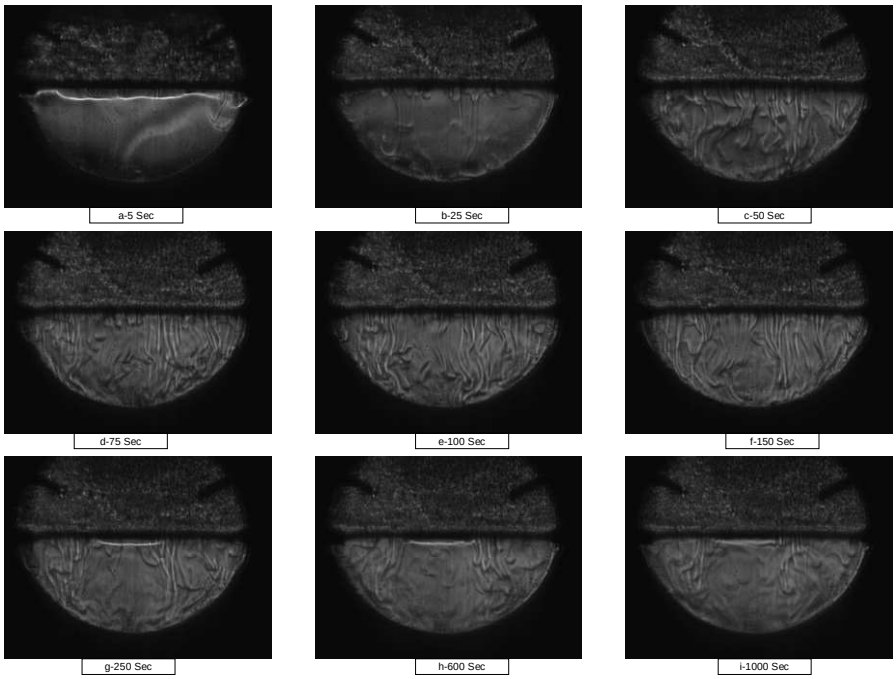

Figure 2-8: Schlieren pattern in CO_2-Brine (10w/w% salt) after different times. It shows fingers in the lower half of the circle. The upper half is filled with CO_2 at 64 bar.

Figure 2-8 shows the Schlieren pattern for a 10 w/w% NaCl solution. Following Eq. (2. 13) we expect again that the refractive index contrast becomes larger than for pure water. One observes that fingering begins at about 25 seconds whereas the fingering starts after 5 seconds in the CO_2 – pure water system. The time for onset of fingering is inversely proportional to Ra^{-2} [13, 16]. This means that the time for onset of gravity fingering is proportional to $(\Delta\rho)^{-2}$. The solubility of CO_2 in 10 w/w% brine is less than in pure water, but larger than in the 25 w/w% case, leading to smaller and larger $\Delta\rho$ values respectively. From t=75 to t=150 seconds a similar instability behavior is observed. As time proceeds, the speed and the number of the fingers decline. The brine- CO_2 system at later stages (600 <t<1000 seconds) shows more unstable behavior than at the corresponding times in the pure water- CO_2 system.

Figure 2-9 shows the Schlieren pattern for the system of pure water- CO_2 at 64 bar. We observe that gravity fingering appears almost immediately; however, as time elapses the number of fingers and the fingering rate decreases. Figure 2-9a shows that the instabilities start from the center and then propagate towards the sides. After 25 seconds the instabilities are visible throughout the whole system. The fingering pattern changes constantly and stays roughly the same between t=25 to t=100 seconds. After about 100 seconds the fingering pattern becomes less than initially, illustrating the evolvement towards a homogeneous concentration distribution.

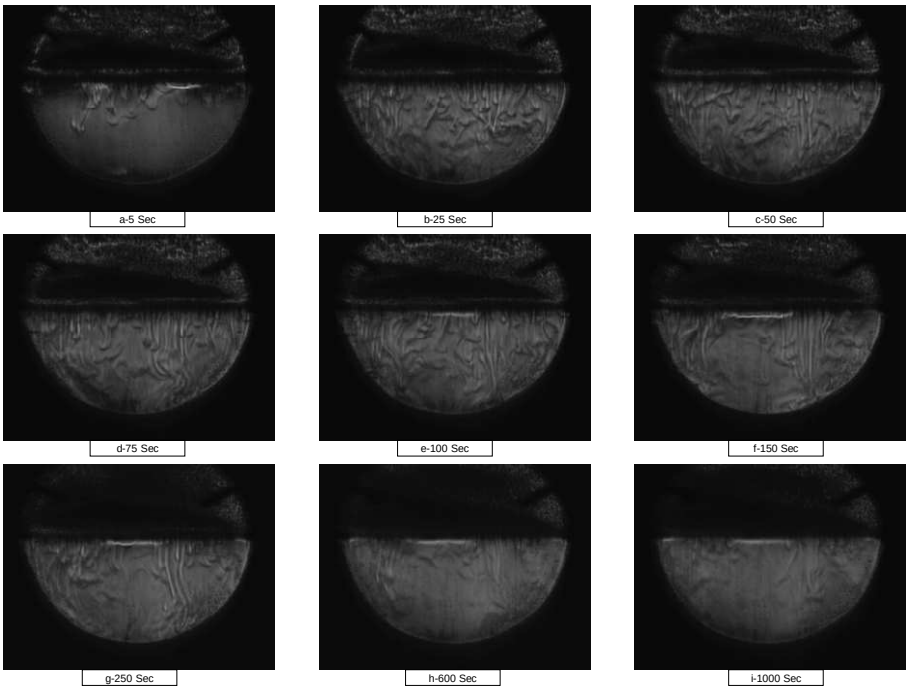

Figure 2-9: Schlieren pattern in CO_2-Water after different times. It shows fingers in the lower half of the circle. The upper half is filled with CO_2 at 64 bar.

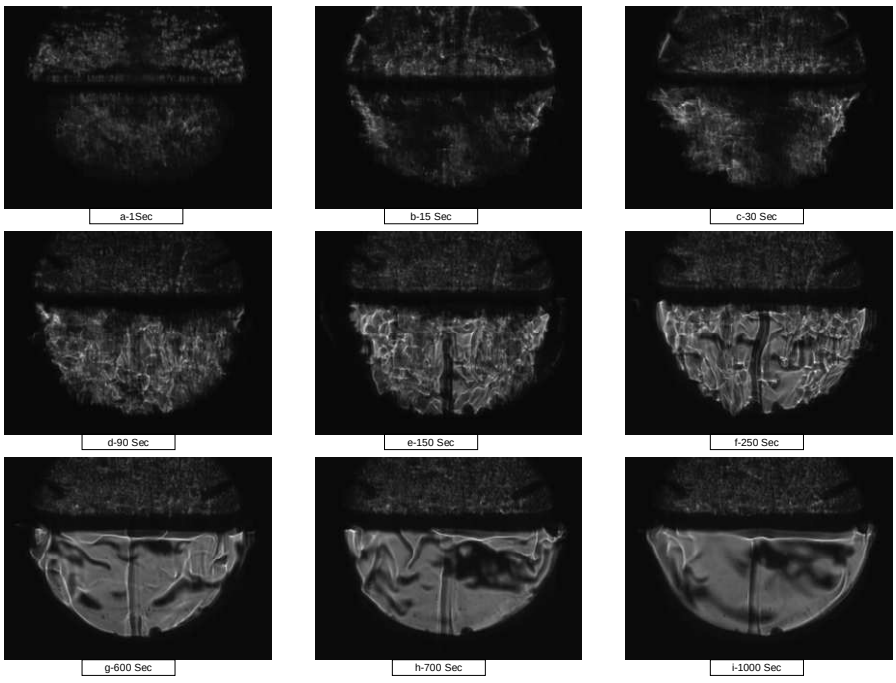

Figure 2-10: Schlieren pattern in CO_2-Oil (nC_{10}) after different times. It shows fingers in the lower half of the circle. The upper half is filled with CO_2 at 64 bar.

Figure 2-10 demonstrates the Schlieren pattern for the system of Oil (n-decane) - CO_2 at 64 bar. Immediately after bringing CO_2 on top of the oleic phase, the system exhibits highly unstable behavior. More interfacial turbulence can be seen in oil-phase experiment than in the aqueous-phase experiments. After 150 seconds a fingering pattern appears in the middle of the cell. From t=600 to t=800 seconds these gravity fingers are observed at both sides of the cell, albeit that the intensity of fingering becomes less. This is the first visualization experiment involving oil. We leave further interpretation of this experiment for future work.

We did an experiment at 84 bar when CO_2 in supercritical condition is brought into contact with water. Figure 2-11 shows the Schlieren pattern in the CO_2 – water system after different times at 84 bar. From the beginning of injection, instability starts. After 5 sec, gravity fingers hit the bottom of the cell. From t=25 to t=150 seconds the instability increases. A similar pattern persists in this period. In comparison with Figure 2-9 at the later stages (600-1000 seconds), a more or less similar behavior is observed for subcritical (Figure 2-9) and super critical CO_2 (Figure 2-11) in contact with water.

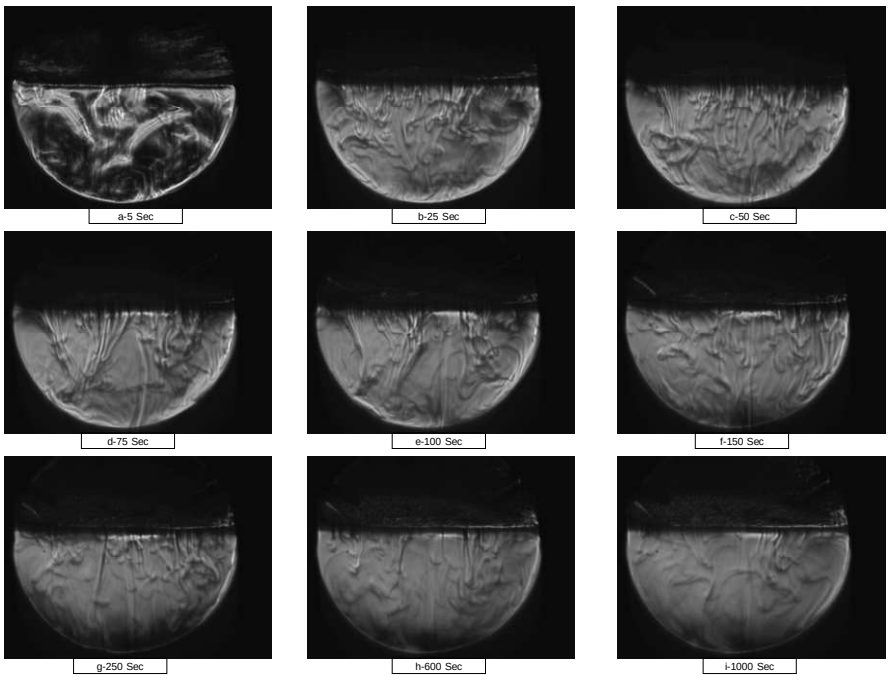

Figure 2-11: Schlieren pattern in CO_2-Water after different times. It shows fingers in the lower half of the circle. The upper half is filled with CO_2 at 84bar

Figure 2-12 summarizes the pressure behavior for the four experiments at 64 bar. As shown in Figure 2-12 the rate of pressure decline decreases in the order of oil, pure water, brine 10w/w% and finally brine 25w/w%. Indeed, due to the high miscibility of CO_2 in oil, the initial pressure decreases dramatically.

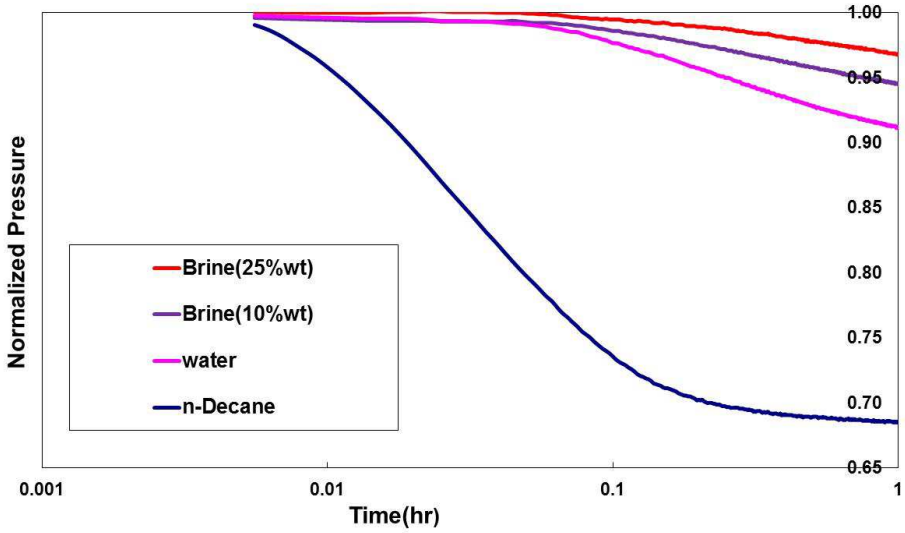

Figure 2-12: Comparison of the pressure history of the experiments in Brine, Water and Oil at 64 bar. A pressure decrease in the upper half of the cell corresponds to a decreasing mass in the upper half of the cell, which must be for reasons of mass conservation transferred to the liquid phase in the lower half of the cell. The pressure derivative can be directly related to the integrated mass transfer rate. The "density or inverse partial molar volume" of the carbon dioxide in the liquid phase is much higher than the molar density in the gas phase, meaning that the transfer of carbon dioxide to the liquid phase entails only a negligible volume increase in the liquid phase.

2.7. NUMERICAL RESULTS

The Numerical modeling of natural convection is challenging because high (spatial and temporal) resolution is required in the regions where natural convection takes place. We use commercial finite element software (COMSOL) to perform the numerical computations. For the liquid phase we apply the creeping flow equation (Eq. (2. 3)), from the fluid flow module and the transport of diluted species (Eq. (2. 4), (2. 5)) from the chemical species transport module. Initial and boundary conditions are given above.

Figure 2-13 to Figure 2-16 show the 3-D numerical simulations corresponding to our experimental conditions. The experimental results are shown in the sequence of increasing strength of natural convection, which has as a consequence that the natural convection is the weakest for the 25w/w% salt solution, somewhat stronger at 10w/w%, again stronger for pure water (0w/w%) and strongest for the n-Decane experiments. The simulations use 49876 tetrahedral elements. The elements are third order for the velocity and second order for the pressure. The elements for the concentration equation are linear.

Figure 2-13 simulates the 25 w/w% situation. The figure shows the onset of natural convection at 50 s where initial perturbation is clearly visible. The upper bound of the concentration remains more or less the same (~300 mol/m3), but at the lower bound it increases from zero to 140 mol/m3. As time proceeds, the fingers become longer and thicker as shown in the top right figure. Subsequently (in bottom left figure) the strength of natural convection becomes less and also the concentration contrast becomes less. The fingers persist in the right bottom figure, albeit that we note that the concentration contrast is decreasing in the range between 140-280 mol/m3. Figure 2-12 shows that the pressure decline for the 25 w/w% solution is slowest.

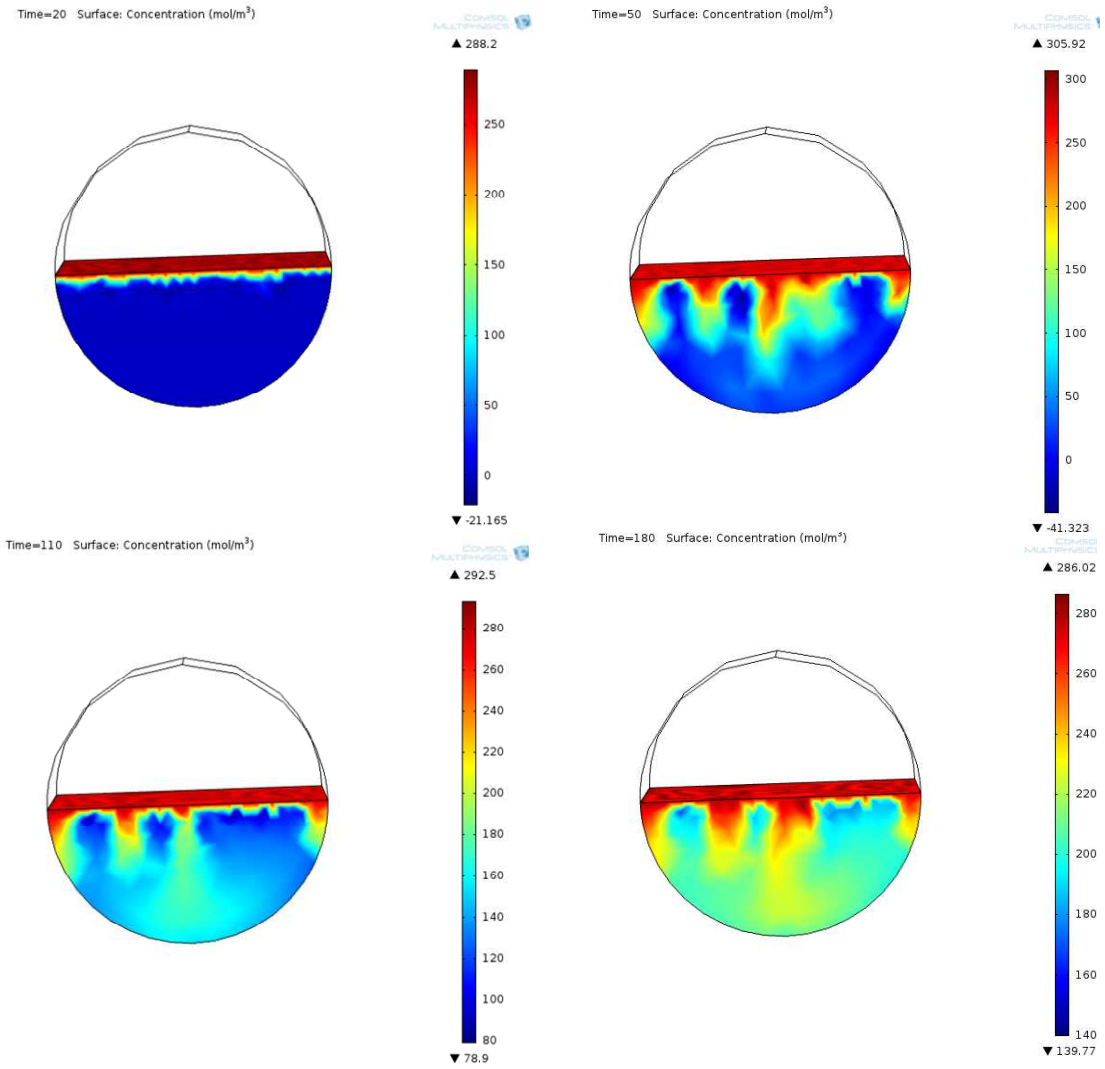

Figure 2-13: Numerical results of classical model 25w/w% brine-CO_2 at 64 bar and 312k, - concentration profile is shown in various times (t=20, 50, 110 and 180 sec).

Figure 2-14 concerns the 10 w/w% situation. The top left figure shows the onset of natural convection at 20 s and the initial perturbation is already superseded by natural convection flow.

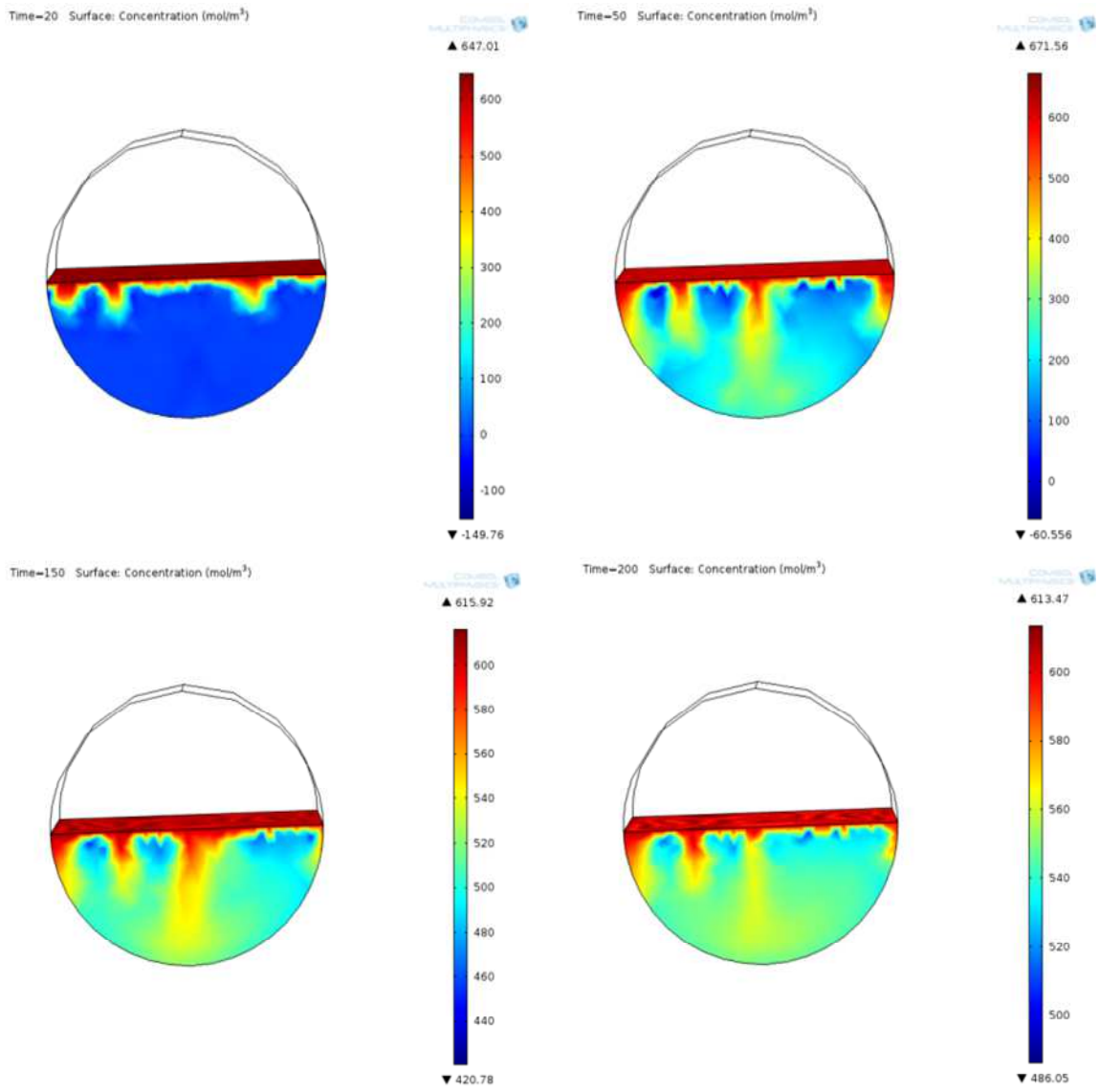

Figure 2-14: Numerical results of classical model 10w/w%-CO_2 brine at 64 bar and 312k, - concentration profile is shown in various times (t=20, 50, 150 and 200 sec).

The upper bound of the concentration remains more or less the same (~700 mol/m^3), but the lower bound increases from zero to 500 mol/m^3. As time proceeds, the fingers become again longer and thicker as shown in the top right figure. Subsequently (in the bottom left figure) the strength of natural convection becomes less and also the concentration contrast becomes less. The fingers persist in the right bottom figure, albeit we note that the concentration contrast is

decreasing in the range between 500-700 mol/m3. Figure 2-12 shows that the pressure decline for the 10 w/w% solution is the second slowest.

Figure 2-15 concerns the pure water phase. The top left figure shows the onset of natural convection at 10 s and the initial perturbation is completely superseded by natural convection flow.

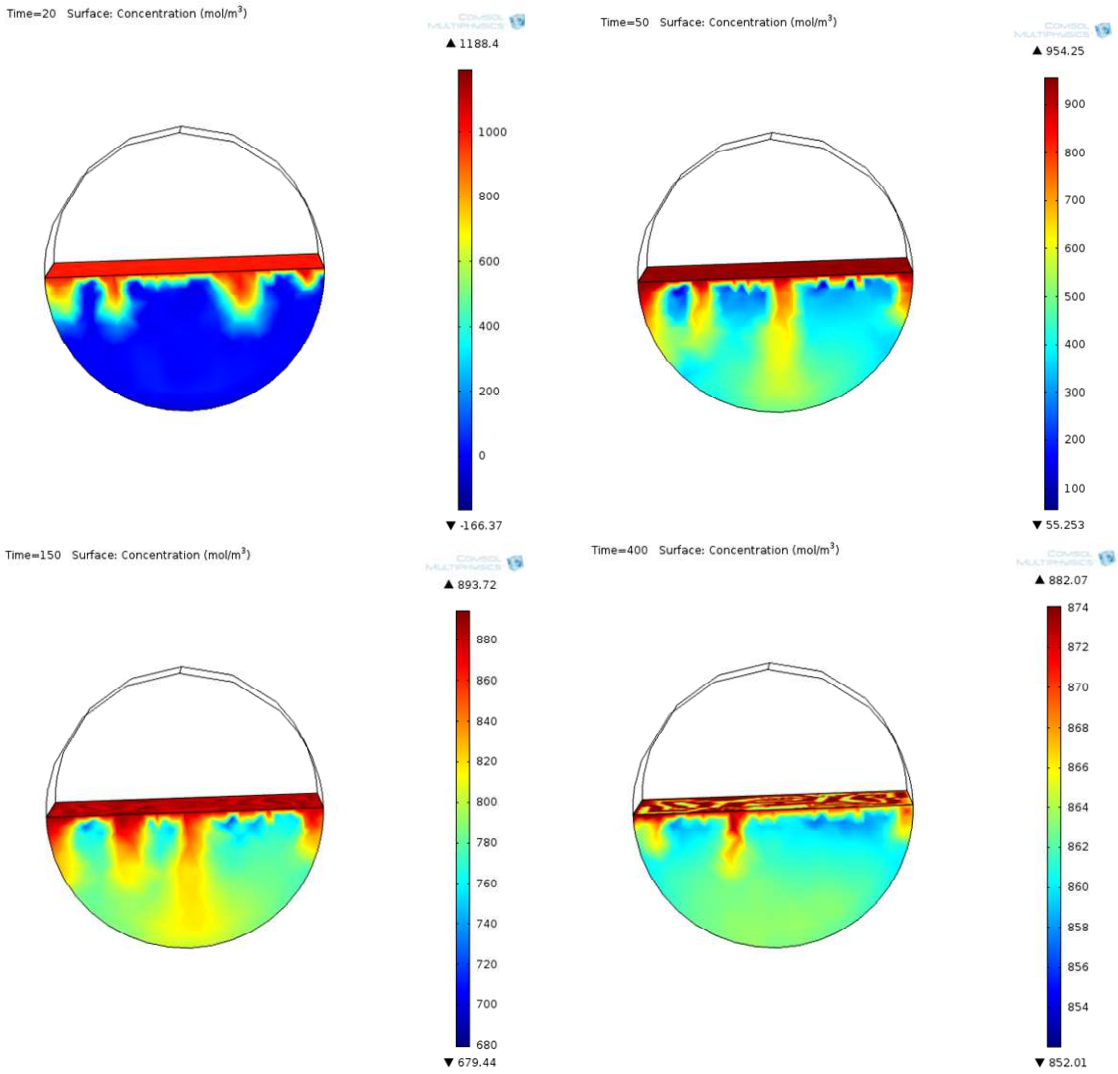

Figure 2-15: Numerical results of classical model pure water-CO_2 at 64 bar and 312k, - concentration profile is shown in various times (t=20, 50, 150 and 400 sec).

The upper bound of the concentration decreases from (~1200 mol/m3) to (~900 mol/m3), whereas the lower bound increases from zero to (~860 mol/m3). As time proceeds, the fingers stay more or less the same as shown in the top right figure. Subsequently (in bottom left figure) the strength of natural convection becomes less and also the concentration contrast becomes less. The fingers

almost disappear in the right bottom figure, which is even more conspicuous if we consider that the concentration contrast is decreasing in the range between (854-874 mol/m3). Figure 2-12 shows that the pressure decline for the 0 w/w% solution is stronger than for the 10 w/w% solution.

Figure 2-16 shows the numerical simulation for the oleic phase. The top left figure shows that the on-set of natural convection occurs at 20 seconds.

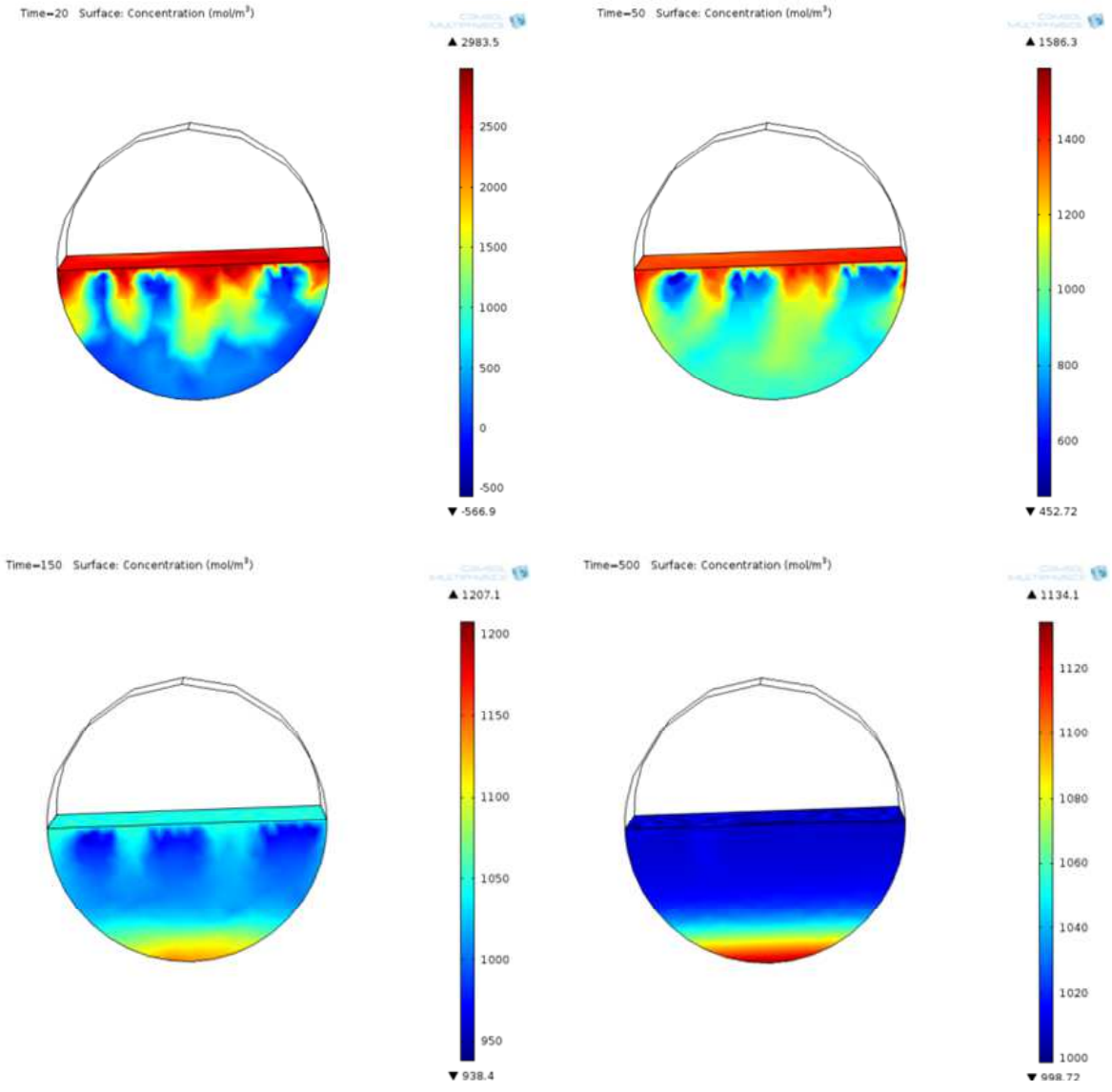

Figure 2-16: Numerical results of classical model Decane-CO_2 at 64 bar and 312K, - concentration profile is shown in various times (t=20, 50, 150 and 500 sec).

The upper bound of the concentration decreases from (~2700 mol/m^3) to (1400 mol/m^3), whereas the lower bound increases from zero to (1000 mol/m^3). As time increases the fingers become less conspicuous. Figure 2-12 shows that the pressure decline for oleic phase is stronger than for the other cases.

Figure 2-17 compares the measured pressure history with results obtained with numerical simulation. The computed results show qualitatively the same trends as the experimental results albeit that the computed transfer rate is larger.

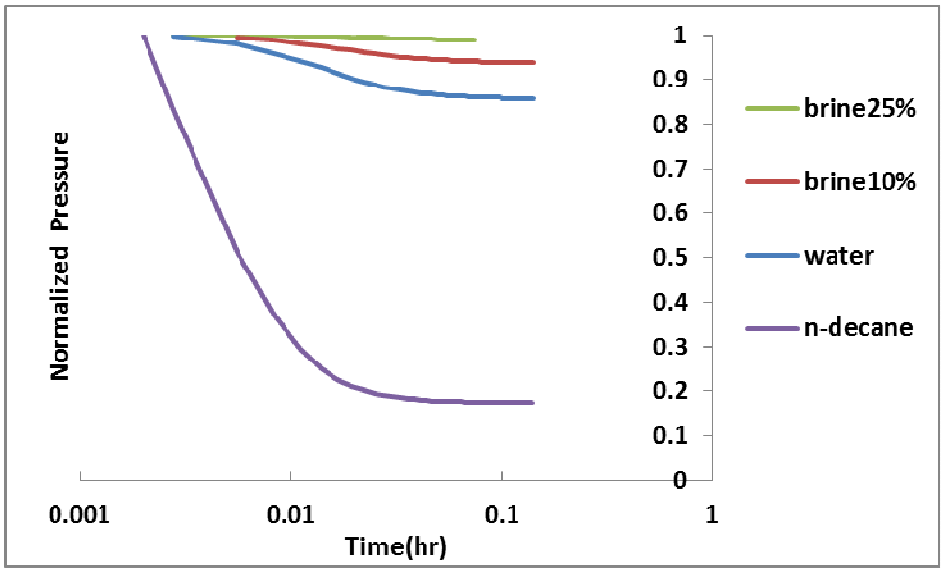

Figure 2-17: Comparison of the pressure history of the modeling in Brine, Water and Oil at 64 bar.

This is in particular conspicuous for the oil result. Indeed, comparison of the experimental results to the numerical results shows only qualitative agreement. We conjecture in the numerical section that the grid cells are too large to capture the mm-scale fine structure of the gravity fingers. It is technically not possible to use smaller grid cells as this will lead to prohibitively long computation times. In comparison to the onset of instability there is some correspondence between experiments and numerical results. In the numerical model, the number of fingers is much less than in the experimental results. Also in the numerical calculations the fingers are much larger. The main qualitative correspondence between simulations and experiments is that there is a region of high concentration gradient near the gas–liquid interface. We leave simulations with finer grids for a better understanding to future work.

2.8. CONCLUSIONS

- Dissolution of CO_2 in an aqueous (or oleic) phase forms a mixture that is denser than the carbon dioxide free water or brine (oleic phase). This causes a local density increase, which induces natural convection currents (gravity fingers) when gaseous carbon dioxide is brought above the liquid phase. This enhances the rate of mixing of CO_2 in the liquid phase.
- We designed and built a cylindrical transparent high pressure cell in which gravity induced fingers (playing a major role in the enhanced mixing process) could be observed, e.g., by mounting the cylinder horizontally and filling the bottom half with liquid and the top-half with gaseous or supercritical carbon dioxide.
- We developed a Schlieren set-up that can be used to observe the gravity induced fingers based on refractive index variations. Gravity fingers have been observed in an aqueous phase with various concentrations of sodium chloride (0-25 w/w %) or with an oleic phase (n-decane). The experiments show that natural convection currents are weakest in highly concentrated brine and strongest in oil.
- The Schlieren pattern consists of a dark region near the equator and a lighter region below it. The dark region indicates a region where the refractive index increases downward, either due to the presence of a gas liquid interface, or due to the thin diffusion layer, which also appears in numerical simulations.
- It is possible to use commercial software (COMSOL Multiphysics) to simulate the natural convection process in 3-D albeit with grid cells that are too large to capture the mm-scale fine structure of the gravity fingers. As the distance between the windows is 11.6 mm it can be expected that the concentration is not uniform in the axial direction. This leads initially to a scattering region with a lighter appearance in the Schlieren pattern. For later times the erratic behavior decreases and the effect of individual gravity fingers can be observed.
- To our knowledge this is the first time that gravity fingers in the oil phase are visualized. The set-up can screen any fluid for its relative importance of natural convection flows.

2.9. NOMENCLATURE

C = concentration (mol/m^3)

C_g = concentration (mol/m^3)

D = molecular diffusion coefficient, (m^2/ s)

D_g= molecular diffusion coefficient in gas phase, (m^2/ s)

k = permeability, mD

β = volumetric expansion coefficient (m^3/mol)

V=velocity (m/s)

P=pressure (bar)

t=time

v = kinematic viscosity (m^2/s)

ρ = density (kg/m^3)

A = the area exposed to CO_2 (m^2)

μ = viscosity of the solvent (kg.m.s)

g = acceleration due to gravity (kg/m)

Ra= Rayleigh number

K_H =Henry's constant

n= refractive index

n_w= refractive index of pure water

n_{CO2} =refractive index of pure CO_2

$\rho_w^{(0)}$ = density of pure water at the reference temperature(kg/m^3)

α = polarizability

L= Avogadro's number

$m_{w,CO2}$= molality of carbon dioxide in the water phase(mol/kg)

$\gamma_{w,CO2}$ = activity coefficient

$f_{g,CO2(g)}$= fugacity of carbon dioxide in the gas phase(bar)

Subscripts

o = reference value of the quantity

g = gas

i = initial value

w = water

2.10. REFERENCES

1. Eftekhari, A.A., H. Van Der Kooi, and H. Bruining, *Exergy analysis of underground coal gasification with simultaneous storage of carbon dioxide*. Energy, 2012. **45**(1): p. 729-745.
2. Van der Meer, L., *Investigations regarding the storage of carbon dioxide in aquifers in the Netherlands*. Energy Conversion and Management, 1992. **33**(5): p. 611-618.
3. Gmelin, L., *Gmelin Handbuch der anorganischen Chemie, 8. Auflage. Kohlenstoff, Teil C3, Verbindungen*, 1973, ISBN 3-527-81419-1.
4. Bachu, S., W. Gunter, and E. Perkins, *Aquifer disposal of CO< sub> 2</sub>: Hydrodynamic and mineral trapping*. Energy Conversion and Management, 1994. **35**(4): p. 269-279.
5. Class, H., et al., *A benchmark study on problems related to CO_2 storage in geologic formations*. Computational Geosciences, 2009. **13**(4): p. 409-434.
6. Elder, J., *The unstable thermal interface*. J. Fluid Mech, 1968. **32**(1): p. 69-96.
7. Ennis-King, J., I. Preston, and L. Paterson, *Onset of convection in anisotropic porous media subject to a rapid change in boundary conditions*. Physics of Fluids, 2005. **17**(8): p. 084107-084107-15.
8. Foster, T.D., *Onset of convection in a layer of fluid cooled from above*. Physics of Fluids, 1965. **8**: p. 1770.
9. Gasda, S.E., Numerical models for evaluating CO_2 storage in deep saline aquifers: Leaky wells and large-scale geological features, . Ph.D. Thesis. Available at http://arks.princeton.edu/ark:/88435/dsp01j098zb09n., 2010.
10. Nordbotten, J.M. and M.A. Celia, *Geological Storage of CO_2: Modeling Approaches for Large-Scale Simulation*2011: Wiley. com.
11. Nordbotten, J.M., M.A. Celia, and S. Bachu, *Injection and storage of CO_2 in deep saline aquifers: Analytical solution for CO_2 plume evolution during injection*. Transport in porous media, 2005. **58**(3): p. 339-360.
12. Ranganathan, P., et al., *Numerical simulation of natural convection in heterogeneous porous media for CO_2 geological storage*. Transport in porous media, 2012. 95(1): p. 25-54.
13. Riaz, A., et al., *Onset of convection in a gravitationally unstable diffusive boundary layer in porous media*. Journal of Fluid Mechanics, 2006. 548: p. 87-111.
14. Walker, K.L. and G.M. Homsy, *Convection in a porous cavity*. J. Fluid Mech, 1978. **87**(Part 3): p. 449-474.
15. Van Duijn, C., G. Pieters, and P. Raats, *Steady flows in unsaturated soils are stable*. Transport in porous media, 2004. **57**(2): p. 215-244.
16. Meulenbroek, B., R. Farajzadeh, and H. Bruining, *The effect of interface movement and viscosity variation on the stability of a diffusive interface between aqueous and gaseous CO_2*. Physics of Fluids (1994-present), 2013. **25**(7): p. 074103.
17. Myint, P.C. and A. Firoozabadi, *Onset of convection with fluid compressibility and interface movement*. Physics of Fluids, 2013. **25**: p. 094105.
18. Lapwood, E., *Convection of a fluid in a porous medium*. Proceedings of the Cambridge, 1948.
19. Weir, G., S. White, and W. Kissling, *Reservoir storage and containment of greenhouse gases*. Energy Conversion and Management, 1995. **36**(6): p. 531-534.
20. Farajzadeh, R., et al., *Mass transfer of CO_2 into water and surfactant solutions*. Petroleum Science and Technology, 2007. **25**(12): p. 1493-1511.
21. Farajzadeh, R., et al., *Numerical simulation of density-driven natural convection in porous media with application for CO_2 injection projects*. International journal of heat and mass transfer, 2007. **50**(25): p. 5054-5064.
22. Farajzadeh, R., P.L. Zitha, and J. Bruining, *Enhanced mass transfer of CO_2 into water: experiment and modeling*. Industrial & Engineering Chemistry Research, 2009. **48**(13): p. 6423-6431.
23. Yang, C. and Y. Gu, *Accelerated mass transfer of CO_2 in reservoir brine due to density-driven natural convection at high pressures and elevated temperatures*. Industrial & Engineering Chemistry Research, 2006. **45**(8): p. 2430-2436.

24. Nazari Moghaddam, R. and B. Rostami, *Reply to the "Comments on the Paper 'Quantification of Density-Driven Natural Convection for Dissolution Mechanism in CO_2 Sequestration'by R. Nazari Moghaddam et al.(2011)"*. Transport in porous media, 2012. **93**(1): p. 175-178.
25. Okhotsimskii, A. and M. Hozawa, *Schlieren visualization of natural convection in binary gas–liquid systems*. Chemical engineering science, 1998. **53**(14): p. 2547-2573.
26. Kneafsey, T.J. and K. Pruess, *Laboratory flow experiments for visualizing carbon dioxide-induced, density-driven brine convection*. Transport in porous media, 2010. **82**(1): p. 123-139.
27. Settles, G. S. "Schlieren and Shadowgraph Techniques: Visualizing Phenomena in Transparent Media. 2001." Springer.
28. Parkhurst, D.L. and C. Appelo, *Description of input and examples for PHREEQC version 3- A computer program for speciation, batch-reaction, one-dimensional transport, and inverse geochemical calculations*. US Geological Survey Techniques and Methods, Book 6, Modeling Techniques, 2013.
29. Randall, M. and C.F. Failey, *The Activity Coefficient of Gases in Aqueous Salt Solutions*. Chemical Reviews, 1927. **4**(3): p. 271-284.
30. Feynman, R., R. Leighten, and M. Sands, *The Feynman Lectures on Physics, Edison-Wesley Pub*, 1965, Comp.
31. Song, Y., et al., *Measurement on CO_2 Solution Density by Optical Technology*. Journal of Visualization, 2003. **6**(1): p. 41-51.
32. Subedi, D., et al., *Study of temperature and concentration dependence of refractive index of liquids using a novel technique*. Kathmandu University Journal of Science, Engineering and Technology, 2006. **2**(1): p. 1-7.
33. Mosteiro, L., et al., *Density, speed of sound, refractive index and dielectric permittivity of (diethyl carbonate+ n-decane) at several temperatures*. The Journal of Chemical Thermodynamics, 2001. **33**(7): p. 787-801.
34. Bao, B., et al., *Detecting Supercritical CO_2 in Brine at Sequestration Pressure with an Optical Fiber Sensor*. Environmental science & technology, 2012. **47**(1): p. 306-313.
35. Gatej, A., J. Wasselowski, and P. Loosen, *Using adaptive weighted least squares approximation for coupling thermal and optical simulation*. Applied Optics, 2012. **51**(28): p. 6718-6725.
36. Rimmer, M.P. *Ray tracing in inhomogeneous media*. in *1983 International Techincal Conference/Europe*. 1983. International Society for Optics and Photonics.
37. Sharma, A., D.V. Kumar, and A.K. Ghatak, *Tracing rays through graded-index media: a new method*. Applied Optics, 1982. **21**(6): p. 984-987.
38. van der Net, A., et al., *Simulating and interpretating images of foams with computational ray-tracing techniques*. Colloids and Surfaces A: Physicochemical and Engineering Aspects, 2007. **309**(1): p. 159-176.
39. Wu, Z.S., et al., *Improved algorithm for electromagnetic scattering of plane waves and shaped beams by multilayered spheres*. Applied Optics, 1997. **36**(21): p. 5188-5198.

Chapter 3

Effect of salinity and pressure on the rate of mass transfer in aquifer storage of carbon Dioxide

ABSTRACT

The growing concern about global warming has increased interest in improving the technology for the geological storage of carbon dioxide (CO_2) in aquifers. One issue is the limited storage space for carbon dioxide. Part of the storage space is in a gas tongue overlaying the aquifer. However, more storage space is available in aquifer. Storage in the aquifer has the advantage that the partial molar volume of dissolved carbon dioxide is about twice as small as the partial molar volume of the gas phase under optimal conditions.

One important aspect for aquifer storage is the rate of transfer between the overlying gas layer and the aquifer below. It is generally accepted that density driven natural convection is an important mechanism that enhances the mass transfer rate. The density effects occur because water with dissolved carbon dioxide has a higher density than fresh water or brine.

There is a lack of experimental work that study the transfer rate into water saturated porous medium at in-situ conditions, i.e., above critical temperatures and at pressures above 60 bar. Representative natural convection experiments require relatively large volumes (e.g., a diameter 8.5 cm and a length of 23 cm). We studied the transfer rate experimentally for both fresh water and brine (2.5, 5 and 10 w/w %). The experiment uses a high pressure ISCO pump to keep the pressure constant and allows determining the corresponding injection rate and cumulative injected volume. To our knowledge this is the first transfer experiments at constant pressure.

A log-log plot reveals that the mass transfer rate is proportional to $t^{0.8}$, and thus much faster than the predicted by Fick's law in the absence of natural convection currents. Moreover, the

experiments show that natural convection currents are weakest in highly concentrated brine and strongest in pure water.

KEYWORDS*: CO_2, Enhanced mass transfer, Natural convection*

Published in: submitted to journal of EAGE.

3.1. INTRODUCTION

The International Energy Agency (IEA) proposes large-scale investments in carbon capture and storage (CCS) to mitigate the impact of carbon dioxide (CO_2) emissions from the power and industrial sectors. In fact, IEA explicitly claims that two-thirds of today's proven reserves of fossil fuels still need to be in the ground in 2050 if the world is to achieve the 2°C goal, unless carbon capture and storage (CCS) technology can be widely deployed [1]. Carbon sequestration options include storage in oil and gas reservoirs, saline formations, un-mineable coal seams, basalts, and shales. Perhaps the most commonly considered target repository for CO_2 is a deep saline aquifer. However, concerns for storage in saline formations contain energy requirement [2], cost, long-term storage, impact on seismicity, and the logistics of sequestration [3] prevent large scale implementation. Eftekhari et al., [4] investigated the practical exergy requirement in CO_2 capture processes. They showed that exergy consumption for capture varies between 0.5-10 MJ/kg CO_2, corresponding to 2.5% - 50% of the exergy of methane. It illustrates the importance of the methods chosen and the effect of energy consumed to carry out carbon capture and storage. Michael et al., [5] reviewed the experience from existing storage operations for geological storage of CO_2 in saline aquifers. Experience with CO_2 injection at the pilot projects (Frio, Ketzin, Nagaoka and US Regional Partnerships) and existing operations (Sleipner, Snøhvit and In Salah) show that CO_2 geological storage in saline aquifers is technically feasible. By the end of 2008, approximately 20 Mt of CO_2 had been successfully injected into saline aquifers by existing operations. The highest injection rate and total storage volume for a single storage operation are approximately 1 Mt CO_2/year and 25 Mt, respectively. A benchmark study on problems related to CO_2 storage in geologic formations were carried out by Class et al., [6]. They mention several problems such as: leakage through a well, spillage of methane into the atmosphere, and low injectivity and heterogeneity of the reservoirs. Quantitative estimation of CO_2 leakage from geological storage was also studied by Celia et al., [7]. Their analytical solutions suggest a promising avenue for leakage analysis at the large scale.

It can be expected that optimal storage [4] of carbon dioxide (CO_2) in aquifers improves by dissolution of CO_2 in formation brine because the virtual density (inverse partial molar volume) of dissolved CO_2 in water (1333 kg/m^3) is more favorable than its density in the supercritical gas-phase. The sequestration capacity of CO_2 in aquifers would be of the order of 2% of the reservoir volume, if CO_2 would not dissolve in the aqueous phase [8]. Injected CO_2 moves upward to the top of the reservoir forming a gas layer due to buoyancy forces. The CO_2 transfer rate from the gas layer to the aquifer below would be slow if it were only determined by molecular diffusion. CO_2 mixes with the water (or brine) to form a denser aqueous phase (e.g., in a pure CO_2-water

mixture, the density increase $\Delta\rho \sim 8$ kg/m^3 at 30 bar, see, [9]). A denser phase above a less dense phase initiates convective currents that enhance the dissolution rate, thus accelerating dissolution of CO_2 in the aqueous phase. The initial stage of natural convection in a saturated porous layer with a denser fluid on top of a lighter fluid has been extensively studied by means of a linear stability analysis, numerical simulations and the energy method ([6, 10-25]).

Experimental work can be categorized in two fields: visualization of fingers and quantification of the dissolution rate. Visualization experiments are designed to show the unstable flow when water saturated with CO_2 overlays a column of carbon dioxide free water (or brine) and to visualize the formation, initiation, and development of fingers. Okhotsimskiis et al., [26] visualized the convective currents in a binary CO_2-water system and qualitatively evaluated the experimental results, based on Marangoni and free (or natural) convection effects in the absence of a porous medium. Kneafsey and Pruess [27] used a pH indicator to visualize the formation of fingers due to the dissolution of CO_2 in pure water and brine in a Hele-Shaw cell with a permeability around 40,000 Darcy. Khosrokhavar et al. in a previous paper [14] applied the Schlieren method to show the effect of gravity induced fingers in a high pressure cell equipped with windows, in which subcritical or supercritical CO_2 is brought above a liquid water, brine, or oil layer at constant temperature, and compared the results with numerical computations. Neufeld et al., [28] presented a new analogue fluid system that reproduces the convective behavior of an CO_2-enriched brine. Laboratory experiments and high-resolution numerical simulations illustrate that the convective flux scales with the Rayleigh number to the 4/5 power, in contrast with a classical linear relationship. MacMinn et al., [29] studied the spreading and convective dissolution of carbon dioxide in vertically confined, horizontal aquifers. They conducted the laboratory experiments with analog fluids (water and a mixture of methanol and ethylene glycol) and compared the experimental results with simple theoretical models. Their experiments show that the spreading of the buoyant current is characterized by a parabola-like advance and retreat of its leading edge.

Farajzadeh et al., [30, 31] performed a set of pressure decay experiments to quantify the enhanced mass transfer of CO_2 in water, surfactant solutions, and oil. They showed that the pressure decay results do not match the solution of the Fick's second law. Nazari Moghaddam et al., [32] carried out pressure decay experiments in two PVT-cells to investigate the CO_2 dissolution in bulk water and a second set of experiments to study CO_2 dissolution in water saturated porous media with a permeability range of 121 to 2546 Darcy. Based on the experimental results, they calculate a pseudo-dissolution coefficient for CO_2 in water. More recently Moortgat et al., [33] numerically investigated CO_2 injection in vertical and horizontal cores. They showed that an analysis of CO_2

core flooding may provide important parameters for field-scale problems. Benson et al., [34] mention the main criteria for successful large-scale geologic CO_2 storage. They showed that optimizing the design and operation of injection projects will depend on knowledge of the injectivity, trapping capacity, the distribution of CO_2 in the subsurface and the overall areal extent of the subsurface plume.

The objective of this chapter is to design and construct an experimental set-up, with which the effect of salinity and pressure on the rate of mass transfer in aquifer storage of carbon dioxide can be elucidated.

The structure of the chapter is as follows: first we describe our experimental set-up and briefly explain the procedure. Then we investigate the onset and development of natural convection and quantify the mass transfer rate in our experimental configuration and interpret the results. Finally we end the chapter with some concluding remarks.

3.2. EXPERIMENTAL SET-UP

The experimental set up, shown in Figure 3-1, consists of a stainless steel vessel with an inside diameter of 8.43 cm and a height of 22.7 cm (see Figure 3-2). It is positioned vertically in an oven with a temperature control accuracy of 0.02 K. The top opening of the vessel is connected to a pressure transducer with an accuracy of 0.01 bar. The pressure is recorded by data acquisition software every 5 seconds.

The experimental procedure is as follows: First, the vessel is filled with known mass of sand with a known particle size distribution. 90% percent of the Cylinder is filled with sand pack to ensure that the sand particles are completely packed, the vessel is shaken by hammering the wall for 60 minutes. The vessel is mounted in the oven and filled with helium at 8 bar. We use the helium detector to check the connections for the leakage. Afterward we pressurized the cylinder by He to 100 bar. Then we record the helium pressure for 24 hours. If there is no noticeable pressure decline (no leakage) we flush the sand pack with CO_2 4-6 times. Then, we connect the set up to a vacuum pump for 24 hours. The vacuuming step is necessary to prevent the formation of bubbles of gas in the water saturated zone .Then a known mass of water is injected through valve 5 to saturate the sand pack. The vacuum in the vessel is enough to suck water inside. Then we bring CO_2 into the ISCO PUMP at 60 and 100 bar. Both the ISCO pump and cylinder containing the sandpack are in the oven to keep the temperature constant. We leave the set-up in the oven for 24 hours to reach thermal equilibrium at a constant temperature of 35°C. When the system reached

thermal equilibrium, we start the data acquisition system and inject CO_2 at constant pressure into the vessel through valve 3.

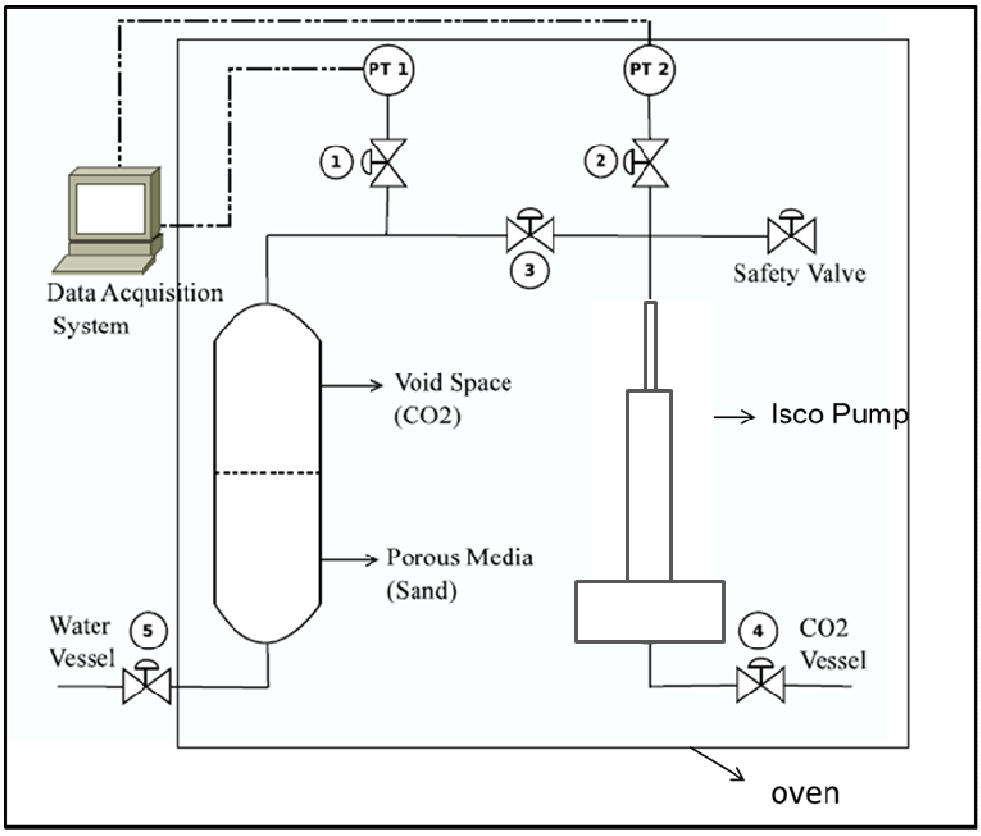

Figure 3-1: Schematic drawing of the experimental set-up. Mention purpose of all valves

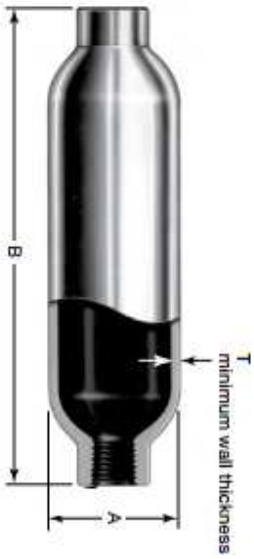

Figure 3-2: Cylindrical high pressure cell. (A=88.9 mm, B(Height)=227mm and T=4.6mm)

The position of the piston, which is adjusted to keep the pressure constant, is measured as a function of time. From this the consumed volume history is determined and recorded every 5 seconds for about 40 hours.

3.3. EXPERIMENTAL RESULTS & DISCUSSION

We carried out five experiments all at a constant temperature and pressure. Figure **3-3** shows the five experimental results after 40 hours at temperatures, pressures and salinities (T, P, c) = (308 K, 100 bar, 10 w/w%), (308 K, 100 bar, 5 w/w%), (308 K, 100 bar, 2.5 w/w%), (308 K, 100 bar, 0 w/w%) and (308 K, 60 bar, 0 w/w%). It illustrates that increasing salinity decreases the consumed CO_2.

Figure **3-3**-a to Figure **3-3**-e show the consumed volume versus time for the five experiments, respectively. To show the importance of enhanced dissolution of CO_2, the results are compared to the pure diffusion model. Initially, the consumed volume is zero. By dissolving CO_2 in water (or the NaCl solution), the number of moles of CO_2 in the sand pack increases and consequently the volume measured in the ISCO pump decreases. The consumed volume is controlled by the rate of mass transfer of CO_2 into water (NaCl solution), which is diffusion controlled at the start of the process. However, experimental curve deviates from the pure diffusion curve predicted by a diffusion model and has a slope bigger than $\sqrt{t}$. As the slope is larger than 0.5 it shows that in all cases we have enhanced diffusion. The deviation from pure diffusion, if it occurs, starts before 30 seconds and would be smaller than known onset times in porous media (see Table 3-2).

Figure **3-3**a presents the result for a 10 w/w% NaCl solution at 100 bar and 35°C. At this salt concentration there is a smaller density difference between the carbon dioxide solution and the pure brine solution [35] and consequently the Rayleigh number is relatively low. The experiment starts after admitting carbon dioxide into the cell at the required pressure. At 5000 seconds, 2.50 cm^3 of carbon dioxide was consumed. After that the slope of experimental curve has changed. From 5000 to 140000 seconds, another 7.50 cm^3 of carbon dioxide dissolved. In comparison to the theoretical diffusion model, the number of moles dissolved in the high pressure cell, i.e., the experimental set-up is about five times bigger. In the early stages of the experiment the consumption rate of carbon dioxide is faster than in the later stages.

Figure **3-3**b shows the experimental curve for a 5 w/w% NaCl solution at 100 bar and 35°C. Following Eq. (3-1) we expect that more carbon dioxide is dissolved than for the 10w/w% solution. Table 3-2 shows that the Rayleigh number decreases for increasing salt concentrations. Also the Henry's constant is smaller for decreasing salinity. The solubility of CO_2 in 5 w/w% NaCl

solution is less than in pure water, but larger than in the 10 w/w% case, leading to smaller and larger $\Delta\rho$ values respectively. From t=0 to t=5000 seconds 2.75 cm^3 of carbon dioxide has been dissolved. As time proceeds, the slope of the curve is increasing. Between t=5000 and t=55000 about another 6.35 cm^3 of carbon dioxide dissolved and after that the slope has changed again.

Figure **3-3**c shows the result for the system of a 2.5 w/w% NaCl solution at 100 bar and 35°C. We observe that the deviation from diffusion model appears in early stages; however, as time elapses the slope of the curve increases. Figure **3-3**c shows that at t=5000 seconds, the consumed volume was about 3.15 cm^3. From t=5000 to t=100000 seconds the volume dissolved has increased to 12.80 cc and after that till the end of experiment it fluctuates to reach its end value.

Figure **3-3**d demonstrates the experimental result for the CO_2 – water system at 100 bar and 35°C. From t=0 to t=6000 seconds the experiment run with lower slope in comparison to late stages. A more or less similar behavior is observed for subcritical critical CO_2 - water system (Figure **3-3**-e).

Figure **3-3**e illustrates the experimental pattern for the CO_2–water system at 60 bar and 35°C. After bringing CO_2 to the cell, the system exhibits similar behavior in comparison to other experimental results however the instability occurred later. After 5000 seconds around 14cm3 of carbon dioxide dissolved. From t=3000 to t=140000 seconds the slope of experiment has smoothly changed. In comparison with supercritical experiments, at 60 bar the consumed volume is larger. To investigate late time behavior in our experimental approach, we have plotted consumption rate of volume in experimental set-up versus time. The results are shown in Figure 3-4-e. One observes more or less behavior for all experiments in late stages. At 100 bar, in all cases the fast decrease in rate can be seen, after hitting the bottom of the cell, it starts to increase and fluctuate to reach a plateau. At 60 bar the same process occurred in later times. In our experimental results, the surface tension increases [36]. It could be a possible reason to have both mechanisms (natural convection and Marangoni effect) in our study [37]. We leave more investigation for future work.

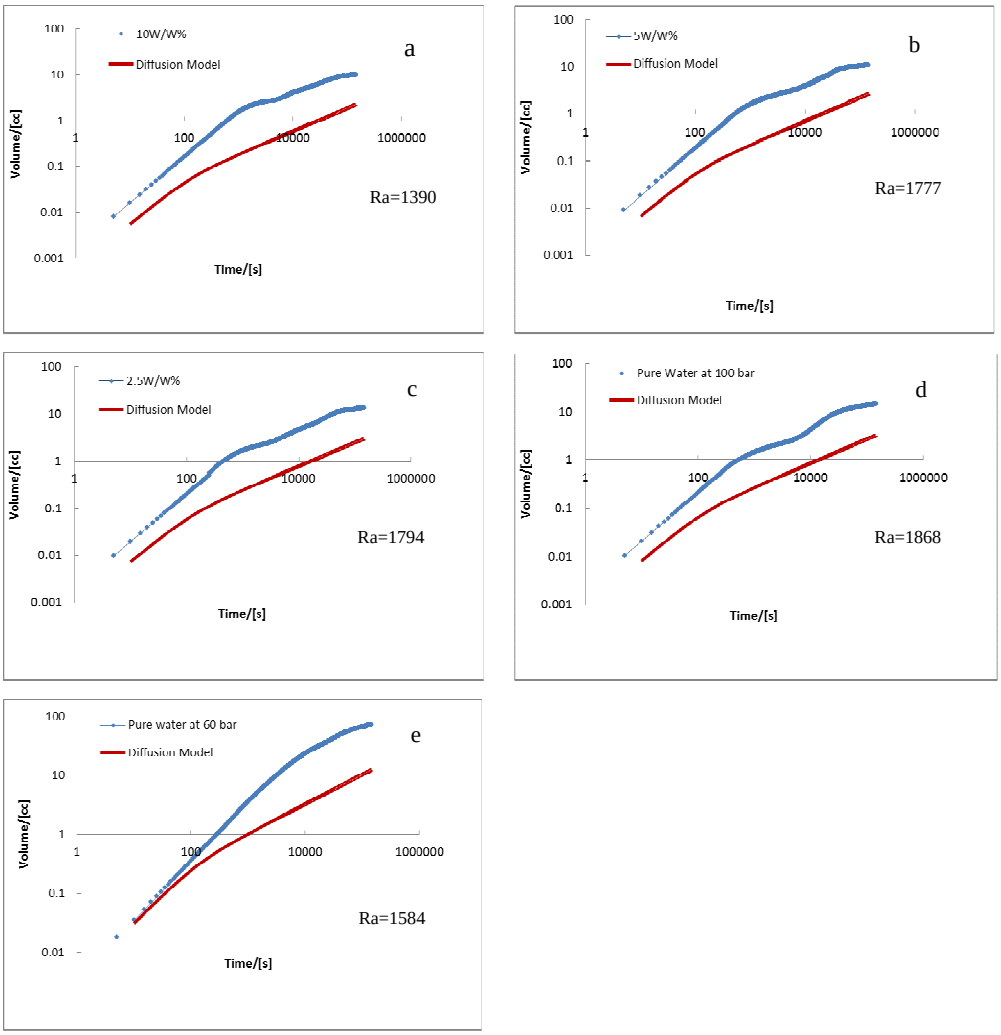

Figure 3-3: Experimental results at 100 bar and 308k. It demonstrates four experiments at different salinity from 0 wt% to 10 wt%. By increasing the salinity, the amount of CO_2 dissolved in the brine decreased. Experimental result at 60 bar and 308K, it shows at constant pressure, about 72 cc CO_2 was consumed

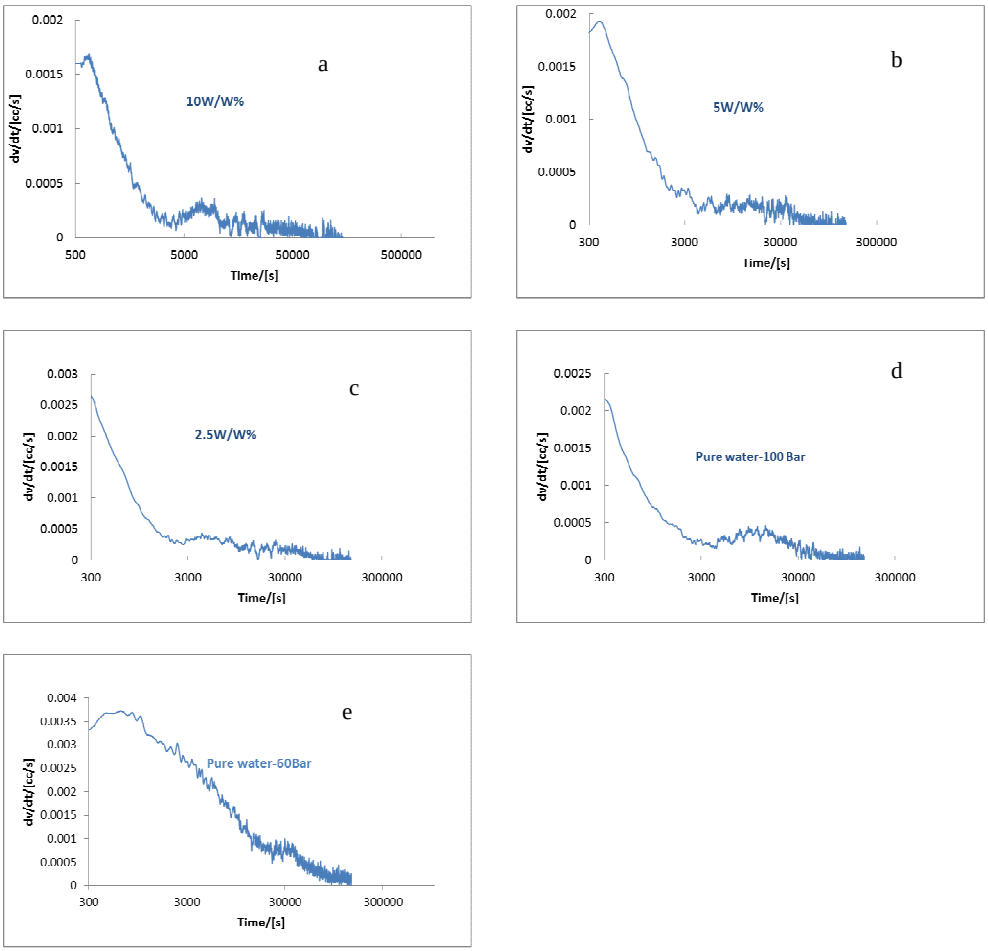

Figure 3-4: The consumption rate of volume is plotted versus time.

3.4. DATA ANALYSIS

We carried out five experiments all at a constant temperature and pressure. To illustrate the importance of the enhanced dissolution of CO_2, the results are compared to results computed with a diffusion model.

By dissolution, CO_2 starts to diffuse into the sand pack, which is saturated with water (or NaCl solution) the part of the moles of CO_2 is transferred from the ISCO pump to the sand pack. The amount of carbon dioxide dissolved in the aqueous phase in the sand pack is controlled by the rate of mass transfer of CO_2. The mass transfer is initially diffusion controlled. However, after

some time the experimental curve deviates from the diffusion model. An accurate experimental measurement of the flux for the actual CO_2-brine system is difficult. For porous media, a large number of numerical studies [12, 18] show that the onset time of convection is inversely proportional to the Rayleigh number, which can be expressed as,

$$t_0 = c_0 Ra^{-1} = c_0 \left(\frac{\varphi \mu \sqrt{D}}{kg\Delta\rho} \right)^2 \qquad (3.1)$$

where μ [Pa.s] is the viscosity of the aqueous phase, φ [-] is the porosity of the porous medium, D [m^2/s] is the binary diffusion coefficient of carbon dioxide in the brine saturated porous medium, g [9.81 m/s^2] is the acceleration due to gravity, k [m^2] is the permeability of the porous medium, and $\Delta\rho$ [kg/m^3] is the difference between the density of pure solvent and the solvent saturated with the solute. Moreover, c_0 is a constant value and it covers a range between 55 and 4500. Many investigations are applied to quantify the onset time. Our experimental work is summarized in Table 3-1.

Table 3-1: The summary of experimental work.

	p[bar]	*T*[C°]	Salinity	*k*	*φ*	*μ* [38]	$\Delta\rho_{[35]}$	*D [39]*	$K_{H[Pa.m^3/mol]}$	*Ra*
Experiment 1	100	35	10W/W%	59×10^{-12}	0.40	9.34×10^{-4}	7.32	1.30×10^{-9}	1250	1390
Experiment 2	100	35	5W/W%	59×10^{-12}	0.40	8.56×10^{-4}	9.86	1.50×10^{-9}	1050	1777
Experiment 3	100	35	2.5W/W%	59×10^{-12}	0.40	8.25×10^{-4}	11.32	1.75×10^{-9}	900	1794
Experiment 4	100	35	0.0W/W%	59×10^{-12}	0.40	8.00×10^{-4}	12.91	2×10^{-9}	750	1868
Experiment 5	60	35	0.0W/W%	59×10^{-12}	0.40	7.99×10^{-4}	10.97	2×10^{-9}	600	1584

The experimental onset times are presented in Table 3-2 and are compared to the theoretical relations, derived by Riaz et al. [18], Ennis-King [12], Hassanzadeh et al. [40] , Xu et al. [41], Pau et al. [42] and Meulenbroek et al [21].

Table 3-2: The experimental onset times are compared with different theoretical models.

	Xu et al [41]	Ennis-King et al [12]	Riaz et al [18]	Pau et al [42]	Hassanzadeh et al [40]	Meulenbroek et al[21]	Experimental onset time/[sec] (this chapter)
Experiment 1	761	789	3695	18126-37152	5061	556	~early stages
Experiment 2	405	420	1966	9646-19772	2693	296	~ early stages
Experiment 3	333	345	1618	7939-19272	2216	243	~ early stages
Experiment 4	275	285	1337	6559-13444	1831	201	~ early stages
Experiment 5	382	396	1855	9101-18654	2541	279	~ early stages

In order to quantify the time evolution of the flux, we describe the late time behavior when the plumes have not yet reached the bottom boundary. This period begins in the neighborhood of the start of nonlinear behavior of mass transfer rate versus time. We follow [43] to characterize the mass transfer rate of CO_2 dissolved in aqueous phase as a function of the Rayleigh number. Comparison between our result and other scientific work has been summarized in Table 3-3.

Table 3-3: Comparison between Current experimental result and other scientific works

	Backhhaus et al [44]	Slim et al[45]	Neufeld et al[28]	Nield and Bejan [46]	Farajzadeh et al[47]	Hidalgo et al[48]	Our experimental result
Experimental And numerical works to find a relation between Rayleigh Number and mas transfer rate.	$Sh \sim Ra^{0.75}$	$Sh \sim Ra$	$Sh \sim Ra^{0.83}$	$Sh \sim Ra$	$dm/dt \sim Ra^{0.832}$	$Sh \sim Ra$	$dm/dt \sim Ra^{0.8283}$

3.5. CONCLUSIONS

- Dissolution of CO_2 in an aqueous phase forms a mixture that is denser than the carbon dioxide free water or brine. This causes a local density increase, which induces natural convection currents (gravity fingers) when gaseous carbon dioxide is brought above the liquid phase. This enhances the rate of mixing of CO_2 in the liquid phase.
- We designed and built a cylindrical high pressure cell in which gravity induced fingers (playing a major role in the enhanced mixing process) could have occurred, e.g., by mounting the cylinder horizontally and filling the 90% with sand pack (k=59 Darcy and

porosity =40%) and then saturating with water or brine and the top with gaseous or sub-supercritical carbon dioxide at constant pressure.

- The experiments show that natural convection currents are weakest in highly concentrated brine and strongest in pure water.
- The experiments show that CO_2 consumption is bigger in subcritical than supercritical condition.
- The experimental results propose a semi linear relation between mass transfer rate and Rayleigh number.
- To our knowledge, this is the first time that such of experiments are carried out at constant pressure injection in the lab scale with considering the effect of salinities.

3.6. NOMENCLATURE

C = concentration (mol/m^3)

C_g = concentration (mol/m^3)

D = molecular diffusion coefficient, (m^2/ s)

D_g= molecular diffusion coefficient in gas phase, (m^2/ s)

k = permeability, mD

u=velocity (m/s)

P=pressure (bar)

t=time

ρ = density (kg/m^3)

μ = viscosity of the solvent (kg.m.s)

g = acceleration due to gravity (kg/m^2)

Ra= Rayleigh number

3.7. REFERENCES

1. International Energy Agency, *World Energy Outlook 2012*, 2012, OECD Publishing.
2. Iijima, M., T. Nagayasu, T. Kamijyo, and S. Nakatani, *MHI's Energy Efficient Flue Gas CO_2 Capture Technology and Large Scale CCS Demonstration Test at Coal-fired Power Plants in USA*. Mitsubishi Heavy Industries Technical Review, 2011. **48**(1): p. 26.
3. Tao, Z. and A. Clarens, *Estimating the Carbon Sequestration Capacity of Shale Formations Using Methane Production Rates*. Environ Sci Technol, 2013. **47**(19): p. 11318-11325.
4. Eftekhari, A.A., H. Van Der Kooi, and H. Bruining, *Exergy analysis of underground coal gasification with simultaneous storage of carbon dioxide*. Energy, 2012. **45**(1): p. 729-745.
5. Michael, K., A. Golab, V. Shulakova, J. Ennis-King, G. Allinson, S. Sharma, and T. Aiken, *Geological storage of CO_2 in saline aquifers—A review of the experience from existing storage operations*. International Journal of Greenhouse Gas Control, 2010. **4**(4): p. 659-667.
6. Class, H., A. Ebigbo, R. Helmig, H.K. Dahle, J.M. Nordbotten, M.A. Celia, P. Audigane, M. Darcis, J. Ennis-King, and Y. Fan, *A benchmark study on problems related to CO_2 storage in geologic formations*. Computational Geosciences, 2009. **13**(4): p. 409-434.
7. Celia, M.A., S. Bachu, J.M. Nordbotten, S.E. Gasda, and H.K. Dahle. *Quantitative estimation of CO_2 leakage from geological storage: Analytical models, numerical models and data needs*. in *Proceedings of 7th International Conference on Greenhouse Gas Control Technologies.(GHGT-7)*. 2004.
8. Van der Meer, L., *Investigations regarding the storage of carbon dioxide in aquifers in the Netherlands*. Energy Conversion and Management, 1992. **33**(5): p. 611-618.
9. Gmelin, L., *Gmelin Handbuch der anorganischen Chemie, 8. Auflage. Kohlenstoff, Teil C3, Verbindungen*, 1973, ISBN 3-527-81419-1.
10. Bachu, S., W. Gunter, and E. Perkins, *Aquifer disposal of CO_2: Hydrodynamic and mineral trapping*. Energy Conversion and Management, 1994. **35**(4): p. 269-279.
11. Elder, J., *The unstable thermal interface*. J. Fluid Mech, 1968. **32**(1): p. 69-96.
12. Ennis-King, J., I. Preston, and L. Paterson, *Onset of convection in anisotropic porous media subject to a rapid change in boundary conditions*. Physics of Fluids, 2005. **17**(8): p. 084107-084107-15.
13. Foster, T.D., *Onset of convection in a layer of fluid cooled from above*. Physics of Fluids, 1965. **8**: p. 1770.
14. Gasda, S.E., Numerical models for evaluating CO_2 storage in deep saline aquifers: Leaky wells and large-scale geological features, . Ph.D. Thesis. Available at http://arks.princeton.edu/ark:/88435/dsp01j098zb09n., 2010.
15. Nordbotten, J.M. and M.A. Celia, *Geological Storage of CO_2 : Modeling Approaches for Large-Scale Simulation*2011: Wiley. com.
16. Nordbotten, J.M., M.A. Celia, and S. Bachu, *Injection and storage of CO_2 in deep saline aquifers: Analytical solution for CO_2 plume evolution during injection*. Transport in porous media, 2005. **58**(3): p. 339-360.
17. Ranganathan, P., R. Farajzadeh, H. Bruining, and P.L. Zitha, *Numerical simulation of natural convection in heterogeneous porous media for CO_2 geological storage*. Transport in porous media, 2012. **95**(1): p. 25-54.
18. Riaz, A., M. Hesse, H. Tchelepi, and F. Orr, *Onset of convection in a gravitationally unstable diffusive boundary layer in porous media*. Journal of Fluid Mechanics, 2006. **548**: p. 87-111.
19. Walker, K.L. and G.M. Homsy, *Convection in a porous cavity*. J. Fluid Mech, 1978. **87**(Part 3): p. 449-474.
20. Van Duijn, C., G. Pieters, and P. Raats, *Steady flows in unsaturated soils are stable*. Transport in porous media, 2004. **57**(2): p. 215-244.
21. Meulenbroek, B., R. Farajzadeh, and H. Bruining, *The effect of interface movement and viscosity variation on the stability of a diffusive interface between aqueous and gaseous CO_2*. Physics of Fluids (1994-present), 2013. **25**(7): p. 074103.
22. Myint, P.C. and A. Firoozabadi, *Onset of convection with fluid compressibility and interface movement*. Physics of Fluids, 2013. **25**: p. 094105.
23. Pruess, K., T. Xu, J. Apps, and J. Garcia, *Numerical modeling of aquifer disposal of CO_2*. Spe Journal, 2003. **8**(1): p. 49-60.
24. Dentz, M. and D.M. Tartakovsky, *Abrupt-interface solution for carbon dioxide injection into porous media*. Transport in porous media, 2009. **79**(1): p. 15-27.
25. Moortgat, J., A. Firoozabadi, and M. Moravvej Farshi. *A new approach to compositional modeling of CO2 injection in fractured media compared to experimental data*. in *SPE Annual Technical Conference and Exhibition*. 2009.

26. Okhotsimskii, A. and M. Hozawa, *Schlieren visualization of natural convection in binary gas–liquid systems*. Chemical engineering science, 1998. **53**(14): p. 2547-2573.
27. Kneafsey, T.J. and K. Pruess, *Laboratory flow experiments for visualizing carbon dioxide-induced, density-driven brine convection*. Transport in porous media, 2010. **82**(1): p. 123-139.
28. Neufeld, J.A., M.A. Hesse, A. Riaz, M.A. Hallworth, H.A. Tchelepi, and H.E. Huppert, *Convective dissolution of carbon dioxide in saline aquifers*. Geophysical research letters, 2010. **37**(22).
29. MacMinn, C.W., J.A. Neufeld, M.A. Hesse, and H.E. Huppert, *Spreading and convective dissolution of carbon dioxide in vertically confined, horizontal aquifers*. Water Resources Research, 2012. **48**(11).
30. Farajzadeh, R., A. Barati, H.A. Delil, J. Bruining, and P.L. Zitha, *Mass transfer of CO_2 into water and surfactant solutions*. Petroleum Science and Technology, 2007. **25**(12): p. 1493-1511.
31. Farajzadeh, R., P.L. Zitha, and J. Bruining, *Enhanced mass transfer of CO_2 into water: experiment and modeling*. Industrial & Engineering Chemistry Research, 2009. **48**(13): p. 6423-6431.
32. Moghaddam, R.N., B. Rostami, P. Pourafshary, and Y. Fallahzadeh, *Quantification of density-driven natural convection for dissolution mechanism in CO_2 sequestration*. Transport in porous media, 2012. **92**(2): p. 439-456.
33. Moortgat, J., A. Firoozabadi, Z. Li, and R.r. Esp? sito, *CO2 Injection in Vertical and Horizontal Cores: Measurements and Numerical Simulation*. Spe Journal, 2013. **18**(2): p. 331-344.
34. Benson, S.M., F. Hingerl, B. Li, R. Pini, H. Tchelepi, and L. Zuo, *Investigations in Geologic Carbon Sequestration: Multiphase Flow of CO_2 and Water in Reservoir Rocks*. 2013.
35. Duan, Z. and R. Sun, *An improved model calculating CO_2 solubility in pure water and aqueous NaCl solutions from 273 to 533 K and from 0 to 2000 bar*. Chemical geology, 2003. **193**(3): p. 257-271.
36. Li, X., E. Boek, G.C. Maitland, and J.M. Trusler, *Interfacial Tension of (Brines+ CO_2):(0.864 NaCl+ 0.136 KCl) at Temperatures between (298 and 448) K, Pressures between (2 and 50) MPa, and Total Molalities of (1 to 5) mol· kg−1*. Journal of Chemical & Engineering Data, 2012. **57**(4): p. 1078-1088.
37. Arendt, B., D. Dittmar, and R. Eggers, *Interaction of interfacial convection and mass transfer effects in the system CO_2–water*. International journal of heat and mass transfer, 2004. **47**(17): p. 3649-3657.
38. Bando, S., F. Takemura, M. Nishio, E. Hihara, and M. Akai, *Viscosity of aqueous NaCl solutions with dissolved CO_2 at (30 to 60) C and (10 to 20) MPa*. Journal of Chemical & Engineering Data, 2004. **49**(5): p. 1328-1332.
39. Sell, A., H. Fadaei, M. Kim, and D. Sinton, *Measurement of CO_2 Diffusivity for Carbon Sequestration: A Microfluidic Approach for Reservoir-Specific Analysis*. Environmental science & technology, 2012. **47**(1): p. 71-78.
40. Hassanzadeh, H., M. Pooladi-Darvish, and D.W. Keith, *Scaling behavior of convective mixing, with application to geological storage of CO_2*. AIChE journal, 2007. **53**(5): p. 1121-1131.
41. Xu, X., S. Chen, and D. Zhang, *Convective stability analysis of the long-term storage of carbon dioxide in deep saline aquifers*. Advances in water resources, 2006. **29**(3): p. 397-407.
42. Pau, G.S., J.B. Bell, K. Pruess, A.S. Almgren, M.J. Lijewski, and K. Zhang, *High-resolution simulation and characterization of density-driven flow in CO_2 storage in saline aquifers*. Advances in water resources, 2010. **33**(4): p. 443-455.
43. Farajzadeh, R., B. Meulenbroek, D. Daniel, A. Riaz, and J. Bruining, *An empirical theory for gravitationally unstable flow in porous media*. Computational Geosciences, 2013. **17**(3): p. 515-527.
44. Backhaus, S., K. Turitsyn, and R. Ecke, *Convective instability and mass transport of diffusion layers in a Hele-Shaw geometry*. Physical review letters, 2011. **106**(10): p. 104501.
45. Slim, A.C., M. Bandi, J.C. Miller, and L. Mahadevan, *Dissolution-driven convection in a Hele–Shaw cell*. Physics of Fluids (1994-present), 2013. **25**(2): p. 024101.
46. Nield, D.A. and A. Bejan, *Convection in porous media*2006: springer.
47. Farajzadeh, R., B. Meulenbroek, D. Daniel, A. Riaz, and J. Bruining, *An empirical theory for gravitationally unstable flow in porous media*. Computational Geosciences, 2013. **17**(3): p. 515-527.
48. Hidalgo, J.J., J. Fe, L. Cueto-Felgueroso, and R. Juanes, *Scaling of convective mixing in porous media*. Physical review letters, 2012. **109**(26): p. 264503.

Chapter 4

Sorption of CH_4 and CO_2 on Belgium Carboniferous Shale Using a Manometric Set-up

ABSTRACT

Shale gas resources are globally abundant and the development of these resources can increase CH_4 production. It is of interest to study the possibility of enhancing CH_4 production by CO_2 injection (Enhanced Gas Recovery- EGR). Some studies indicate that, in shale, five molecules of CO_2 can be stored for every molecule of CH_4 produced. The technical feasibility of Enhanced Gas Recovery (EGR) needs to be investigated in more detail. The amount of extracted natural gas from shale has increased rapidly over the past decade. A typical shale gas reservoir combines an organic-rich deposition with extremely low matrix permeability. One important parameter in assessing the technical viability of (enhanced) production of shale gas is the sorption capacity. Our focus is on the sorption of CH_4 and CO_2. Therefore we have chosen to use the manometric method to measure the excess sorption isotherms of CO_2 at 318 K and of CH_4 at 308, 318 and 336 K and at pressures up to 105 bar on Belgium dry black shale from a depth of 745 m. The shale was obtained from a former coal mine in Zolder in the Campina Basin (North Belgium), which contains Westphalian coal and coal associated sediments of Northwest

European origin. We derive the equations for excess sorption in the manometric set-up. Only a few measurements have been reported in the literature for high-pressure gas sorption on shales, and interest is largely focused on shales occurring outside Europe. The excess sorption isotherm shows an initial increase to a maximum value of 0.175 ± 0.004 mmol/gram for CO_2 and then starts to decrease until it becomes zero at 82 bar and subsequently the excess sorption becomes negative. Similar behaviour was also observed for other shales and coal reported in the literature. The experiments on CH_4 show, as expected, decreasing sorption for increasing temperature. We apply an error analysis based on Monte-Carlo simulation. It shows that the error is increasing with increasing pressure, but that the manometric set-up can be used to determine the sorption capacity of CO_2 and CH_4 on the black shale with sufficient accuracy.

KEYWORDS: *CO_2, CH_4, Sorption, Shale, Monte Carlo simulation*

Published in: International Journal of Coal Geology volumes 128–129, 1 August 2014, Pages 153–161

4.1. INTRODUCTION

Shale gas resources are globally abundant and the development of these resources can increase the CH_4 production, a fossil fuel with potentially minimal carbon footprint if sound operational practices are adhered and the latest technological advances are implemented [1, 2]. A typical shale gas reservoir combines an organic-rich deposition with extremely low matrix permeability [3]. The production of natural gas has been greatly amplified in the United States in recent years due to development of shale gas plays and the U.S. is now the largest producer of natural gas in the world [4]. Canada and the United States, the two countries that have made most progress in the extraction of shale gas, are producing 25% of the global natural gas [4]. Advanced technologies for shale gas extraction will increase shale gas production in the United States and Canada. It is expected that shale gas will account for 49% of the total gas production in the United States by 2035, up from 23% in 2010. In that case both countries will drill thousands of wells in next decade if the gas shale development becomes increasingly economical [5].

Estimates of technically recoverable shale gas in the United States differ but are generally considered in excess of about 660 trillion (10^{12}) cubic feet. In Canada there is estimated a large potential of gas in place in shale formations (one quadrillion (10^{15}) cubic feet) [6]. China has 1,115 trillion cubic feet of technically recoverable shale gas [7]. China has the largest estimated shale gas resources and Argentina, estimated to have 802 trillion cubic feet of technically recoverable shale gas, has the second largest global shale gas resources. Eastern Europe is estimated to have 424 trillion cubic feet of shale gas [5]. There have been estimates that Poland, for example, would provide domestic natural gas for 300 years at the country's current level of use if shale gas reserves were exploited [5]. Recently the most intense shale gas exploration occurred in Poland where over 42 wells have been drilled [8]. According to McGlade and Sorrell [9], Poland and France are expected to have the largest shale gas resources in the European countries. Due to several reasons , the development of gas shale has not been successful in European countries [10]. Key hindrances include: uncertainty in the estimation of technically recoverable gas shale resources, the requirement of large number of wells in dense populated areas, lack of field data, environmental risk, lack of infrastructure, operational cost, water source and land access. However, technological developments, e.g., using CO_2 for hydraulic fracturing [11, 12], may solve some of the technological issues.

The Energy Resources Conservation Board/Alberta Geological Survey (ERCB/AGS) initiated a project in 2007 to evaluate shale gas resources in Alberta and determine the quantity and spatial extent of these resources. In this project, Beaton et al., [13] measured CH_4 sorption isotherms on

several shale samples. They showed that the data could be fitted by a Langmuir isotherm. The samples originating from depths between 2000-3000 m in Canada at in-situ temperatures between 60-80° C show maximum sorption capacities of CH_4 between 11-26 scf per ton ~(0.012-0.029 mmol/g), which has to be compared to 800 scf/ton found for coal Batistutta et al., [14]. Indeed it is mentioned by Hall et al., [15] that CH_4 sorption in shales is about 10-30 times lower than the sorption in coals. Weniger et al., [16] studied gas sorption behavior of CH_4 and CO_2 in coals and shales in the Prana Basin, Brazil. They show a correlation between the total organic carbon (TOC) and the sorption capacity. They find that for the sorbed CH_4, $[CH_4]_{ads}$ = 0.009 TOC (%) + 0.026 (mol/ kg), and for sorbed CO_2, $[CO_2]_{ads}$ = 0.008 TOC (%) + 0.183 (mol/kg). As a result the sorption capacity on mineral matter for CO_2 is much stronger. Ross and Bustin [17] investigated the effect of shale composition, pore structure and CH_4 sorption for potential shale gas reservoirs in the Western Canadian Sedimentary Basin (WCSB). They also showed that CH_4 sorption on dried and moisture equilibrated shales increases with the total organic carbon (TOC) content. Yuan et al., [18] performed an experimental and modelling study of CH_4 sorption and diffusion in shale. They showed gas sorption and diffusivity were significantly reduced in moist samples, showing that water reduces the gas storage capacity and the transport rate in shale on the laboratory scale. Gasparik et al., [19] carried out a set of experiments to investigate high-pressure sorption of CH_4 on black shales in the Netherlands. They indicate that, TOC does not affect the sorption capacity. They also present a simple and efficient experimental approach to determine the effect of temperature on high-pressure CH_4 sorption in moist organic-rich shales [20].

Concerns about rising concentrations of CO_2 in the atmosphere have led to many experimental [16, 21-25] and numerical studies [26-32] aimed to store anthropogenic CO_2 in the geological formations [33-35]. Methods proposed to reduce CO_2 emission include its storage in saline aquifers, depleted gas and oil reservoirs or unminable coal seams [14, 21, 36, 37]. A roadmap and criteria for the site selection for CO_2 sequestration in geological media has been presented in [36]. Bachu [36] mentions as most important steps: selecting appropriate sites for storage that are sufficiently close to sources of CO_2 and their suitability for long time storage. Busch et al., [22, 38] investigated gas sorption behavior in Muderong shales (Australia) and also studied the effect of physical sorption and chemical reactions while CO_2 is injected in shaly caprock. For their shale samples it was observed that the sorption capacity of CO_2 decreases with decreasing moisture content. They also reported negative excess sorption for dry shale beyond 95 bar. Kang et al., [24] measured the total CO_2 storage capacity of organic-rich shales at supercritical conditions as a function of pore pressure by considering the pore compressibility and sorption effects. The results show that kerogen, the organic part of the shale, enhances CO_2 sorption on shales.

Most work on sequestration of CO_2 in depleted gas reservoirs is based on storage. Some studies, however, have indicated that CO_2 injection can also be used as a method of enhancing shale gas recovery [39, 40]. The injection of CO_2 may increase the rate and the volume of natural gas recovered from a reservoir [34] as CO_2 can be trapped in gas shales due to occupation of sorption sites that were originally filled with CH_4. Shale gas formations include organic materials that may store large amounts of sorbed natural gas, from 20% to 80% of the original-gas-in-place. Recent work demonstrates that five CO_2 molecules could displace one CH_4 molecule [41]. This means that by storing CO_2 in shale gas formation, chances for gas recovery may increase. On the other hand, we can approximately store 12 kg of CO_2 and produce 1 kg of CH_4. 1 kg of CH_4 can produce 55 Mega joules energy. To store 1 kg of CO_2, 1 Mega joule is consumed on compression costs. It illustrates that in the storing part, we obtain 55 Mega joules energy [42] while we spend 12 Mega joules energy for compression. It shows the benefit of EGR prospect. If we take into account the consumption energy in separation of CO_2 in Carbon Capture and Storage (CCS) projects, we can say that there still is a gain in terms of energy even considering storage of CO_2 [43]. Godec et al., [44] showed that by injecting CO_2 in the Marcellus gas shale formation in the Eastern United States, 7% enhanced gas production can be realized. They theoretically demonstrated that CO_2 can be sequestered with 100% CH_4 in place in both free and sorbed phase.

There are only a few experimental papers dealing with European shales e.g., [19, 38] . Most European researchers used samples from other parts of the world [16, 38]. It is important to also make an inventory of shales occurring in Europe and this chapter wants to contribute to a European data base.

We have chosen to measure the sorption isotherms of CO_2 at 318 K and CH_4 at 308, 318 and 336 K at pressures up to 105 bar by using the manometric method [45] on Belgium dry black shale from a depth of 745 m, which consists of Illite, Kaolinite, Chlorite, Quartz and organic matter. It was obtained from the former coal mine in Zolder in the Campina Basin (North Belgium), which contains Westphalian coal and coal associated sediments of Northwest European origin.

The chosen temperature and pressure range is representative for in situ conditions. In Europe suitable conditions for CO_2 storage are at depths above 500 meters, with correspondingly high reservoir pressures and temperatures (308-338 K, 60-150 bar), [14] .

The chapter is organized as follows: first we describe the experimental set-up and materials. Then we give the experimental procedure and error analysis. We continue the chapter with a results and discussion section. We confirm that an accurate void volume determination is essential for the accurate measurement of excess sorption. We end with some conclusions.

4.2. EXPERIMENTAL METHOOD

The manometric method for determining sorption capacities uses the principle of mass balance. A reference cell (Figure **4-1**) is filled with a given amount of gas at a pressure P. After opening a valve mounted in a connecting tube between the reference cell and the sample cell, the pressure in both cells reaches an equilibrium pressure. The excess sorption measurement requires, apart from the equilibrium pressure, the determination of the void volume excluding the sample volume. The void volume measurement is based on a stepwise introduction of Helium in the reference cell and subsequently allowing Helium to expand in the sample cell. Using the pressure before and after expansion and using an equation of state (EOS) for Helium Mc-Carthy and Arp., [46] we can determine the void volume because the Helium sorption on the sample is considered to be negligible. We repeat the steps thus increasing the pressure for reasons of validating the void volume determination procedure. Ross and Bustin., [47] investigated the impact of an accurate void volume value on the determination of sorption capacities in microporous shale gas reservoirs. They suggest that Helium due to its small size overestimates the void volume accessible to CO_2. Therefore the void volume measurement by Helium can lead to an apparent negative excess sorption measurement.

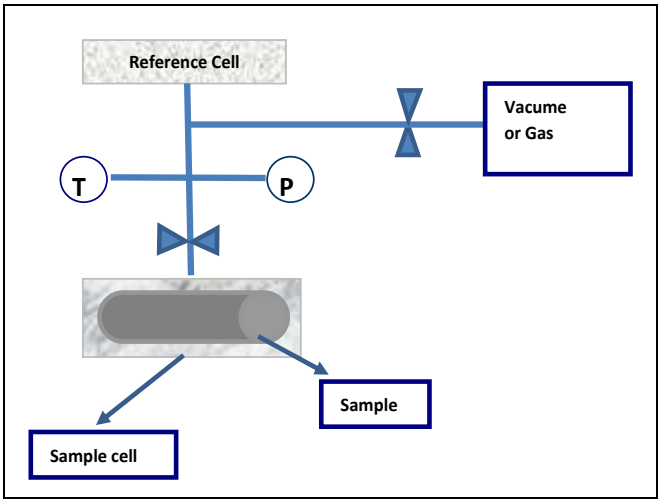

Figure 4-1: Drawing of manometric set-up.

The procedure used here to obtain the excess sorption of CO_2 and CH_4 follows the same procedure as used for the void volume determination with Helium, except that the sorption CO_2 and CH_4 is not negligible. Using the known void volume it is now possible to determine the excess sorption as is explained in more detail in the section “Data Analysis”. We use the term excess sorption for the

data m_{ads}^{N} obtained from Eqs. (1) and (2), which disregard the change in void volume due to the presence of sorbed molecules, swelling or other possibilities.

4.3. APPARATUS

The manometric set-up is described in detail in previous papers [14, 45], but is also described here for reasons of easy reference. The full flow scheme around the manometric set-up is shown in Figure **4-2** and consists of a sample cell A and a reference cell B. The reference cell B consists of tubing with a total volume of 3.524×10^{-6} m^3. Two similar sample cells are used in our experiments; a second sample cell can be prepared while the experiment with the first sample cell is running. The volumes of the two sample cells are 78.33×10^{-6} m^3 and 75.90×10^{-6} m^3. A Paroscientific pressure sensor monitors the pressure continuously. Its precision and accuracy are reported by the manufacturer as 0.1kPa and 1kPa in the temperature range of interest. However, our instrument was calibrated in 2012 by the manufacturer to remove any systematic error. The PT100 temperature sensor monitors the temperature continuously. Its precision and accuracy are reported by the manufacturer as 20mK and 1mK respectively. Valves (1, 2, 3, and 4) with low leakage characteristics are used in the set-up. However, they can only operate at experimental temperatures below 340 K. The thermostatic bath has a volume of about $40\times10^{-3}m^3$. A temperature control device keeps the temperature of the bath constant within 20 mK. The gas added to the setup is pressurized with a booster.

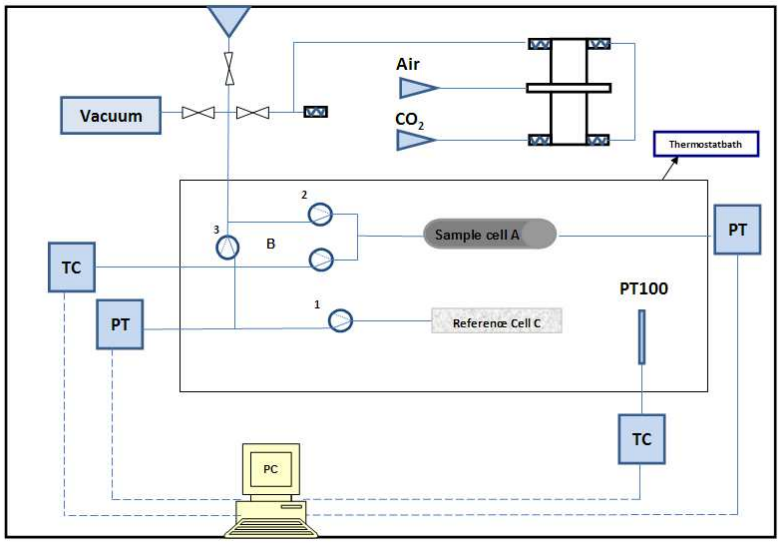

Figure 4-2 : Schematic drawing of the manometric set-up [45].

4.4. SAMPLE PREPARATION AND MATERIAL USED

The experiments are performed with Carboniferous black shale from Belgium. The procedure is as follows: first, from a large source sample, pieces of 2-5 cm were hammered out. These pieces were granulized together and then sieved to a size of 40-100 µm. No further homogenization procedure was performed.

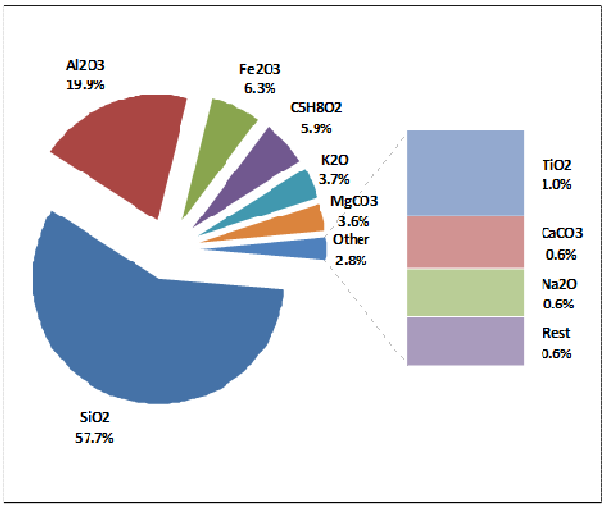

Figure 4-3: The XRF result of the black shale.

Secondly, we determined the mineral composition and elemental composition using XRF on an additional sample from the granulized stock and an XRD on a previously obtained sample from the same source. The XRF results, shown in Figure **4-3**, indicate that the main part of the shale consists of SiO_2. The XRD results, shown in Figure **4-4**, demonstrate that the sample contains 53.70% clay minerals, 26.82% quartz and 6.58 vol% of organic matter.

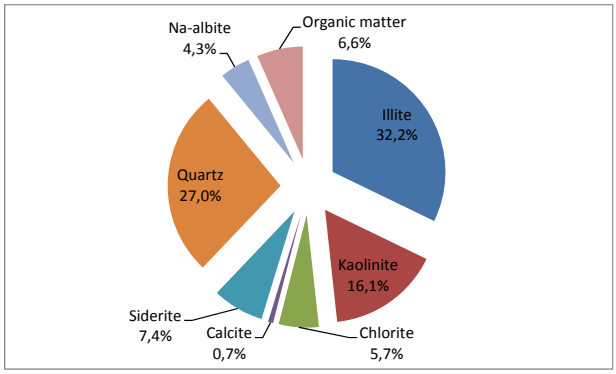

Figure 4-4: The XRD result of the black shale.

Before placing the sample cell, it has been dried in an oven for 24 hours at 378 K under vacuum conditions in order to remove the moisture content. The scanning electron microscope (SEM) image of our sample is presented in Figure **4-5**.

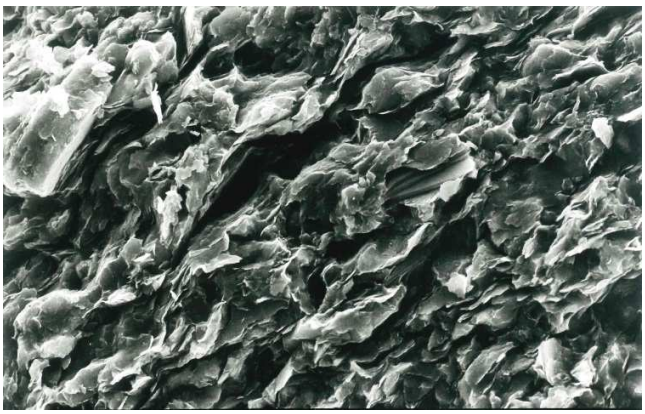

Figure 4-5: Scanning electron microscope (SEM) image of the black shale.

4.5. EXPERIMENTAL PROCEDURE

An experiment comprises the following four sequential procedures: (1) He (helium) leakage test, (2) Void volume measurement by a He sorption experiment, (3) actual sorption experiment with CO_2 or CH_4, and (4) control measurement of the He sorption. The second He sorption experiment in step 4 ensures that the volume accessible to gas has not changed during the experiment [45]. The He leak rate is determined at 18 MPa and the experimental temperature for more than 24 h. Prior to the experiments, a drying procedure was carried out as described here: the sample holder containing sample was weighed and put in the oven at a temperature of 373 K, where it was also evacuated for 24 hours. The sample was weighed again after this procedure, but no significant change in weight was measured. Subsequently it was put in the experimental set up and evacuated for another 24 hours before the actual sorption. Subsequently we fill the reference cell by opening valve "3" to a pressure P_f .Then we close valve "3". Thereafter we open valve "4" and measure the equilibrium pressure. Then we again close valve "4" and fill the reference cell by opening valve "3" to filling pressure P_f. Subsequently we repeated the procedure (See Figure **4-2**).

4.6. DATA ANALYSIS

Measured properties are the initial and final pressure and temperature in the reference and sample cell; these are converted to density values, in mole/dm^3, using highly accurate EOS [48, 49]. The volume accessible to gas in the sample, V_v, i.e., the *void volume* in m^3, is determined from the He sorption experiments as mentioned above. The sample mass, M in g, is determined

by weighing, before the sample cell is built into the setup. We refer to Figure **4-6** for the derivation of an expression for the cumulative sorbed mass. Using that the mass for the conditions shown at the left side of Figure **4-6** is equal to the mass shown at the right side we find

$$V_r\rho_f^N + V_v\rho_{eq}^{N-1} + m_{ads}^{N-1} = V_r\rho_{eq}^N + V_v\rho_{eq}^N + m_{ads}^N, \tag{4. 1}$$

which can be rearranged to

$$V_r\left(\rho_f^N - \rho_{eq}^N\right) - V_v\left(\rho_{eq}^N - \rho_{eq}^{N-1}\right) = m_{ads}^N - m_{ads}^{N-1}, \tag{4. 2}$$

The equation has been derived previously see [14, 45].

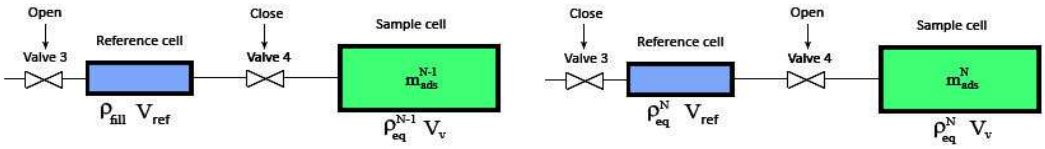

Figure 4-6: Data analysis after bringing gas to sample cell.

4.7. RESULTS AND DISSCUSION

In this section we present the results of the sorption experiments of CO_2 and CH_4 on black shale. We applied Eq. 2 to obtain the sorption values. First we discuss the CO_2 experiments. We carried out two experiments at a temperature of 318 K and pressures up to 85 bar. Figure **4-7**a, b plots the excess sorption versus the pressure, while Figure **4-8**a, b plots the excess sorption versus the density. We use the Span-Wagner EOS to obtain the density [48]. Error bars (see below how they are obtained) are included. The plots cover a pressure range between 0-90 bar. For both experiments at about 82 bar the excess sorption is zero. The experiments show that the excess sorption is the same within experimental error, with a maximum between 0.153 ± 0.006 mmol/gm and 0.175 ± 0.004 mmol/g. This corresponds to the sorption values reported by Weniger et al. [16] who obtained 0.187mmol/g for shale with this carbon content, i.e., $[CO_2]_{ads}$ = 0.008 TOC(%) + 0.183 (mol/kg), as already mentioned in the introduction . At a pressure of about 82 bar, the excess sorption becomes negative. The low pressure at which zero excess sorption occurs can be due one or the combination of the following: (1) overestimation of the void volume as Helium can penetrate in corners that are not easily accessed by CO_2 molecules (2) the finite density of the sorbed phase, (3) reaction of CO_2 with the minerals, (4) changing of the void volume during the experiment and (5) the behaviour of CO_2 [23, 50-54] near the critical point. The void volume measurements are validated with Argon and Helium at the end of experiment. It

proves that there is no change in void volume before and after introducing the gases, i.e., CO_2 or CH_4 to the sample.

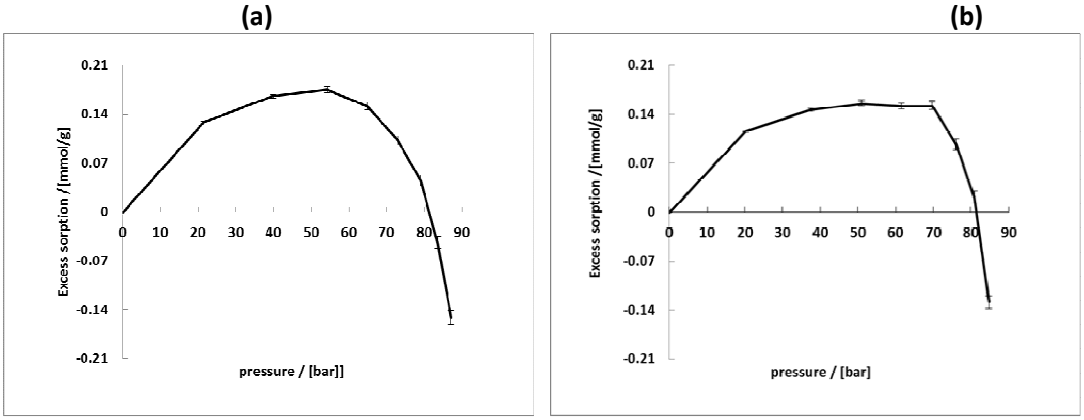

Figure 4-7: (a) Excess sorption of CO_2 on black shale as a function of pressure at a temperature of 318 *K*.
(b) Excess sorption of CO_2 on black shale as a function of pressure at a temperature of 318 *K*.

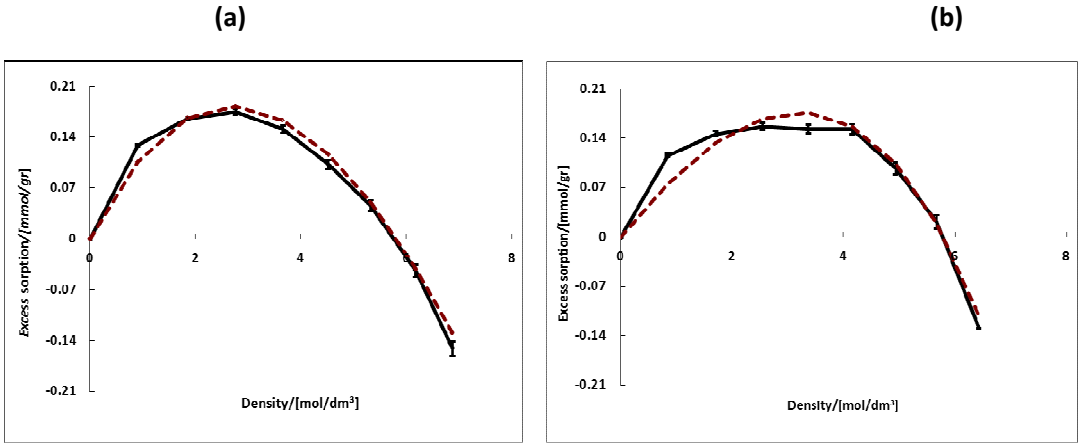

Figure 4-8: (a) Excess sorption of CO_2 on black shale as a function of density at a temperature of 318 *K*.
(b) Excess sorption of CO_2 on black shale.

Negative excess sorption values were also observed by Busch et al., [38] and Ross and Bustin [47]. Busch et al., [38] report experiments on CO_2 absorption on Paleozoic shale from the Warndt-Luisenthal coal mine in the German Saar area. Their experiments cover a pressure range between zero and 200 bar. From about 80 bar onwards their results on dry shale show a decrease, with zero excess sorption at 95 bar. After reaching an excess sorption of "-1 kg/ton" their excess sorption remains constant, i.e., at a much lower value than observed by us. The maximum excess sorption value measured by Busch et al., [38] is 5.5 kg/ton, which can be compared with our maximum of 7.90 kg/ton.

We also plot a theoretical curve in Figure **4-8**a, b (red line-Dash line), which is a Langmuir sorption isotherm (with two parameters) multiplied by a correction factor (with one parameter) to account for the density of the sorbed phase, disregarding other mechanisms that vary the void volume.

$$M_{ads} = \frac{a\rho}{1+b\rho}\left(1-\frac{\rho}{\rho_a}\right), \qquad (4.3)$$

It appears that a curve that plots the sorbed mass per unit mass of sorbent versus the density of the gas can describe the experiments within experimental data. The EXCEL solver was used to fit the experimental data to obtain optimized parameters for Eq. (3). EXCEL uses the Generalized Reduced Gradient Algorithm to find the parameters. The sorption isotherm in the first experiment (Figure **4-8**-a) is well described by Eq. (3). The second experiment, shown in the right panel (Figure **4-8**-b), was obtained with the sample from the same batch. For densities < 4 mol/dm^3 Eq. (4. 3) is not adequate to describe the sorption behaviour in this experiment. At higher densities there is a good fit. This would indicate that the finite density of the sorbed phase can account for the declining excess sorption. A zero excess sorption value would indicate that the density of the sorbed phase is the same as the density of the free phase. This suggests that the sorbed phase density is 5.80 mol/dm^3 = 255 kg/m^3. The density, ρ_a, is the inverse partial molar volume of CO_2. The partial molar volume describes the increase in volume of the sorbing medium when a mole of CO_2 is sorbed on it. The density ρ_a = 255 kg/m^3 obtained for sorption on shale is very small with respect to equivalent densities (inverse partial molar volumes when CO_2 dissolves in water or brine [55-57] or in ionic melts [58-61] or sorbs on polymers [62].

Rother et al., [63] have also observed negative sorption of CO_2 in mesoporous CPG-10 Silica. They mention that the pore size can affect the value of the excess sorption and may change the pressure at which the maximum excess sorption occurred. The gas density at which the excess sorption of CO_2 on coal becomes zero is 880 kg/m^3 by table 5 from [14] and the gas density at which the excess sorption of CO_2 on CPG-10 Silica becomes zero is 700 kg/m^3 [63]. This density can be equated to the inverse partial molar volume or the sorbed density respectively on coal and CPG-10 Silica. The density of dissolved CO_2 in water is 1333 kg/m^3 [64] . However, the sorbed density of CO_2 in our shale experiment is much lower, i.e., 255 kg/m^3. Even if the black shale sample consists of 27 % of quartz and 6.6 % of organic carbon and the sorption capacity of black shale is relatively low, we infer that the low value of the sorbed phase density is indicative of sorption on the clay mineral [63].

In order to put error bars in the plot, we conducted an error analysis based on a Monte Carlo simulation. This simulation considers all random errors in the experimental measurements. The precision of the pressure and temperature is given by the manufacturer who calibrated the instrument. The systematic error in the pressure was also calibrated by the manufacturer. We corrected for the systematic error and only kept the random errors. However, in the Monte Carlo simulation, we used the systematic error in the temperature as random error, but this error is very small. It is assumed that experimental errors are normally distributed. In our case we consider variations in the temperature, the pressure, the reference volume and the volume ratio. The Monte Carlo method is used to obtain a probability distribution of experimental quantities, in our case the excess sorption [mmol/g]. It uses repeated random sampling of temperature, pressure and void volume. For the volume ratio (void volume / reference volume) and the reference volume we used the standard deviation of the measured values with Helium pycnometry as random error. For each equilibrium step we applied Eqs. (1) and (2) and calculated the measured excess sorption value m_{ads}^{N} adding a randomly sampled standard deviation for the pressure, temperature and volumes to the measured values. This procedure was repeated four hundred times. Thus we obtain for each equilibrium pressure step four hundred excess sorption values. By putting in ascending order we used the standard procedure to obtain the cumulative distribution function of the excess sorption values. By inverting this cumulative distribution function we can obtain the corresponding value of Z, i.e., a variable in its standard normal form. By plotting our experimental data m_{ads}^{N} versus Z, where $m_{ads}^{N} = \sigma Z+\mu$, we find the average value μ, $m_{ads}^{N}(P,T,V_r,V_v)$, and the standard deviation σ. The standard deviation determines the length of the error bars. The results are shown in Figure **4-7** to Figure **4-11** plots the excess sorption versus pressure and the error bars indicate the standard deviation. Figure **4-8** gives the same plot, but now versus the density obtained using the Span Wagner EOS [48].

Figure **4-9** to Figure **4-11** present excess sorption of CH_4 on black shale as a function of pressure. Figure **4-9** shows excess sorption of CH4 at 308 *K*. it increases to its maximum at (0.0392 ± 0.003 mmol/g) and after that it starts to decrease to 0.034± 0.005 mmol/g at about 110 bar. Figure **4-10** indicates the excess sorption of CH_4 at 318 K. It starts to increase to its maximum at 0.022 ± 0.006 mmol/g then it decreases to reach zero at about 104 bar. After that the negative sorption can be observed. By increasing the pressure the uncertainty increases. Figure **4-11** demonstrates CH4 sorption at 336 K. Among three experiments, at 336 K, excess sorption of CH4 has a maximum of at least 0.014±0.005.

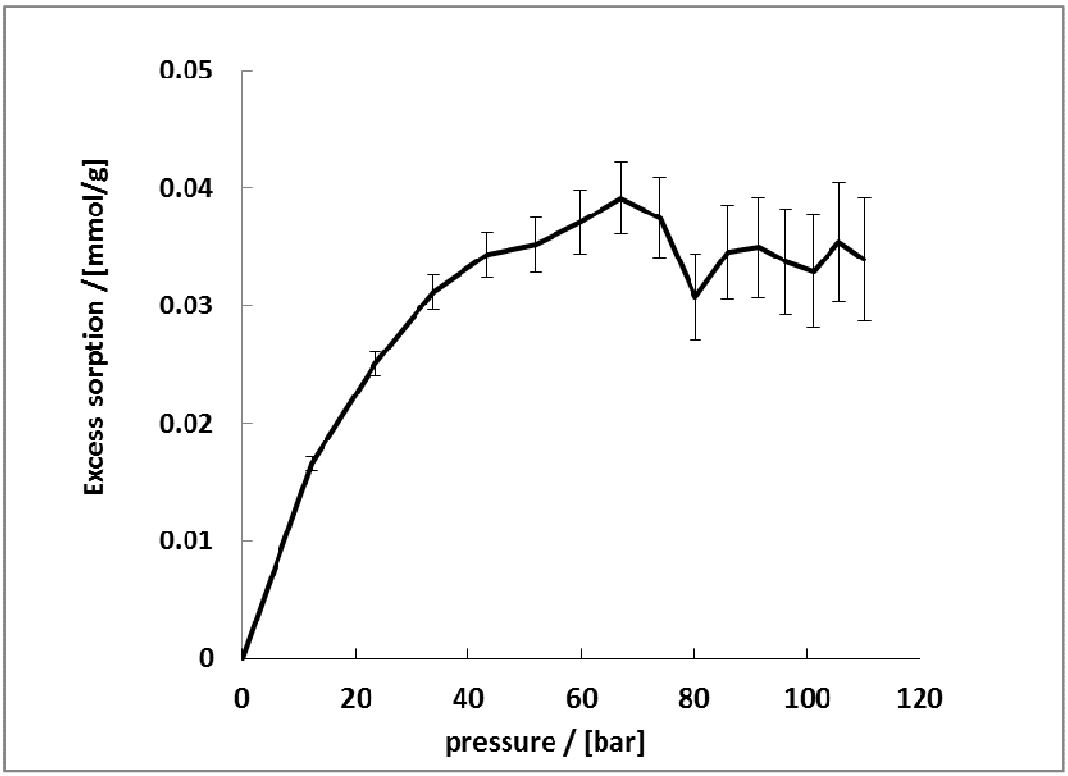

Figure 4-9: Excess sorption of CH_4 on black shale as a function of pressure at 308 K.

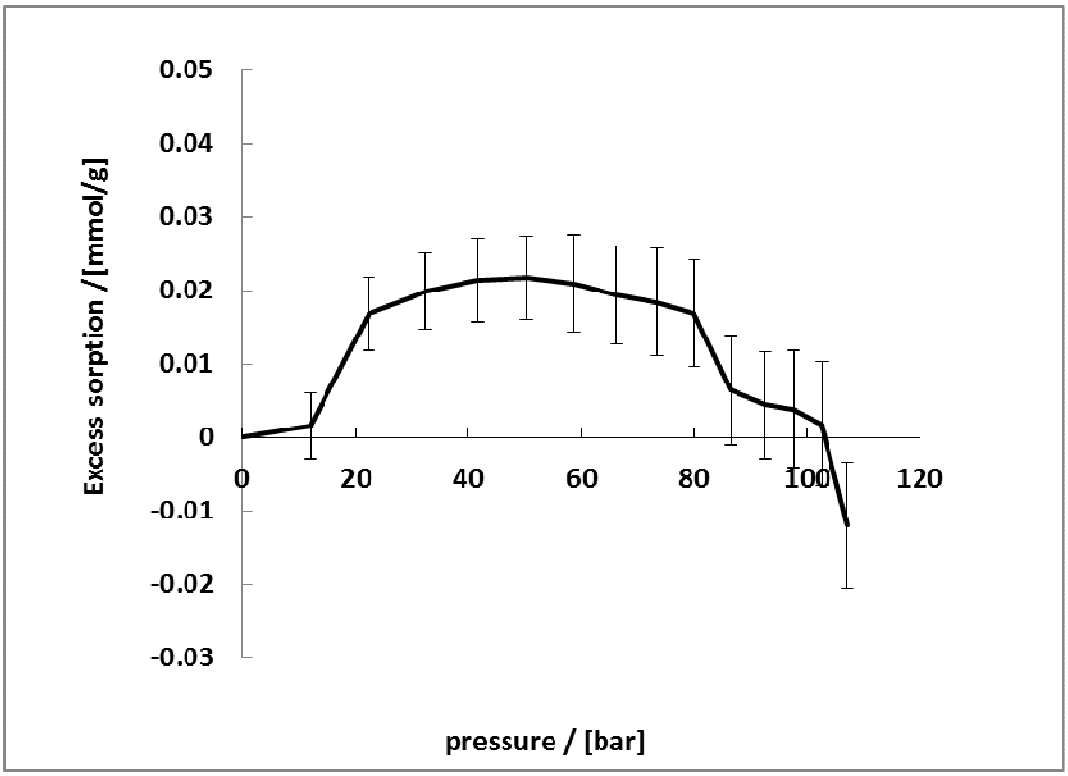

Figure 4-10: Excess sorption of CH_4 on black shale as a function of pressure at 318 K.

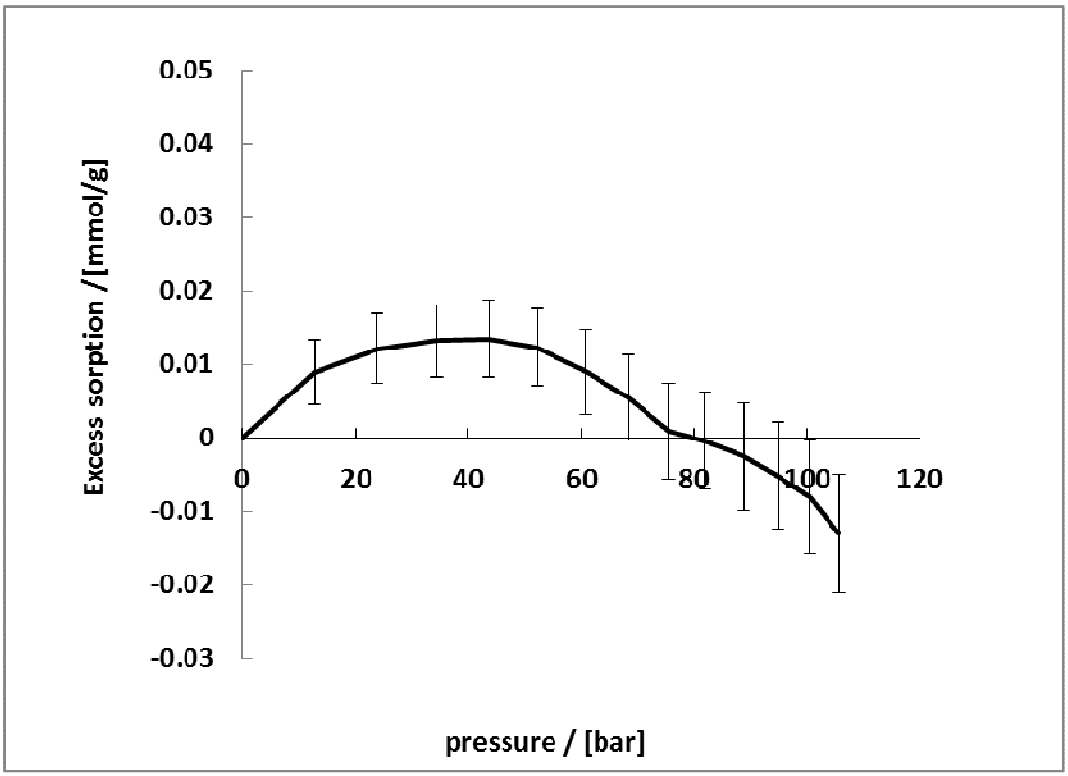

Figure 4-11: Excess sorption of CH4 on black shale as a function of pressure at 336 K.

The figure shows that negative sorption starts around 80 bar. Figure **4-7**:11 suggest that the standard deviation at high pressures is of the order of 0.005mmol/g. Figure **4-12** compares excess sorption at different temperatures. That the value measured at 318 K and 12 bar is lower than the value at 336 K and 12 bar must be attributed to experimental error as indicated by the error bars. For all other data it shows that by increasing the temperature, the amount of excess sorption decreases. Ross and Bustin [47] report experiments for CH_4 sorption on moist Jurassic and Devonian shales. They find a maximum CH_4 sorption of 0.05 cc @ STP / g corresponding to 0.002 mmol/g, which is much smaller than the CO_2 sorption. They also observed negative sorption. For all experiments, the void volume measurements are validated with Argon and Helium at the end of experiment, showing that there is no significant change in the void volume before and after introducing the gases, i.e., (CO_2 and CH_4) to the sample. Investigations of CH_4 sorption on shale done by other scientists are summarized in Table **4-1**.

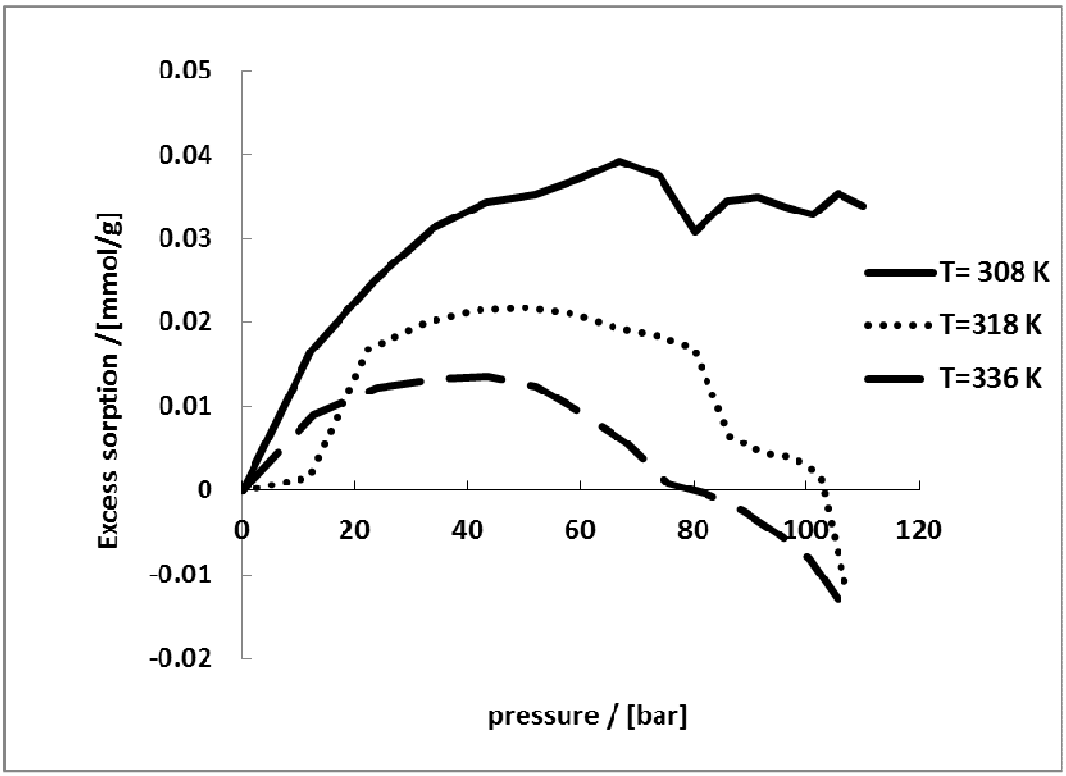

Figure 4-12: Comparison of Excess sorption of CH_4 on black shale as a function of pressure in three different temperatures.

Table 4-1: The CH_4 sorption amounts on shales. The effects are shown with three abbreviations: N (negative), P (positive) and NE (no effect). [a]S: Shale, [b]V: Volumetric and M:Manometric. [c]No trend for organic-lean Sample.

Author	Year	Gas	Sample[a]	TOC	Moisture	Method[b]	Sorption
Ross et al., [47]	2007	CH_4	S	-	N	V	0.002 mmol/g
Ross et al., [17]	2008	CH_4	S	P		V	0.4 to 4 cc/g at T=30° C
Weniger et al., [16]	2010	CH_4	S	P	N	M	=0.009 TOC(%) + 0.026 mmol/g
Chareonsuppanimit et al.,[65]	2011	CH_4	S	P[c]	-	V	=0.035 mmol/g at T=55 C
Gasparik et al.,[19]	2012	CH_4	S	NE	N	M	0.05 to 0.3 mmol/g at T=65° C
Gasparik et al., [66]	2013	CH_4	S	P	N	M	For carboniferous sample, 0.03 to 0.09 mmol/g at T=65° C and different TOC

4.8. CONCLUSIONS

- It is possible to use the manometric set-up to accurately measure excess sorption of CO_2 and CH_4 on Belgian carboniferous black shale at temperatures of 308, 318 and 336 K and in a pressure range between 0- 105 bar.
- The CO_2 excess sorption isotherm shows an initial increase to a maximum value of 0.175 ± 0.004 mmol/gram-shale before it starts to decrease until it becomes zero at 82 bar, which can be converted using the Span-Wagner EOS to a gas-density of 255 kg/m^3. Subsequently the excess sorption becomes negative.
- The CH_4 excess sorption isotherm at 308 K shows an initial increase to a maximum value of 0.0392 ± 0.003 mmol/gram-shale. The CH_4 excess sorption isotherm at 318 K shows an initial increase to a maximum value of 0.022 ± 0.006 mmol/gram-shale before it decreases until it becomes zero at 104 bar. Subsequently the excess sorption becomes negative. We see the same behaviour for CH_4 sorption at 336 K; however, its maximum is about 0.014±0.005 mmol/ gram-shale. As expected the CH_4 excess sorption isotherm at 308K is the largest. Indeed, the experiments on CH_4 show a decreasing sorption at increasing temperature. In comparison to the experiment that we have done for CO_2 at 318 K, the amount of excess CO_2 sorption is about 7 times higher than CH_4 sorption. It validates the idea that sorption capacity of CO_2 is much higher than of CH_4.

4.9. NOMENCLATURE

EGR	Enhance Gas Recovery
TOC	Total Organic Carbon
CCS	Carbon Capture and Storage
EOS	Equation of State
SEM	Scanning Electron Microscope
XRF	X-Ray Fluorescence, the elemental composition analysis
XRD	X-Ray Diffraction, the mineral composition analysis
T	Temperature
P	Pressure
P_f	filling pressure
ρ	Density of the gas
ρ_{eq}^{N-1}	Equilibrium density of gas in step N-1

ρ_{eq}^{N} Equilibrium density of gas in step N

ρ_{f}^{N} Density of the gas filled in the reference cell step N

V_r Volume of reference cell

V_v Void volume

V_v^N Void volume measured in step N

V_v^0 Void volume measured by Helium prior to the gas sorption experiment

m_{ads}^{N-1} Sorbed mass in step N-1

m_{ads}^{N} Sorbed mass in step N

ΔV_{sw}^{N} The changes in void volume of the sample due to its swelling in step N

ΔV_{ads}^{N} The changes in void volume of the sample due to the sorption in step N

ΔV_{react}^{N} The changes in void volume of the sample due to the reaction in step N

4.10. REFERENCES

1. Shaoul, J.R., L.F. Van Zelm, and H.J. De Pater. *Damage mechanisms in unconventional gas well stimulation-A new look at an old problem*. in *SPE Middle East Unconventional Gas Conference and Exhibition*. 2011. Society of Petroleum Engineers.
2. Campin, D. *Environmental Regulation of Hydraulic Fracturing in Queensland*. in *SPE Annual Technical Conference and Exhibition*. 2013. Society of Petroleum Engineers.
3. U.S. Energy Information Administration, *Technically* Recoverable *Shale Oil and Shale Gas Resources: An Assessment of 137 Shale Formations in 41 Countries Outside the United States*, 2013, U.S. Department of Energy: Washington, D.C.
4. BP Statistical Review of World Energy, w.b.c., 2012.
5. *Speight, J.G., Shale Gas Production Processes 2013, Gulf Professional Publishing: Boston. p. i-iii.*
6. *NEB. A Primer for Understanding Canadian Shale Gas*. . National Energy Board, Calgary, Alberta, Canada, November 2009.
7. International Energy Agency, *World Energy Outlook 2012*, 2012, OECD Publishing.
8. Karcz, P.a., M. Janas, and I. Dyrka, *Polish shale gas deposits in relation to selected shale gas prospective areas of Central and Eastern Europe*.
9. McGlade, C., J. Speirs, and S. Sorrell, *Unconventional gas – A review of regional and global resource estimates*. Energy, 2013. **55**: p. 571-584.
10. Geny, F., *Can unconventional gas be a game changer in European markets? Oxford Institute for Energy Studies. Nat Gas Ser 2010; 46: 120*. 2010.
11. Sinal, M.L. and G. Lancaster, *Liquid CO Fracturing: Advantages And Limitations*. Journal of Canadian Petroleum Technology, 1987. **26**(05).
12. Ishida, T., K. Aoyagi, T. Niwa, Y. Chen, S. Murata, Q. Chen, and Y. Nakayama, *Acoustic emission monitoring of hydraulic fracturing laboratory experiment with supercritical and liquid CO_2*. Geophysical Research Letters, 2012. **39**(16).
13. Beaton, A., *Rock Eval, Total Organic Carbon and Adsorption Isotherms of the Duvernay and Muskwa Formations in Alberta: Shale Gas Data Release*2010: Alberta Geological Survey.

14. Battistutta, E., P. Van Hemert, M. Lutynski, H. Bruining, and K.-H. Wolf, *Swelling and sorption experiments on methane, nitrogen and carbon dioxide on dry Selar Cornish coal*. International Journal of Coal Geology, 2010. **84**(1): p. 39-48.
15. Hall, F., Z. Chunhe, K. Gasem, R. Jr, and Y. Dan. *Adsorption of pure methane, nitrogen, and carbon dioxide and their binary mixtures on wet Fruitland coal*. in *SPE Eastern Regional Meeting*. 1994.
16. Weniger, P., W. Kalkreuth, A. Busch, and B.M. Krooss, *High-pressure methane and carbon dioxide sorption on coal and shale samples from the Paraná Basin, Brazil*. International Journal of Coal Geology, 2010. **84**(3): p. 190-205.
17. Ross, D.J. and R. Marc Bustin, *The importance of shale composition and pore structure upon gas storage potential of shale gas reservoirs*. Marine and Petroleum Geology, 2009. **26**(6): p. 916-927.
18. Yuan, W., Z. Pan, X. Li, Y. Yang, C. Zhao, L.D. Connell, S. Li, and J. He, *Experimental study and modelling of methane adsorption and diffusion in shale*. Fuel, 2014. **117**: p. 509-519.
19. Gasparik, M., A. Ghanizadeh, P. Bertier, Y. Gensterblum, S. Bouw, and B.M. Krooss, *High-Pressure Methane Sorption Isotherms of Black Shales from The Netherlands*. Energy & Fuels, 2012. **26**(8): p. 4995-5004.
20. Gasparik, M., A. Ghanizadeh, Y. Gensterblum, and B.M. Krooss, *"Multi-temperature" method for high-pressure sorption measurements on moist shales*. Review of Scientific Instruments, 2013. **84**(8): p. 085116.
21. Khosrokhavar, R., G. Elsinga, A. Mojaddam, R. Farajzadeh, and J. Bruining. *Visualization of Natural Convection Flow of Super Critical CO_2 in Water by Applying Schlieren Method*. in *SPE EUROPEC/EAGE Annual Conference and Exhibition*. 2011.
22. Busch, A., S. Alles, Y. Gensterblum, D. Prinz, D.N. Dewhurst, M.D. Raven, H. Stanjek, and B.M. Krooss, *Carbon dioxide storage potential of shales*. International Journal of Greenhouse Gas Control, 2008. **2**(3): p. 297-308.
23. Gensterblum, Y., P. Van Hemert, P. Billemont, A. Busch, D. Charriére, D. Li, B. Krooss, G. De Weireld, D. Prinz, and K.-H. Wolf, *European inter-laboratory comparison of high pressure CO_2 sorption isotherms. I: Activated carbon*. Carbon, 2009. **47**(13): p. 2958-2969.
24. Kang, S.M., E. Fathi, R. Ambrose, I. Akkutlu, and R. Sigal, *Carbon dioxide storage capacity of organic-rich shales*. SPE Journal, 2011. **16**(4): p. 842-855.
25. Farajzadeh, R., P.L. Zitha, and J. Bruining, *Enhanced mass transfer of CO_2 into water: experiment and modeling*. Industrial & Engineering Chemistry Research, 2009. **48**(13): p. 6423-6431.
26. Eftekhari, A.A., H. Van Der Kooi, and H. Bruining, *Exergy analysis of underground coal gasification with simultaneous storage of carbon dioxide*. Energy, 2012.
27. Meulenbroek, B., R. Farajzadeh, and H. Bruining, *The effect of interface movement and viscosity variation on the stability of a diffusive interface between aqueous and gaseous CO_2*. Physics of Fluids (1994-present), 2013. **25**(7): p. 074103.
28. Nordbotten, J.M. and M.A. Celia, *Geological Storage of CO_2: Modeling Approaches for Large-Scale Simulation*2011: Wiley. com.
29. Nordbotten, J.M., M.A. Celia, and S. Bachu, *Injection and storage of CO_2 in deep saline aquifers: Analytical solution for CO_2 plume evolution during injection*. Transport in porous media, 2005. **58**(3): p. 339-360.
30. Ranganathan, P., R. Farajzadeh, H. Bruining, and P.L. Zitha, *Numerical simulation of natural convection in heterogeneous porous media for CO_2 geological storage*. Transport in porous media, 2012. **95**(1): p. 25-54.
31. Gasda, S.E., Numerical models for evaluating CO_2 storage in deep saline aquifers: Leaky wells and large-scale geological features, . Ph.D. Thesis. Available at http://arks.princeton.edu/ark:/88435/dsp01j098zb09n., 2010.
32. Kumar, A., M. Noh, G. Pope, K. Sepehrnoori, S. Bryant, and L. Lake. *Reservoir Simulation of CO_2 Storage in Deep Saline Aquifers, paper SPE-89343*. in *Society of Petroleum Engineers Fourteenth Symposium on Improved Oil Recovery, Tulsa, OK*. 2004.
33. Orr, F., *Storage of carbon dioxide in geologic formations*. Journal of petroleum technology, 2004. **56**(9): p. 90-97.
34. Regan, M., *A Review of the Potential for Carbon Dioxide (CO_2) Enhanced Gas Recovery in Australia*. Cooperative Research Centre for Greenhouse Gas Technologies, Canberra. CO_2CRC Publication No: RPT07-0802. 39p, 2007.
35. Tao, Z. and A. Clarens, *Estimating the Carbon Sequestration Capacity of Shale Formations Using Methane Production Rates*. Environ Sci Technol, 2013. **47**(19): p. 11318-11325.
36. Bachu, S., *Sequestration of CO_2 in geological media in response to climate change: road map for site selection using the transform of the geological space into the CO_2 phase space*. Energy Conversion and Management, 2002. **43**(1): p. 87-102.
37. Bachu, S., W. Gunter, and E. Perkins, *Aquifer disposal of CO_2 : Hydrodynamic and mineral trapping*. Energy Conversion and Management, 1994. **35**(4): p. 269-279.

38. Busch, A., S. Alles, B.M. Krooss, H. Stanjek, and D. Dewhurst, *Effects of physical sorption and chemical reactions of CO_2 in shaly caprocks*. Energy Procedia, 2009. **1**(1): p. 3229-3235.
39. Blok, K., R. Williams, R. Katofsky, and C.A. Hendriks, *Hydrogen production from natural gas, sequestration of recovered CO_2 in depleted gas wells and enhanced natural gas recovery*. Energy, 1997. **22**(2): p. 161-168.
40. Oldenburg, C., K. Pruess, and S.M. Benson, *Process modeling of CO_2 injection into natural gas reservoirs for carbon sequestration and enhanced gas recovery*. Energy & Fuels, 2001. **15**(2): p. 293-298.
41. Liu, F., K. Ellett, Y. Xiao, and J.A. Rupp, *Assessing the feasibility of CO_2 storage in the New Albany Shale (Devonian–Mississippian) with potential enhanced gas recovery using reservoir simulation*. International Journal of Greenhouse Gas Control, 2013. **17**: p. 111-126.
42. LeVan, M., G. Carta, and D. Green, *Perry's Chemical Engineers' Handbook, 2007*, Section.
43. Iijima, M., T. Nagayasu, T. Kamijyo, and S. Nakatani, *MHI's Energy Efficient Flue Gas CO_2 Capture Technology and Large Scale CCS Demonstration Test at Coal-fired Power Plants in USA*. Mitsubishi Heavy Industries Technical Review, 2011. **48**(1): p. 26.
44. Godec, M., G. Koperna, R. Petrusak, and A. Oudinot, *Potential for Enhanced Gas Recovery and CO_2 Storage in the Marcellus Shale in the Eastern United States*. International Journal of Coal Geology, 2013.
45. Van Hemert, P., H. Bruining, E.S.J. Rudolph, K.-H.A. Wolf, and J.G. Maas, *Improved manometric setup for the accurate determination of supercritical carbon dioxide sorption*. Review of Scientific Instruments, 2009. **80**(3): p. 035103-035103-11.
46. McCarty, R. and V. Arp, *A new wide range equation of state for helium*. Advances in cryogenic engineering, 1990. **35**: p. 1465-1475.
47. Ross, D.J. and R. Marc Bustin, *Impact of mass balance calculations on adsorption capacities in microporous shale gas reservoirs*. Fuel, 2007. **86**(17): p. 2696-2706.
48. Span, R. and W. Wagner, *A new equation of state for carbon dioxide covering the fluid region from the triple-point temperature to 1100 K at pressures up to 800 MPa*. Journal of physical and chemical reference data, 1996. **25**: p. 1509.
49. Wagner, W. and R. Span, *Special Equations of State for Methane, Argon, and Nitrogen for the Temperature Range from 270 to 350 K at Pressures up to 30 MPa*. International journal of thermophysics, 1993. **14**(4): p. 699-725.
50. Gensterblum, Y., P. Van Hemert, P. Billemont, E. Battistutta, A. Busch, B. Krooss, G. De Weireld, and K.-H. Wolf, *European inter-laboratory comparison of high pressure CO_2 sorption isotherms II: Natural coals*. International Journal of Coal Geology, 2010. **84**(2): p. 115-124.
51. Goodman, A., A. Busch, G. Duffy, J. Fitzgerald, K. Gasem, Y. Gensterblum, B. Krooss, J. Levy, E. Ozdemir, and Z. Pan, *An inter-laboratory comparison of CO_2 isotherms measured on Argonne premium coal samples*. Energy & Fuels, 2004. **18**(4): p. 1175-1182.
52. Sakurovs, R., S. Day, S. Weir, and G. Duffy, *Application of a modified Dubinin-Radushkevich equation to adsorption of gases by coals under supercritical conditions*. Energy & Fuels, 2007. **21**(2): p. 992-997.
53. Staib, G., R. Sakurovs, and E.M.A. Gray, *A pressure and concentration dependence of CO_2 diffusion in two Australian bituminous coals*. International Journal of Coal Geology, 2013. **116**: p. 106-116.
54. Yu, H., W. Guo, J. Cheng, and Q. Hu, *Impact of experimental parameters for manometric equipment on CO_2 isotherms measured: Comment on "Inter-laboratory comparison II: CO_2 isotherms measured on moisture-equilibrated Argonne premium coals at 55° C and up to 15 MPa" by Goodman et al.(2007)*. International Journal of Coal Geology, 2008. **74**(3): p. 250-258.
55. Carroll, J.J. and A.E. Mather, *The system carbon dioxide-water and the Krichevsky-Kasarnovsky equation*. Journal of solution chemistry, 1992. **21**(7): p. 607-621.
56. Enick, R.M. and S.M. Klara, *CO_2 solubility in water and brine under reservoir conditions*. Chemical Engineering Communications, 1990. **90**(1): p. 23-33.
57. Parkinson, W.J. and N. De Nevers, *Partial molal volume of carbon dioxide in water solutions*. Industrial & Engineering Chemistry Fundamentals, 1969. **8**(4): p. 709-713.
58. Duncan, M.S. and C.B. Agee, *The partial molar volume of carbon dioxide in peridotite partial melt at high pressure*. Earth and Planetary Science Letters, 2011. **312**(3): p. 429-436.
59. Huang, X., C.J. Margulis, Y. Li, and B.J. Berne, *Why Is the Partial Molar Volume of CO_2 So Small When Dissolved in a Room Temperature Ionic Liquid? Structure and Dynamics of CO_2 Dissolved in [Bmim+][PF6-]*. Journal of the American Chemical Society, 2005. **127**(50): p. 17842-17851.
60. Jalili, A.H., A. Mehdizadeh, M. Shokouhi, A.N. Ahmadi, M. Hosseini-Jenab, and F. Fateminassab, *Solubility and diffusion of CO_2 and H_2S in the ionic liquid 1-ethyl-3-methylimidazolium ethylsulfate*. The Journal of Chemical Thermodynamics, 2010. **42**(10): p. 1298-1303.
61. Kumełan, J., D. Tuma, and G. Maurer, *Partial molar volumes of selected gases in some ionic liquids*. Fluid Phase Equilibria, 2009. **275**(2): p. 132-144.

62. Kamiya, Y., Y. Naito, and D. Bourbon, *Sorption and partial molar volumes of gases in poly (ethylene-co-vinyl acetate)*. Journal of Polymer Science Part B: Polymer Physics, 1994. **32**(2): p. 281-286.
63. Rother, G., E.G. Krukowski, D. Wallacher, N. Grimm, R.J. Bodnar, and D.R. Cole, *Pore size effects on the sorption of supercritical CO_2 in mesoporous CPG-10 silica*. The Journal of Physical Chemistry C, 2011. **116**(1): p. 917-922.
64. Gmelin, L., *Gmelin Handbuch der anorganischen Chemie, 8. Auflage. Kohlenstoff, Teil C3, Verbindungen*, 1973, ISBN 3-527-81419-1.
65. Chareonsuppanimit, P., S.A. Mohammad, R.L. Robinson Jr, and K.A. Gasem, *High-pressure adsorption of gases on shales: Measurements and modeling*. International Journal of Coal Geology, 2012. **95**: p. 34-46.
66. Gasparik, M., P. Bertier, Y. Gensterblum, A. Ghanizadeh, B.M. Krooss, and R. Littke, *Geological controls on the methane storage capacity in organic-rich shales*. International Journal of Coal Geology, 2013.

Chapter 5

Shale Gas Formations and Their Potential for Carbon Storage: Opportunities and Outlook

ABSTRACT

Shale gas resources are proving to be globally abundant and the development of these resources can support the geologic storage of CO_2 (carbon dioxide) to mitigate the climate impacts of global carbon emissions from power and industrial sectors. This chapter reviews global shale gas resources and considers both the opportunities and challenges for their development. It then provides a review of the literature on opportunities to store CO_2 in shale, thus possibly helping to mitigate the impact of CO_2 emissions from the power and industrial sectors. The studies reviewed indicate that the opportunity for geologic storage of CO_2 in shales is significant, but knowledge of the characteristics of the different types of shale gas found globally is required. The potential for CO_2 sorption as part of geologic storage in depleted shale gas reservoirs must be assessed with respect to the individual geology of each formation. Likewise, the introduction of CO_2 into shale for enhanced gas recovery (EGR) operations may significantly improve both reservoir performance and economics. Based on this review, we conclude that there is a very good opportunity globally regarding the future of geologic storage of CO_2 in depleted shale gas formations and as part of EGR operations.

KEYWORDS: *Shale gas, Shale formations, EGR, CO_2 storage in geological formations, Natural gas production*

Published in: Environmental Processes, 2014 1:595–611 DOI 10.1007/s40710-014-0036-4.

5.1. INTRODUCTION

Global and national energy outlooks to 2030 and beyond indicate growing global energy demand, particularly in non-OECD countries, and a continued dominant role for fossil fuels in the world's energy mix, even as utilization of renewable energy sources grows faster than utilization of fossil fuels [1-3]. The future energy landscape will see natural gas play an increasing role for energy supply, particularly in light of the substantial quantities of unconventional gas reserves now being exploited in the United States and plans to exploit similar unconventional resources in many other countries. Even though natural gas is a cleaner burning fossil energy source than coal or oil (Carbon emissions from electricity generation are approximately 400 gCO_2/kWh for natural gas, 785 to 1,005 gCO_2/kWh for coal, depending on type, and 635 to 715 gCO_2/kWh for oil products, depending on type) [4], it still produces greenhouse gas (GHG) emissions and will only compliment rather than fully replace coal and oil for energy in the stationary and transportation sectors. Therefore, addressing the joint challenge of growing energy demand and the potential of climate change consequences from the resulting GHG emissions requires coordinated action at the global scale. Immediate and effective actions are needed to maintain the atmospheric concentration of GHGs to 450 ppm or less, which is the level consistent with maintaining global temperature change below 2°C relative to pre-industrial levels and the associated social, economic and environmental consequences [5]. The International Energy Agency (IEA) estimates that key actions include large-scale investments in carbon capture and storage (CCS) to mitigate the impact of CO_2 (carbon dioxide) emissions from the power and industrial sectors. In fact, IEA explicitly states that unless CCS technology is widely deployed by 2050, approximately two-thirds of proven fossil fuel reserves need to remain un-extracted if the world is to achieve the 2°C goal [6].

Carbon sequestration options include storage in depleted oil and gas reservoirs, saline formations, un-mineable coal seams, basalts, and shales. Perhaps the most commonly considered target repository for CO_2 is deep saline aquifers. However, documented concerns for storage in saline formations include cost, long-term storage, impact on seismicity, and the logistics of sequestration [7]. Enhanced recovery of tight oil, coal bed methane and other unconventional fossil fuels, known as enhanced gas recovery (EGR) or enhanced oil recovery (EOR), using CO_2 is receiving interest as an opportunity for carbon sequestration because of the economic benefits it affords and the existing infrastructure that can be leveraged [7].

The potential for the geologic storage of CO_2 in shale formations that have undergone hydraulic fracturing for extraction is being explored for several reasons [8] such as shales are broadly distributed; availability of infrastructure of wells, pipeline and so on; decrease in pore pressure caused by gas production in the shale formation before CO_2 injection.

Development of shale resources may benefit CO_2 storage because the innovations developed are directly transferable, particularly those that relate to well completion, like new methods for well cementing, advanced horizontal drilling techniques, and enhancement of field treatment skills for saline water [9]. Thus, understanding the behavior of CO_2 in shale is an important part of advancing the opportunity for the economic geologic storage of CO_2, particularly because of the fact that the geological characteristics of a particular storage site often have important influences on the design of related CO_2 capture and transportation infrastructure [4].

This chapter examines the global unconventional hydrocarbon landscape with a focus on the assessment of recoverable shale gas resources. The opportunity for geologic storage of CO_2 in shale formations (as well as other natural gas reservoirs that include shales) is then considered through a review of the types of shales globally, and the CO_2 storage capacity and EGR opportunities in shale formations.

5.2. GLOBAL SHALE RESOURCES

According to the World Energy Outlook [6], the remaining technically recoverable natural gas resources by the end of 2011 globally reached 790 Tcm (trillion cubic meters). This includes both conventional and unconventional resources and is slightly greater than the estimate of 719 Tcm provided by McGlade, Speirs [10] in their recent review of regional and global unconventional gas estimates. A breakdown of the amount of each type of resource globally [6] is shown in Table **5-1**.

The U.S. Energy Information Administration (EIA) estimates that roughly 32% of total estimated global natural gas resources are in shale formations [11]. The top 10 countries for technically recoverable shale gas resources for which EIA has made a shale resource assessment are shown in Table **5-2** [11].

Table 5-1: Technically recoverable natural gas resources by end-2011 [6]

Region	Conventional (Tcm)	Unconventional (Tcm)				Total (Tcm)
		Tight gas	Shale gas	Coalbed methane	Sub-total	
E. Europe/Eurasia	144	11	12	20	44	187
Middle East	125	9	4	-	12	137
Asia-Pacific	43	21	57	19	94	137
OECD America	47	11	47	9	67	114
Africa	49	10	30	0	40	88
Latin America	32	15	33	-	48	80
OECD Europe	24	4	16	2	22	46
World	462	81	200	47	328	790

Table 5-2: Top 10 countries with technically recoverable shale gas resources [11]. Estimates for the United States include those from the Energy Information Administration (EIA) and Advanced Resources International (ARI)

Rank	Country	Shale Gas (Tcf)
1	China	1,115
2	Argentina	802
3	Algeria	707
4	United States	665 (EIA), 1,161 (ARI)
5	Canada	573
6	Mexico	545
7	Australia	437
8	South Africa	390
9	Russia	285
10	Brazil	245

Although the data shown in Table **5-1** and Table **5-2** suggest a significant CO_2 storage opportunity via exploitable shale resources, the data represent technically recoverable resources which differ from economically recoverable resources. According to the EIA's definitions [11]: technically recoverable natural gas is that which can be produced with current technologies, regardless of natural gas prices and production costs; economically recoverable resources are resources that can be produced profitably under current market conditions. The costs of well drilling and completion, the amount of natural gas produced from an average well over its lifetime, and the prices received for gas production define the economic recoverability of gas resources.

As specifically stated by the EIA, the economic recoverability is influenced by factors such as ownership of mineral rights that provide economic incentive for development, availability of experienced independent operators and contractors, existing infrastructure, and the availability of water resources for use in hydraulic fracturing [11]. It should also be noted that estimates of both technically and economically recoverable shale gas resources are uncertain and continually undergoing revision based on updated information.

Given the substantial variation across the world's shale formations in both geological and non-geological factors, the extent to which technically recoverable shale resources will prove to be economically recoverable is very uncertain. China, for instance, holds the most technically recoverable reserves of shale gas globally (Table **5-2**) and was once considered well positioned to replicate the United States' shale gas success. However, problems comprising poor infrastructure, political disputes, and the fact that the shale gas formations are much deeper than expected, have made economic shale gas recovery extremely challenging in China [12]. Although not assessed in EIA's coverage, large amounts of potentially productive shales exist in other countries around the

world, including most of the countries in the Middle East and North Africa (MENA) [13, 14]. According to Baker Hughes, Saudi Arabia [15] has more than 16.8 Tcm of shale gas reserves. However, several of the obstacles already noted make MENA countries hamper the development of tight and shale gas. The obstacles stated by Martin [14]include: high cost of MENA field-development operations (i.e., the cost of drilling and completing in the MENA countries is said to be 2.5 to 5 times higher than similar operations in the United States); lack of fiscal incentives; lack of infrastructure; competition from alternative fossil sources; discomfort with wellbore-scale experimentations; lack of wellbore-specific information; and difficulty in doing business generally. The conclusion, therefore, is that shale gas resources are abundant but many factors must converge in order to make shale gas extraction profitable. These factors include technology innovation, government policy, private sector entrepreneurship, land and mineral rights ownership, market structure, geology, water availability, and natural gas pipeline infrastructure, to name a few. Hence, the policy and market environment are key factors in determining the potential for profitable shale gas production in a particular country. Therefore, the opportunity for geological storage of CO_2 in shale resources is dependent on success in overcoming a large number of development challenges that would make the shale resources available for storage. If these challenges can be overcome, then not only will abundant hydrocarbon resources become available, but potentially very good repositories for geologic storage of CO_2 will also result.

5.3. CURRENT STATUS OF SHALE GAS DEVELOPMENT

World production of unconventional gas, of which shale gas is a subset, was approximately 472 Bcm in 2010, with approximately 76% of production coming from the United States and 13% of production coming from Canada [16]. The opportunity to produce substantial amounts of gas from shale formations in both the United States and Canada is based on the development and application of new technologies for economic shale gas extraction [17, 18]. Unlike China and the MENA region previously discussed, the United States and Canada currently have regulatory and political climates generally conducive for shale gas development. Both countries are predicted to drill thousands of wells in the next decade as shale gas development becomes increasingly economical [19].

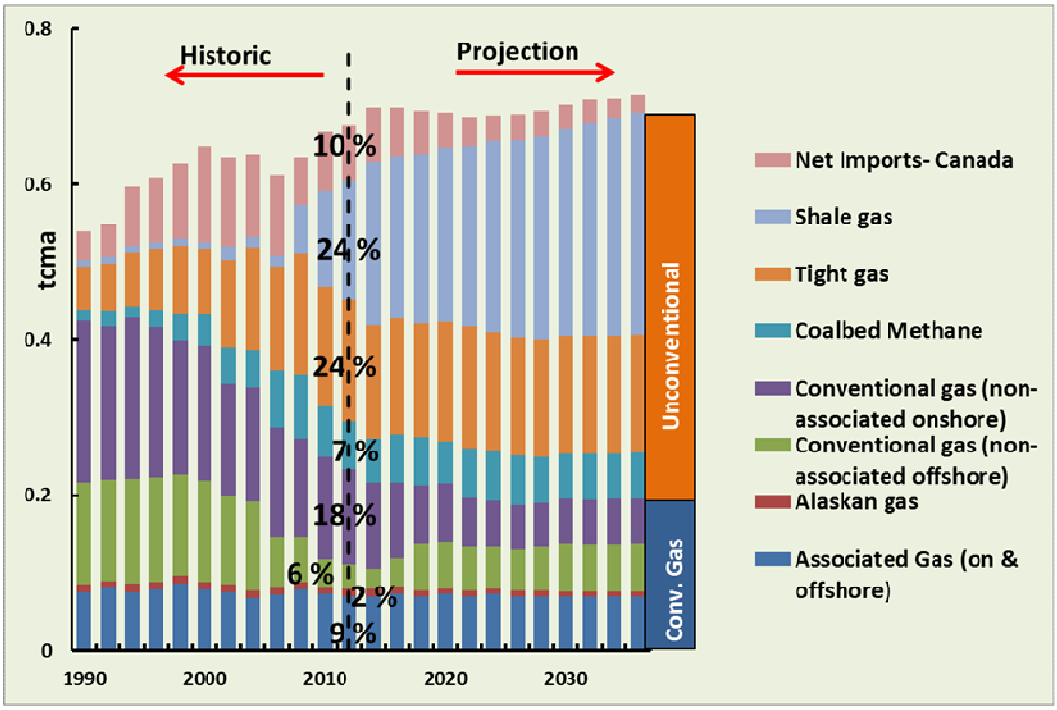

Figure 5-1: US historic gas production record (in Trillion cubic meter per year – Tcma) and forecast till 2035. [108]

During recent years, because of development of shale gas plays, the production of natural gas has been significantly increased in the United States (Figure **5-1**). The U.S. is now the largest producer of natural gas in the world. The most growth in economic extraction of shale gas has been made by Canada and the United States which are producing 25% of global natural gas [20]. Indeed, shale gas is expected to account for 49% of total gas production in the United States by 2035, up from 23% in 2010 (Figure **5-1**). Advances in shale gas extraction technologies have increased shale gas production in the United States and this production is believed to be able to support the United States' energy demand for about 60 years at the current level of use [21]. The main shale resources in the United States are provided in Figure **5-2** [11, 22]. Among these formations, the Marcellus Shale in the Appalachian Basin is the largest one [11].

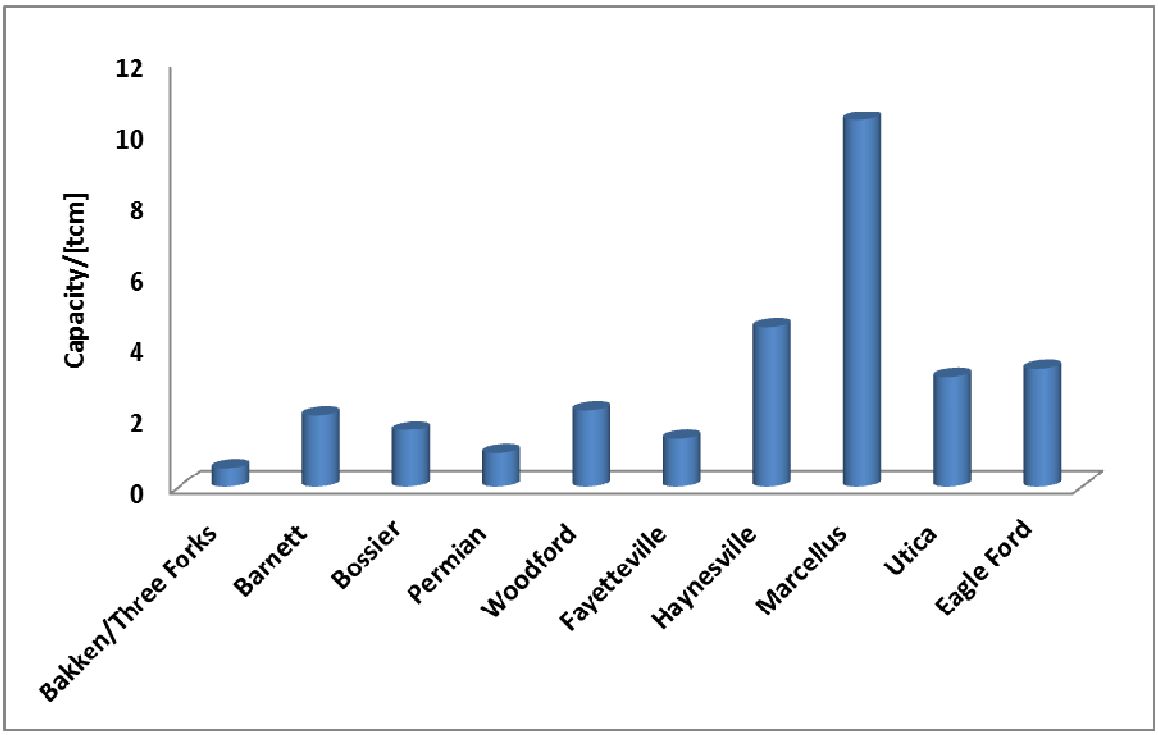

Figure 5-2: Remaining Shale Gas Reserves and Undeveloped Resources in the United States [11].

In Canada, a large potential value for gas-in-place is estimated in shale formations (~28 Tcm) [23]. Gas production from Canadian shales began modestly in 2005 (Figure **5-3**) and has increased rapidly afterward. Natural gas is mainly being produced from Devonian shales in the Horn River Basin and from the Triassic Montney shales and siltstones, both located in northeastern British Columbia and in the Devonian Duvernay Formation in Alberta [24]. The important shales in Canada are shown in Figure **5-4**. Gas production from the Utica Shale in Quebec, Canada was placed under a moratorium until the possible risks for groundwater contamination could be evaluated [25].

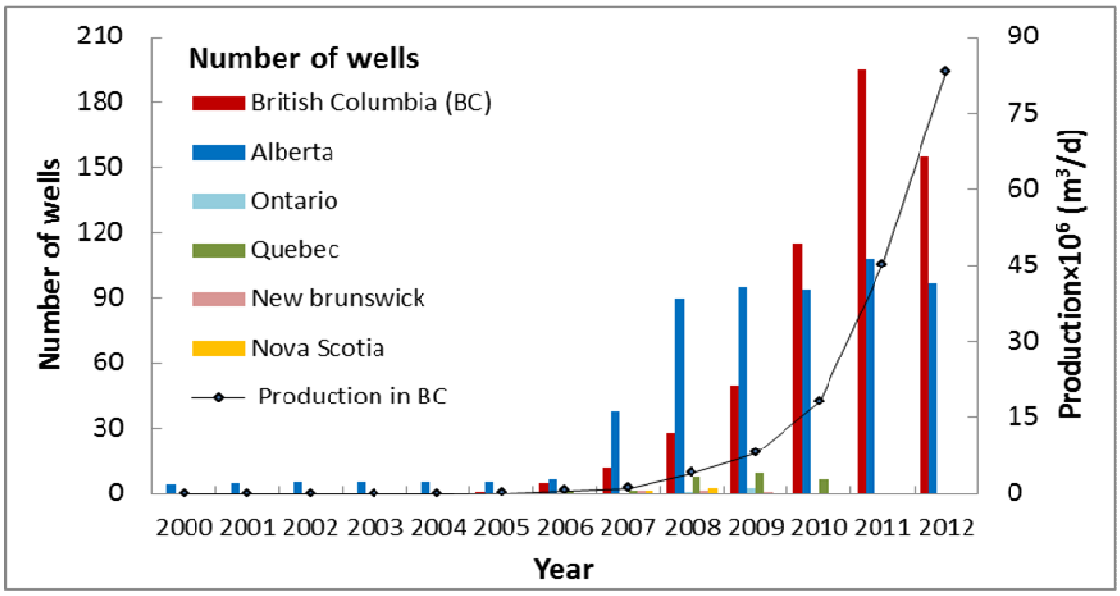

Figure 5-3: Total number of wells drilled yearly for unconventional hydrocarbon per year in Canada and yearly production of shale gas for British Columbia [24].

China is at the early stages of evaluating its shale gas resources [17]. China is planning to increase its shale gas output from nearly zero in 2012 to 6.5 billion cubic meters (Bcm) (per year by 2015 and to 80 to 100 Bcm per year by 2020 [17]. In China, the Sichuan Basin, located in south central China, accounts for 40% of the country's shale resource [19].

Argentina's Neuquén Basin, on Argentina's border with Chile, is the country's largest source of hydrocarbons, accounting for 35% of the country's oil reserves and 47% of the gas reserves. Argentina's biggest energy company, YPF (Yacimientos Petrolíferos Fiscales), was successful in discovering shale gas in the Mendoza province [19].

Australia's natural gas resource is shown in Figure **5-5**. They are dominated by unconventional gas, particularly shale gas and coal seam gas. This indicates the significance of shale gas resources in long-term gas supply for Australia [26].

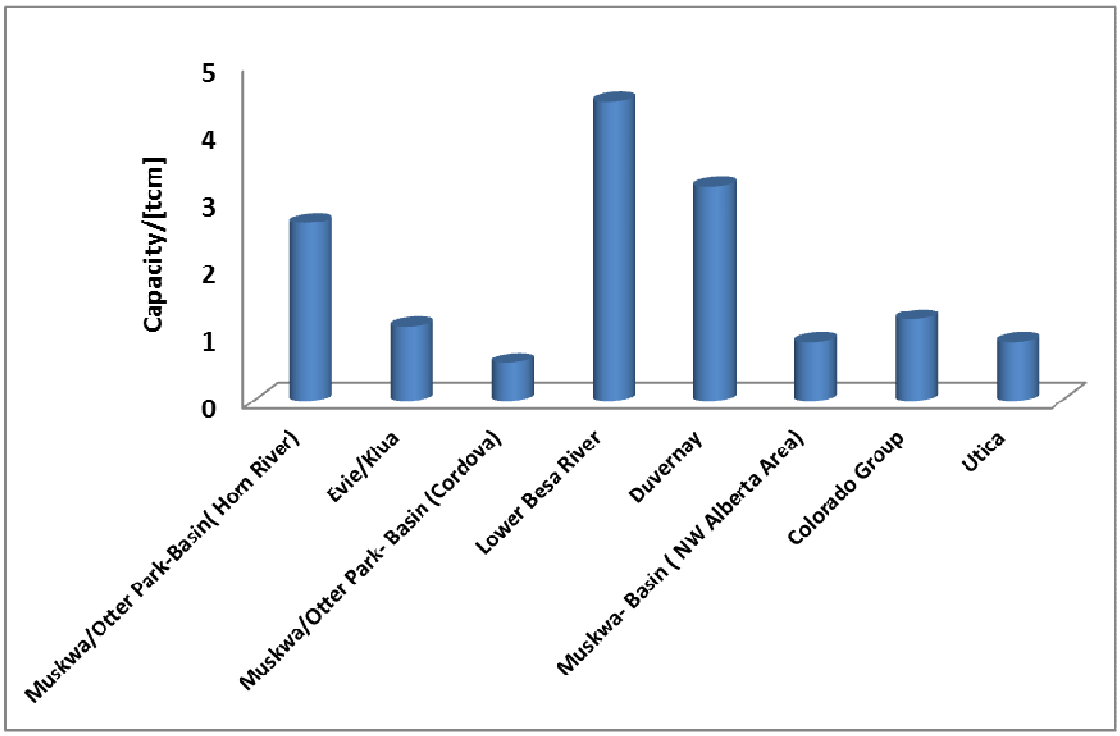

Figure 5-4 : Technically Shale Gas Reserves in Canada [11].

Eastern Europe is estimated to have ~12 Tcm of shale gas resources. This potential provides a great opportunity for Europe to decrease its dependency on natural gas imports. There have been estimates that Poland, for example, would not need to import natural gas for 300 years at the country's current level of use if shale gas reserves were exploited to meet demand [19]. Recently, intense shale gas exploration has occurred in Poland [27] with over 42 wells drilled. Kiersnowski and Dyrka [28] present a brief history and a comparison with other reports of shale gas resources in Poland. According to McGlade, Speirs [10], Poland and France are expected to have the largest shale gas resources among European countries. The development of shale gas has been largely unsuccessful so far in European countries [29] for several reasons [30], including uncertainty in estimating technically recoverable shale gas resources, a lack of field data, perceived environmental risks, lack of infrastructure, operational costs, water scarcity, and land access, similar to issues in the MENA region discussed earlier. The status of shale gas development as of 2013 is shown in Figure **5-6**.

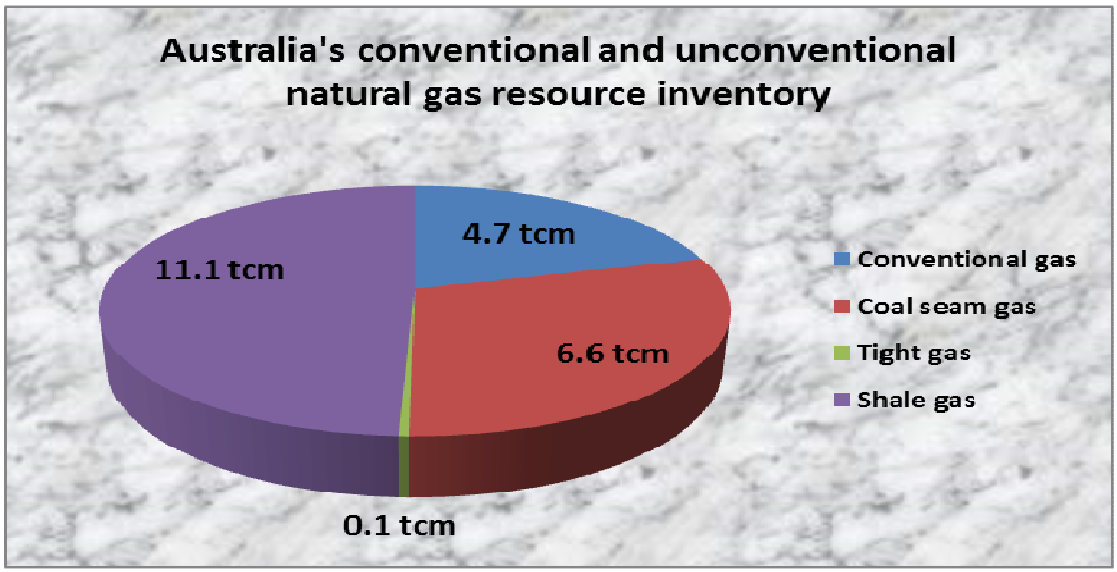

Figure 5-5: Australia's natural gas resources [26]. The differences depend on the methodology (hypotheses) used for the estimation.

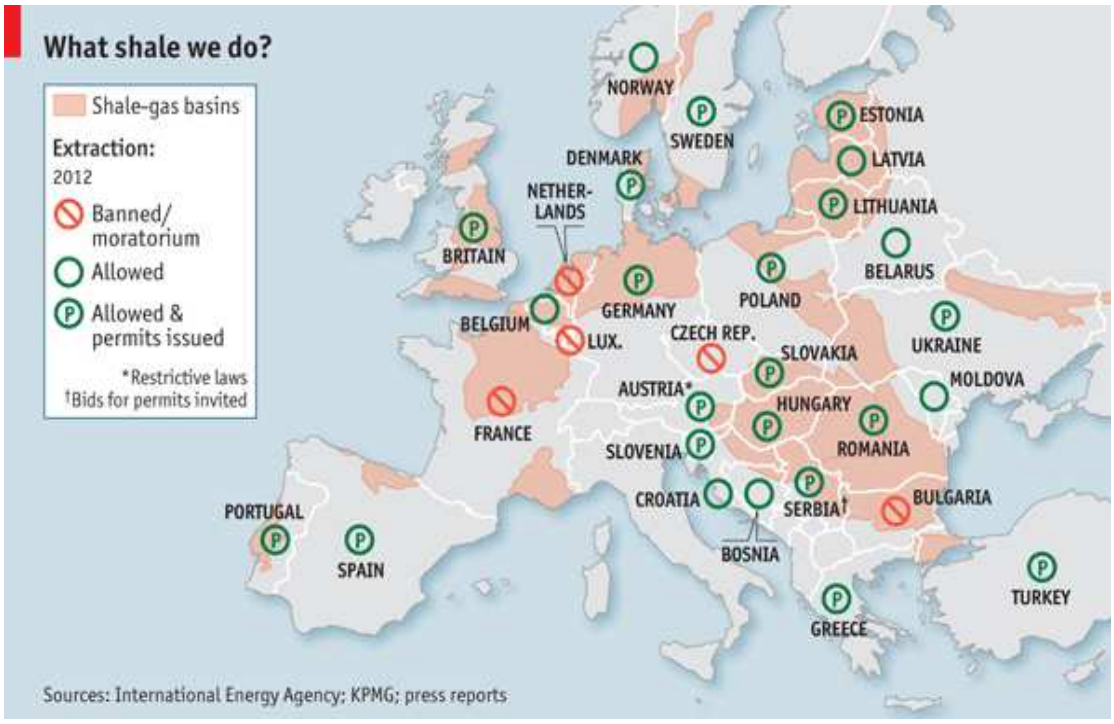

Figure 5-6: Shale gas development status in European countries (as of February 2013) in allowing or banning shale gas development [107].

5.4. TYPES OF GAS SHALES

Unconventional hydrocarbons in the context of this chapter are those hydrocarbons obtained from reservoirs difficult to produce due to physically limiting factors such as low permeability. We focus our attention on shale and tight hydrocarbon formations, with particular consideration given to natural gas. However, it is important to acknowledge that shale oil and liquids play an equally important role in the broader realm of unconventional hydrocarbons. Although the terms "shale" and "tight" are often used interchangeably, we adopt the U.S. Energy Information Administration (EIA) definitions [11] that specifically states that shale formations are a subset of all low permeability tight formations, which includes not just shales but also sandstones and carbonates. Tight gas reservoirs are geologically similar to conventional reservoirs except that they have much lower permeability of less than 0.1 millidarcy. Shale gas reservoirs have permeability three orders of magnitude (or more) lower than tight gas reservoirs [31] and also differ geologically since shale is a geological rock formation containing clay minerals and organic particles where the shale source rock is also the reservoir. Unconventional gas typically cannot be produced economically unless the well from which it is extracted is stimulated by a hydraulic fracture treatment, a horizontal wellbore, or some other technique to expose more of the reservoir to the wellbore [10, 17].

Shales are divided into dark and light forms based on organic content [32]. The dark form is organic rich whereas the light form is organic lean. A good illustration is in the United States where the Barnett shale, Marcellus shale, Haynesville shale, Fayetteville shale are dark (gray dark) shale [33]. Shale formation defining characteristics are based on age and physical characteristics, including era, period, depth and thickness. A shale gas reservoir is a fine grained shale with organic content [34]. Criteria that are important in characterizing shale gas hydrocarbon potential include: permeability, Total Organic Carbon (TOC) content, thermal maturity of the organic matter and the type of hydrocarbons available in the reservoir [35-39]. Characteristics of shale gas formations in the United States and Canada are summarized in (see Table **5-3**). This suggests that each shale reservoir is unique with regard to the optimal approach to drilling, completion, production and evaluation. Shale gas is a dry gas in many formations albeit some reservoirs produce wet gas. To clarify the terms dry and wet in quantitative measures, dry natural gas is primarily a CH_4 vapor with less than 0.014m^3 of gasoline vapor per 28.32m^3 Wet natural gas contains liquid natural gases (LNGs), such as ethane and butane, in the gas at concentrations of more than 0.014m^3per 28.32m^3 [19]. The gas from shale is generated in two ways: thermogenic (generated from cracking of organic matter or the secondary cracking of oil), and biogenic (generated from microbes such as in the Antrim shale gas field in Michigan) [40]. Mature organic matter typically generates the most gas in the formation. Gas in the formation is

in sorbed and free phases. Thermal maturity, the thickness of organic shale and TOC are effective parameters for the economic viability of a shale gas play. The required thickness to economically develop a shale gas target may decrease by improving and developing drilling and completion techniques [19]. For a more detailed discussion of shale gas geology, see Bruner and Smosna [41].

Table 5-3: Shale Gas Formations in the United States and Canada with their Characteristics [35-39] Characterization of shales is provided by Total Organic Carbon (TOC) and Vitrinite Reflectance (VR). VR indicates maturity of the organic matter and the onset of oil generation in hydrocarbon source rocks is generally correlated with a VR of 0.5-0.6% and the termination of oil generation with VR of 0.85-1.1%. The onset of gas generation is typically associated with VR values of 1.0-1.3% and terminates around 3.0%.

Formation	Period	Location	TOC wt%	Vitrinite Reflectance	Color
Antrim Shale	Late Devonian	Michigan Basin, US	0.5-24	0.4-0.6	Black
Barnett Shale	Mississippian	Fort Worth and Permian Basin, US	3.2	2.25	Dark Gray
Marcellus Shale	Devonian	New York, Ohio, Pennsylvania, West Virginia, US	3.8	1.56	Black
Haynesville Shale	Late Jurassic	Louisiana, East Texas, US	4.2	2.37	Black
Woodford Shale	Devonian-Mississippian	Oklahoma, Texas, US	2	1.51	Gray
Duvernay Shale	Devonian	Alberta, Canada	4-11	0.4-1.41	Dark Brown

5.5. CH_4 CAPACITY, CO_2 STORAGE AND ENHANCED GAS RECOVERY IN SHALES

Currently, natural gas is the third largest energy source in the world and its consumption is predicted to raise substantially in coming years [26]. From an environmental perspective, CH_4 is a hydrocarbon with a carbon footprint that is generally smaller than that of other hydrocarbons used in energy production, although various studies suggest that shale gas production and utilization may result in significant GHG emissions, depending on the total fugitive CH_4 emissions during extraction and utilization [16]. Additionally, extraction of shale gas may have negative impacts on water resources, public health, biodiversity, food supply and soil, if not adequate technical precautions are taken and there is lack of regulatory oversight.

The sorption capacity of both CO_2 and CH_4 on shales is important to understanding the storage capacity of natural gas in different type of shales, as well as the extent to which CO_2 can displace CH_4 in EGR. Shale gas is a combination of sorbed and free natural gas, which is mainly composed of methane (CH_4) and to a much lesser extent ethane, propane and other gases [42, 43]. The sorption capacity of shales is affected by its TOC content, clay minerals and micropore structure.

There is a large body of literature investigating the sorption capacity [44-65]. Beaton et al. [66] measured CH_4 sorption isotherms on several shale samples from Alberta. They showed that the data could be fitted by a Langmuir isotherm. The samples originated from depths between 2,000 and 3,000 m in western Canada at in situ temperatures between 60 and 80° C. They illustrated that maximum sorption capacities of CH_4 vary between 0.012and 0.029 mmol/g. Weniger et al. [67] studied the gas sorption behavior of CH_4 and CO_2in coals and shales in the Parana Basin, Brazil. They demonstrated a correlation between the sorption capacity and the TOC. They found for sorbed CH_4 that $[CH_4]_{ads}$ = 0.009 TOC(%) + 0.026 (mol/kg), but that $[CO_2]_{ads}$ = 0.008 TOC(%) + 0.183 (mol/kg). Therefore, the sorption capacity on mineral matter for CO_2 is much stronger but not very dependent on the TOC. The TOC, however, is the dominating factor for CH_4 sorption. Wang et al. [42] investigated the CH_4 sorption capacity of Paleozoic shales from the Sichuan Basin, China.

Table 5-4: CH_4 sorption amount on shale. The effects are shown with three abbreviation s: TOC: Total Organic Content, V: Volumetric and M: Manometric.

Author	**Year**	**Gas**	**Sample**	**Method**	**CH_4 sorption capacity**
Ross and Marc Bustin [104]	2007	CH_4	Shale	V	0.002 mmol/g
Ross and Marc Bustin [60]	2008	CH_4	Shale	V	0.4 to 4 cc/g at T=30° C
Weniger et al. [67]	2010	CH_4	Shale	M	=0.009 TOC(%) + 0.026 mmol/g
Chareonsuppanimit et al. [105]	2011	CH_4	Shale	V	=0.035 mmol/g at T=55° C
Gasparik et al. [55]	2012	CH_4	Shale	M	0.05 to 0.3 mmol/g at T=65° C
Gasparik et al. [56]	2013	CH_4	Shale	M	For carboniferous sample, 0.03 to 0.09 at T=65° C and different TOC
Rexer et al. [106]	2013	CH_4	Shale	M	0.042-0.176 mmol/g at T=27 to T=200° C
Khosrokhavar et al. [62]	2014	CH_4	Shale	M	0.02-0.04 mmol/g at T=30 ,40 and 63° C

They showed that the TOC content is the controlling factor for CH_4 sorption capacity in these shales. CH_4 sorption experiments were carried out by Zhang et.al [58] on clay-rich rocks at 35° C, 50° C and 65° C, and at CH_4 pressure up to 15 MPa under dry conditions. The experimental results illustrate that the clay mineral type greatly affects CH_4 sorption capacity under experimental conditions. In terms of relative CH_4 sorption capacity: montmorillonite ≫ illite/smectite mixed layer > kaolinite > chlorite > illite. Physisorption is the dominant process for CH_4 absorption on clay minerals and, as a result, in the clay-mineral dominated rocks exist a

linear correlation between CH_4 sorption capacity and surface area. Ross and Marc Bustin [60] showed the effect of shale composition, pore structure and CH_4 sorption for potential shale gas reservoirs in the Western Canadian Sedimentary Basin (WCSB). They demonstrate that CH_4 sorption on dried and moisture equilibrated shales increases with total organic carbon (TOC) content. The results of recent work are summarized in Table 5-4.

In various studies the total CO_2 storage capacity of unmineable coalbeds is estimated to range between 100 and 300 Gt CO_2 [68] and the total storage capacity of deep saline aquifers is estimated to range between 1000 and 10,000 Gt CO_2 [68]. Gas-bearing shales are also a strong candidate for CO_2 storage. To illustrate the importance of shale formations for CO_2 storage, we can refer to work done concerning the Netherlands. The Dutch resource of shale gas is estimated between 48,000 and 230,000 Bcm and if one assumes that technology can be developed to store 1 m^3 of CO_2 for 1m^3 of CH_4 produced and that only one percent of the resource can be recovered, a substantial 480-2,300 Bcm of CO_2, corresponding to 0.9 to 4.35 Gton CO_2, could be stored [69]. This compares very favorably with the annual Dutch emission of 0.17 Gton/year and would allow for several decades of the Dutch yearly CO_2 emissions to be stored [69]. This indicates the potential importance of CO_2 storage in geological formations, and many studies have been undertaken on this topic [70-91]. Methods have been proposed to decrease CO_2 emission through storage in geological formations and criteria for the site selection for CO_2 sequestration in geological formations have been given by [84]. Nuttal et al. [87] estimated the CO_2 sequestration capacity in the organic-rich Devonian black shales in the Big Sandy gas field of Eastern Kentucky to be about 6.8 Gt. Gas sorption behaviour of Muderong shales in Australia were investigated by [85, 86]. Their experiments indicate significant CO_2 storage capacity in the shale formations. For Belgium black shale, Khosrokhavar et al. [62] investigated the sorption capacity for CO_2 is about 7.9 kg/ton of the formation, while Busch et al. [85] showed the sorption capacity for CO_2 is 5.5 kg/ton of the formation for dry samples. These results are consistent with those by Weniger [67], discussed previously regarding the gas sorption behavior of CH_4 and CO_2 in coals and shales in the Parana Basin, Brazil.

Godec et al. [89], based on numerical investigation, concluded that the maximum CO_2 storage capacity for eastern U.S. shale gas is 1.12 million metric tons per square kilometer, and the sorbed CO_2 storage capacity is estimated to be 0.72 million metric tons per square kilometer. The total CO_2 storage capacity of organic-rich shales at supercritical conditions as a function of pore pressure was measured by Kang et al. [92] by considering the pore compressibility and sorption effects. The results state that kerogen, the organic part of the shale, acts as a molecular sieve and accounts for the gas sorption on shales.

5.6. ENHANCED GAS RECOVERY IN SHALES

The most work on sequestration of CO_2 in depleted gas reservoirs is based on storage. Recently some studies have illustrated that CO_2 injection can be considered as a method of EGR [93-96]. The injection of CO_2 may increase the rate and the volume of natural gas recovered from a reservoir [95, 97] as CO_2 can be trapped in shale gas through sorption onto organic materials and clay minerals as a sorbed gas with the parallel displacement of natural gas. Nuttall et al. [95] showed that continuous CO_2 injection (300 tons) over a period of 45 days can lead to significant improvement in recovery. As previously discussed, shale gas formations include organic materials. Large amounts of sorbed natural gas could be stored by organic materials from 20% to 80% of original-gas-in-place. Recent work demonstrates that CO_2 could displace CH_4 with up to a 5:1 ratio on a molecule-by-molecule basis [98] or 14:1 on a mass basis. 1 kg of CH_4 produces approximately 55 MJ [99] of energy. To store 1 kg of CO_2, 1MJ is consumed [100] on compression costs. This suggests that for storage, 55 MJ of energy [99] is obtained while spending only about 14MJ of energy for compression, indicating the potential benefit of EGR from an energy balance perspective. If we take into account the consumption of energy in separation of CO_2 in CCS projects, there is still a net energy gain, even considering storage of CO_2 [100]. This means that by storing CO_2 in a shale gas formation, chances for gas recovery increase without significant energy penalty, and this benefit is in addition to those previously discussed regarding storage of CO_2 in shales as opposed to saline aquifers. Godec et al. [101] showed that by injecting CO_2 in the Marcellus shale in the Eastern United States, a 7% enhancement in gas production can be realized. Al-Hasami et al. [102] investigated the main criteria for CO_2 EGR and found that the density of CO_2 is 2 to 6 times greater than CH_4 at reservoir conditions and this caused the effect of gravity to accelerate the displacement of CH_4. The dissolution of CO_2 in water is higher than the solubility of CH_4 in water and this helps to delay CO_2 breakthrough. The mobility ratio and viscosity of CO_2 are other important parameters for CO_2 EGR projects. Recently, Ishida et al. [103] investigated the application of CO_2 in hydraulic fracturing and found that use of CO_2 may decrease the environmental risk (i.e., contaminated water) and increase the production rate. As a final and critically important consideration, CO_2 EGR projects are only economically feasible when an available supply of CO_2 is close to the shale gas formation as this decreases the cost of infrastructure, transportation, and operation [97].

5.7. CONCLUSIONS

Carbon capture and storage to mitigate the impact of CO_2 emissions from the power and industrial sectors receives increased interest in importance, and sequestration of CO_2 in shale gas formations has significant potential. Shales are widely distributed. Fracked shales have

infrastructure in place that can be used for CO_2 storage. The CO_2 storage in shale formations has reduced potential for induced seismicity relative to CO_2 storage in saline aquifers. Furthermore, EGR using CO_2 presents an interesting opportunity to produce a relatively clean burning fuel while simultaneously promoting environmental sustainability through CO_2 storage. We recognize, however, that various studies suggest that shale gas production and utilization may result in significant GHG emissions depending on the total fugitive CH_4 emissions during extraction and utilization. Additionally, extraction of shale gas may have negative impacts on water resources, public health, biodiversity, food supply and soil without adequate technical precautions and regulatory oversight. Hence, EGR and storage of CO_2 in shale gas formations must be further explored before the environmental benefits can be decisively concluded.

As discussed, technically recoverable shale gas is abundant globally, although only the United States and Canada have made substantial progress in the development and production of shale gas reservoirs. Several countries with substantial technically recoverable shale gas, such as China and countries in the MENA region, are struggling not only with technical challenges for shale gas development, but also financial and regulatory challenges. Nonetheless, there is a great global opportunity for developing large, economically recoverable shale gas resources, and so it is necessary to investigate now how such reservoirs may perform for both CO_2 storage and EGR. Our review of the literature on this topic suggests that CO_2 storage and EGR are viable, yet dependent on shale physical characteristics. Hence, knowledge of shale properties is critical to assessing the economic viability of CO_2 storage in shales.

The literature review in this chapter indicates that shales are in fact a good medium for CO_2 storage with capacities of 5 to 10 kg/ton of formation or approximately 1 million metric tons per square kilometer. This level of storage capacity suggests a substantial opportunity for CO_2 storage in shales. The opportunity for CO_2 storage in shales via EGR becomes even more attractive as significant energy can be extracted with relatively modest energy input. As discussed in this chapter, EGR can be used to exploit the high affinity of shales for CO_2 relative to CH_4 (14:1 on a mass basis).

Although widespread exploitation of shale gas resources and the long-term economic viability of carbon capture and storage are not certain, the state of knowledge regarding geologic storage of CO_2 and EGR in shale formations needs to be improved in order to make these processes viable as the extraction of gas from shale resources gains traction globally. Based on the studies reviewed and information presented in this chapter, we conclude that there is a very good opportunity globally regarding the future of geologic storage of CO_2 in depleted shale gas formations and as a part of EGR operations.

5.8. REFRENCES

1. British Petroleum, BP Energy Outlook 2030, 2013.
2. Exxon Mobil, The Outlook for Energy: A View to 2040, 2013.
3. Shell, New Lens Scenarios: A Shift in Perspective for a World in Transition, 2013.
4. International Energy Agency, CO_2 Emissions From Fuel Combustion: Highlights (2013 Edition), International Energy Agency: France. 2013.
5. IPCC, IPCC, 2014: Summary for Policymakers, in Climate Change 2014, Mitigation of Climate Change, O. Edenhofer, et al., Editors. 2014, Contribution of Working Group III to the Fifth Assessment Report of the Intergovernmental Panel on Climate Change: Cambridge, United Kingdom and New York, NY, USA. 2014.
6. International Energy Agency, World Energy Outlook 2012., 2012, OECD Publishing.
7. Tao, Z. and A. Clarens, Estimating the Carbon Sequestration Capacity of Shale Formations Using Methane Production Rates. Environ Sci Technol, 2013. **47**(19): p. 11318-11325.
8. Rodosta, T., J. Hull, and M. Zoback, Interdisciplinary Investigation of CO_2 Sequestration in Depleted Shale Gas Formations. , 2013, U.S. Department of Energy. .
9. Nicot, J.-P. and I.J. Duncan, Common attributes of hydraulically fractured oil and gas production and CO_2 geological sequestration. . Greenhouse Gases: Science and Technology., 2012. **2**(5): p. 352-368.
10. McGlade, C., J. Speirs, and S. Sorrell, Unconventional gas – A review of regional and global resource estimates. Energy, 2013. **55**: p. 571-584.
11. Kuuskraa, V., S.H. Stevens, and K.D. Moodhe, Technically Recoverable Shale Oil and Shale Gas Resources: An Assessment of 137 Shale Formations in 41 Countries Outside the United States2013.
12. Lux Research, China shale proves difficult. http://blog.luxresearchinc.com/blog/coveragearea/china-innovation/, in Exploration And Production Journal 2013.
13. Ibrahim, R., MENA region moving ahead on shale gas. , 2013, "Manaar Energy Consulting and Project Management". Manaar Monthly Newsletter, http://www.manaarco.com/images/presentations/Manaar20Newsletter20February202013.pdf (Apr. 10, 2013).
14. Martin, A.N., The Potential Pitfalls of Using North American Tight and Shale Gas Development Techniques in the North African and Middle Eastern Environments. SPE Economics & Management, 2012. **3**(4): p. 147-157.
15. Baxter, K. "Saudi Aramco to release design tender for shale gas." MEED News, {http://www.meedinsight.com} (May 5, 2013). 2013.
16. Peduzzi, P. and R. Harding Rohr Reis, Gas fracking: can we safely squeeze the rocks? Environmental Development, 2013. **6**: p. 86-99.
17. Wang, Q., X. Chen, A.N. Jha, and H. Rogers, Natural gas from shale formation–The evolution, evidences and challenges of shale gas revolution in United States. Renewable and Sustainable Energy Reviews, 2014. **30**: p. 1-28.
18. Soeder, D.J., Shale gas development in the United States. In: Al-Megren, Hamid A. (Ed.), Advances in Natural Gas Technology. ISBN: 978-953-51-0507-7 (April 2012, InTech, Rijeka, Croatia, 542 pp. http://www.intechopen.com/books/advances-in-natural-gas-technology)). Advances in Natural Gas Technology. Intech, Croatia, 2012.
19. Speight, J.G., Shale Gas Production Processes., 2013, Gulf Professional Publishing: Boston. p. i-iii.
20. British Petroleum, Statistical Review of World Energy, www.bp.com,2012.
21. NPC, Prudent Development: Realizing the Potential of North America's Abundant Natural Gas and Oil Resources. National Petroleum Council, Washington, DC, ,www.npc.org. 2011.
22. GAO, Information on Shale Resources, Development, and Environmental and Public Health Risks. Report No. GAO-12-732. Report to Congressional Requesters. United States Government Accountability Office, Washington, DC. September, 2012.
23. NEB, A Primer for Understanding Canadian Shale Gas. National Energy Board, Calgary, Alberta, Canada. Accessed online at http://www.neb.gc.ca/clf-nsi/rnrgynfmtn/nrgyrprt/ntrlgs/prmrndrstndngshlgs2009/prmrndrstndngshlgs2009-eng.pdf on January 6, 2012. 2009.
24. Rivard, C., D. Lavoie, R. Lefebvre, S. Séjourné, C. Lamontagne, and M. Duchesne, An overview of Canadian shale gas production and environmental concerns. International Journal of Coal Geology, 2013. **126**: p. 64-76.
25. Lavoie, D., C. Rivard, R. Lefebvre, S. Séjourné, R. Thériault, M. Duchesne, J. Ahad, B. Wang, N. Benoit, and C. Lamontagne, The Utica Shale and gas play in southern Quebec: Geological and hydrogeological syntheses and methodological approaches to groundwater risk evaluation. . International Journal of Coal Geology, 2013. **126**: p. 77-91.

26. Leather, D.T., A. Bahadori, C. Nwaoha, and D.A. Wood, A review of Australia's natural gas resources and their exploitation. Journal of Natural Gas Science and Engineering, 2013. **10**: p. 68-88.
27. Karcz, P.a., M. Janas, and I. Dyrka, Polish shale gas deposits in relation to selected shale gas prospective areas of Central and Eastern Europe. . Przegląd Geologiczny, 2013. **61 (11)**(11).
28. Kiersnowski, H. and I. Dyrka, Ordovician-Silurian shale gas resources potential in Poland: evaluation of Gas Resources Assessment Reports published to date and expected improvements for 2014 forthcoming Assessment. 2013.
29. Geny, F., Can unconventional gas be a game changer in European markets? Oxford Institute for Energy Studies. Nat Gas Ser 2010; 46: 120. 2010.
30. Soeder, D.J., S. Sharma, N. Pekney, L. Hopkinson, R. Dilmore, B. Kutchko, B. Stewart, K. Carter, A. Hakala, and R. Capo, An approach for assessing engineering risk from shale gas wells in the United States. International Journal of Coal Geology, 2014. **126**: p. 4-19.
31. Mokhatab, S., M. ARAUJO FRESKY, and M. Rafiqul Islam, Applications of nanotechnology in oil and gas E&P. . Journal of petroleum technology, 2006. **58 (4)**(4).
32. Hosterman, J.W. and S.I. Whitlow, Munsell color value as related to organic carbon in Devonian shale of Appalachian basin. AAPG Bulletin, 1981. **65**(2): p. 333-335.
33. Blatt, H., R.J. Tracy, and B. Owens, Petrology-Igneous. Sedimentary, and Metamorphic: WH Freeman &Co., New York, 1996: p. 377-380.
34. Bustin, R., A. Bustin, A. Cui, D. Ross, and V. Murthy Pathi. Impact of shale properties on pore structure and storage characteristics. in In: SPE paper 119892 presented at the society of petroleum engineers shale gas production conference in Fort Worth, Texas; November 16–18, 2008. 2008.
35. Chalmers, G.R., R.M. Bustin, and I.M. Power, Characterization of gas shale pore systems by porosimetry, pycnometry, surface area, and field emission scanning electron microscopy/transmission electron microscopy image analyses: Examples from the Barnett, Woodford, Haynesville, Marcellus, and Doig units. AAPG bulletin, 2012. **96**(6): p. 1099-1119.
36. Fowler, M.G., M. Obermajer, and L.D. Stasiuk, Rock-Eval/TOC data for Devonian potential source rocks, Western Canada Sedimentary Basin.2003: Geological Survey of Canada, Open file 1579.
37. Montgomery, S.L., D.M. Jarvie, K.A. Bowker, and R.M. Pollastro, Mississippian Barnett Shale, Fort Worth basin, north-central Texas: Gas-shale play with multi–trillion cubic foot potential. AAPG bulletin, 2005. **89**(2): p. 155-175.
38. Wust, R., B. Nassichuk, R. Brezovski, P. Hackley, and N. Willment. Vitrinite reflectance versus pyrolysis Tmax data: Assessing thermal maturity in shale plays with special reference to the Duvernay shale play of the Western Canadian Sedimentary Basin, Alberta, Canada. in 2013 SPE Unconventional Resources Conference & Exhibition-Asia Pacific. 2013.
39. Brathwaite, L.D., Shale-deposited natural gas: a review of potential. California: California Energy Commission, 2009:33., 2009.
40. Martini, A.M., L.M. Walter, T.C. Ku, J.M. Budai, J.C. McIntosh, and M. Schoell, Microbial production and modification of gases in sedimentary basins: A geochemical case study from a Devonian shale gas play, Michigan basin. AAPG bulletin, 2003. **87**(8): p. 1355-1375.
41. Bruner, K.R. and R. Smosna, A Comparative Study of the Mississippian Barnett Shale, Fort Worth Basin, and Devonian Marcellus Shale, Appalachian Basin. National Energy Technology Laboratory, 2011, DOE/NETL-2011/1478.
42. Wang, S., Z. Song, T. Cao, and X. Song, The methane sorption capacity of Paleozoic shales from the Sichuan Basin, China. Marine and Petroleum Geology, 2013. **44**: p. 112-119.
43. Soeder, D.J., Porosity and permeability of eastern Devonian gas shale. SPE Formation Evaluation. 116–124. 1988.
44. Diaz-Campos, M., I.Y. Akkutlu, and C.H. Sondergeld, New pore-scale considerations for shale gas in place calculations. Society of Petroleum Engineers, Paper SPE 131772, 17p. 2010.
45. Ambrose, R.J., R.C. Hartman, M. Diaz-Campos, I.Y. Akkutlu, and C.H. Sondergeld, Shale gas-in-place calculations part I: new pore-scale considerations. SPE Journal, 2012. **17**(01): p. 219-229.
46. Shabro, V., C. Torres-Verdin, and F. Javadpour. Numerical simulation of shale-gas production: From pore-scale modeling of slip-flow, Knudsen diffusion, and Langmuir desorption to reservoir modeling of compressible fluid. in SPE-144355, paper presented at the Unconventional Gas Conference, SPE, The Woodlands, TX. 2011.
47. Slatt, R.M. and N.R. O'Brien, Pore types in the Barnett and Woodford gas shales: Contribution to understanding gas storage and migration pathways in fine-grained rocks. AAPG bulletin, 2011. **95**(12): p. 2017-2030.
48. Loucks, R.G., R.M. Reed, S.C. Ruppel, and U. Hammes, Spectrum of pore types and networks in mudrocks and a descriptive classification for matrix-related mudrock pores. AAPG bulletin, 2012. **96**(6): p. 1071-1098.
49. Chalmers, G.R. and R.M. Bustin, The organic matter distribution and methane capacity of the Lower Cretaceous strata of Northeastern British Columbia, Canada. International Journal of Coal Geology, 2007. **70**(1): p. 223-239.

50. Bowker, K.A., Barnett shale gas production, Fort Worth Basin: Issues and discussion. AAPG bulletin, 2007. **91**(4): p. 523-533.
51. Curtis, J.B., Fractured shale-gas systems. AAPG bulletin, 2002. **86**(11): p. 1921-1938.
52. Jarvie, D.M., R.J. Hill, T.E. Ruble, and R.M. Pollastro, Unconventional shale-gas systems: The Mississippian Barnett Shale of north-central Texas as one model for thermogenic shale-gas assessment. AAPG bulletin, 2007. **91**(4): p. 475-499.
53. Harris, L.D., W. de Witt Jr, and G. Colton, What are possible stratigraphic controls for gas fields in eastern black shale? Oil Gas J., 1970. **76**(14): p. p. 162–165.
54. Gasparik, M., A. Ghanizadeh, Y. Gensterblum, and B.M. Krooss, "Multi-temperature" method for high-pressure sorption measurements on moist shales. Review of Scientific Instruments, 2013. **84**(8): p. 085116.
55. Gasparik, M., A. Ghanizadeh, P. Bertier, Y. Gensterblum, S. Bouw, and B.M. Krooss, High-Pressure Methane Sorption Isotherms of Black Shales from The Netherlands. Energy & Fuels, 2012. **26**(8): p. 4995-5004.
56. Gasparik, M., P. Bertier, Y. Gensterblum, A. Ghanizadeh, B.M. Krooss, and R. Littke, Geological controls on the methane storage capacity in organic-rich shales. International Journal of Coal Geology, 2013. **123** p. 34 -51.
57. Hartwig, A. and H.-M. Schulz, Applying classical shale gas evaluation concepts to Germany—Part I: The basin and slope deposits of the Stassfurt Carbonate (Ca2, Zechstein, Upper Permian) in Brandenburg. Chemie der Erde-Geochemistry, 2010. **70**: p. 77-91.
58. Ji, L., T. Zhang, K.L. Milliken, J. Qu, and X. Zhang, Experimental investigation of main controls to methane adsorption in clay-rich rocks. Applied Geochemistry, 2012. **27**(12): p. 2533-2545.
59. Lu, X.-C., F.-C. Li, and A.T. Watson, Adsorption measurements in Devonian shales. Fuel, 1995. **74**(4): p. 599-603.
60. Ross, D.J. and R. Marc Bustin, The importance of shale composition and pore structure upon gas storage potential of shale gas reservoirs. Marine and Petroleum Geology, 2009. **26**(6): p. 916-927.
61. Zhang, T., G.S. Ellis, S.C. Ruppel, K. Milliken, and R. Yang, Effect of organic-matter type and thermal maturity on methane adsorption in shale-gas systems. Organic Geochemistry, 2012. **47**: p. 120-131.
62. Khosrokhavar, R., K.-H. Wolf, and H. Bruining, Sorption of CH_4 and CO_2 on a carboniferous shale from Belgium using a manometric setup. International Journal of Coal Geology, 2014. **128**: p. 153-161.
63. Rexer, T.F., E.J. Mathia, A.C. Aplin, and K.M. Thomas, High-pressure Methane Adsorption and Characterization of Pores in Posidonia Shales and Isolated Kerogens. Energy & Fuels, 2014. **28**(5): p. 2886-2901.
64. Gensterblum, Y., A. Busch, and B.M. Krooss, Molecular concept and experimental evidence of competitive adsorption of H_2O, CO_2 and CH_4 on organic material. Fuel, 2014. **115**: p. 581-588.
65. Amann-Hildenbrand, A., P. Bertier, A. Busch, and B.M. Krooss, Experimental investigation of the sealing capacity of generic clay-rich caprocks. . International Journal of Greenhouse Gas Control, 2013. **19**: p. 620-641.
66. Beaton, J.G. Pawlowicz, S.D.A. Anderson, H. Berhane, and a.C.D. Rokosh, Rock Eval, Total Organic Carbon and Adsorption Isotherms of the Duvernay and Muskwa Formations in Alberta: Shale Gas Data Release2010: Alberta Geological Survey, Open File Report 2010-05 .
67. Weniger, P., W. Kalkreuth, A. Busch, and B.M. Krooss, High-pressure methane and carbon dioxide sorption on coal and shale samples from the Paraná Basin, Brazil. International Journal of Coal Geology, 2010. **84**(3): p. 190-205.
68. Wilcox, J., Carbon capture2012: Springer.
69. Khosrokhavar, R., C. Schoemaker, E. Battistutta, K.-H.A. Wolf, and J. Bruining. Sorption of CO_2 in Shales Using the Manometric Set-up. in SPE Europec/EAGE Annual Conference. 2012. Society of Petroleum Engineers.
70. Class, H., A. Ebigbo, R. Helmig, H.K. Dahle, J.M. Nordbotten, M.A. Celia, P. Audigane, M. Darcis, J. Ennis-King, and Y. Fan, A benchmark study on problems related to CO_2 storage in geologic formations. Computational Geosciences, 2009. **13**(4): p. 409-434.
71. Elder, J., The unstable thermal interface. J. Fluid Mech, 1968. **32**(1): p. 69-96.
72. Ennis-King, J., I. Preston, and L. Paterson, Onset of convection in anisotropic porous media subject to a rapid change in boundary conditions. Physics of Fluids, 2005. **17**(8): p. 084107-084107-15.
73. Foster, T.D., Onset of convection in a layer of fluid cooled from above. Physics of Fluids, 1965. **8**: p. 1770.
74. Gasda, S.E., Numerical models for evaluating CO_2 storage in deep saline aquifers: Leaky wells and large-scale geological features, . Ph.D. Thesis. Available at http://arks.princeton.edu/ark:/88435/dsp01j098zb09n., 2010.
75. Riaz, A., M. Hesse, H. Tchelepi, and F. Orr, Onset of convection in a gravitationally unstable diffusive boundary layer in porous media. Journal of Fluid Mechanics, 2006. **548**: p. 87-111.

76. Walker, K.L. and G.M. Homsy, Convection in a porous cavity. J. Fluid Mech, 1978. **87**(Part 3): p. 449-474.
77. Van Duijn, C., G. Pieters, and P. Raats, Steady flows in unsaturated soils are stable. Transport in porous media, 2004. **57**(2): p. 215-244.
78. Myint, P.C. and A. Firoozabadi, Onset of convection with fluid compressibility and interface movement. Physics of Fluids, 2013. **25**: p. 094105.
79. Elenius, M.T. and K. Johannsen, On the time scales of nonlinear instability in miscible displacement porous media flow. Computational Geosciences, 2012. **16**(4): p. 901-911.
80. Pau, G.S., J.B. Bell, K. Pruess, A.S. Almgren, M.J. Lijewski, and K. Zhang, High-resolution simulation and characterization of density-driven flow in CO_2 storage in saline aquifers. Advances in Water Resources, 2010. **33**(4): p. 443-455.
81. Neufeld, J.A., M.A. Hesse, A. Riaz, M.A. Hallworth, H.A. Tchelepi, and H.E. Huppert, Convective dissolution of carbon dioxide in saline aquifers. . Geophysical research letters. , 2010. **37 (22)**(22).
82. MacMinn, C.W., J.A. Neufeld, M.A. Hesse, and H.E. Huppert, Spreading and convective dissolution of carbon dioxide in vertically confined, horizontal aquifers. Water Resources Research, 2012. **48: W11516**(11).
83. Iglauer, S., Dissolution trapping of carbon dioxide in reservoir formation brine–a carbon storage mechanism. Mass Transfer (ed.: Nakajima H), Rijeka: InTech, 2011.
84. Bachu, S., Sequestration of CO_2 in geological media in response to climate change: road map for site selection using the transform of the geological space into the CO_2 phase space. Energy Conversion and Management, 2002. **43**(1): p. 87-102.
85. Busch, A., S. Alles, Y. Gensterblum, D. Prinz, D.N. Dewhurst, M.D. Raven, H. Stanjek, and B.M. Krooss, Carbon dioxide storage potential of shales. International Journal of Greenhouse Gas Control, 2008. **2**(3): p. 297-308.
86. Busch, A., S. Alles, B.M. Krooss, H. Stanjek, and D. Dewhurst, Effects of physical sorption and chemical reactions of CO_2 in shaly caprocks. Energy Procedia, 2009. **1**(1): p. 3229-3235.
87. Nuttall, B.C., C.F. Eble, J.A. Drahovzal, and R.M. Bustin, Analysis of Devonian black shales in Kentucky for potential carbon dioxide sequestration and enhanced natural gas production. Kentucky Geological Survey Report DE-FC26-02NT41442, 2005.
88. Lahann, R., M. Mastalerz, J.A. Rupp, and A. Drobniak, Influence of CO_2 on New Albany Shale composition and pore structure. . International Journal of Coal Geology, 2013. **108**: p. 2-9.
89. Michael Godec, G.K., Robin Petrusak, and a.A. Oudinot, Assessment of Factors Influencing CO_2 Storage Capacity and Injectivity in Eastern U.S. Gas Shales. Energy Procedia, 2013. **37**: p. 6644 – 6655.
90. Khosrokhavar, R., G. Elsinga, R. Farajzadeh, and H. Bruining, Visualization and investigation of natural convection flow of CO_2 in aqueous and oleic systems. Journal of Petroleum Science and Engineering, 2014(0).
91. Bachu, S., W. Gunter, and E. Perkins, Aquifer disposal of CO_2 : Hydrodynamic and mineral trapping. Energy Conversion and Management, 1994. **35**(4): p. 269-279.
92. Kang, S.M., E. Fathi, R. Ambrose, I. Akkutlu, and R. Sigal, Carbon dioxide storage capacity of organic-rich shales. SPE Journal, 2011. **16**(4): p. 842-855.
93. Blok, K., R. Williams, R. Katofsky, and C.A. Hendriks, Hydrogen production from natural gas, sequestration of recovered CO_2 in depleted gas wells and enhanced natural gas recovery. Energy, 1997. **22**(2): p. 161-168.
94. Oldenburg, C., K. Pruess, and S.M. Benson, Process modeling of CO_2 injection into natural gas reservoirs for carbon sequestration and enhanced gas recovery. Energy & Fuels, 2001. **15**(2): p. 293-298.
95. Schepers, K.C., B.C. Nuttall, A.Y. Oudinot, and R.J. Gonzalez. Reservoir modeling and simulation of the Devonian gas shale of eastern Kentucky for enhanced gas recovery and CO_2 storage. in SPE International Conference on CO_2 Capture Storage and Utilization. SPE 126620, 2009. . 2009. Society of Petroleum Engineers.
96. Câmara, G., C. Andrade, A. Silva Júnior, and P. Rocha, Storage of carbon dioxide in geological reservoirs: is it a cleaner technology? Journal of Cleaner Production, 2013. **47**: p. 52-60.
97. Regan, M., A Review of the Potential for Carbon Dioxide (CO_2) Enhanced Gas Recovery in Australia. Cooperative Research Centre for Greenhouse Gas Technologies, Canberra. CO_2CRC Publication No: RPT07-0802. 39p, 2007.
98. Liu, F., K. Ellett, Y. Xiao, and J.A. Rupp, Assessing the feasibility of CO_2 storage in the New Albany Shale (Devonian–Mississippian) with potential enhanced gas recovery using reservoir simulation. International Journal of Greenhouse Gas Control, 2013. **17**: p. 111-126.
99. Perry, R.H., D.W. Green, and J.O. Maloney, Perry's chemical engineer's handbook, in Perry's chemical engineer's handbook1984, McGraw-Hill Book.

100. Iijima, M., T. Nagayasu, T. Kamijyo, and S. Nakatani, MHI's Energy Efficient Flue Gas CO_2 Capture Technology and Large Scale CCS Demonstration Test at Coal-fired Power Plants in USA. . Mitsubishi Heavy Industries Technical Review 2011. **48**(1): p. 26-32.
101. Godec, M., G. Koperna, R. Petrusak, and A. Oudinot, Potential for Enhanced Gas Recovery and CO_2 Storage in the Marcellus Shale in the Eastern United States. . International Journal of Coal Geology, 2013. **118**: p. 95-104.
102. Al-Hasami, A., S. Ren, and B. Tohidi. CO_2 injection for enhanced gas recovery and geo-storage: reservoir simulation and economics. in SPE Europec/EAGE Annual Conference. Society of Petroleum Engineers Inc., Madrid, Spain. http://dx.doi.org/10.2118/94129-MS 2005.
103. Ishida, T., K. Aoyagi, T. Niwa, Y. Chen, S. Murata, Q. Chen, and Y. Nakayama, Acoustic emission monitoring of hydraulic fracturing laboratory experiment with supercritical and liquid CO_2. Geophysical Research Letters, 2012. **39 L16309**(16).
104. Ross, D.J. and R. Marc Bustin, Impact of mass balance calculations on adsorption capacities in microporous shale gas reservoirs. Fuel, 2007. **86**(17): p. 2696-2706.
105. Chareonsuppanimit, P., S.A. Mohammad, R.L. Robinson Jr, and K.A. Gasem, High-pressure adsorption of gases on shales: Measurements and modeling. International Journal of Coal Geology, 2012. **95**: p. 34-46.
106. Rexer, T.F., M.J. Benham, A.C. Aplin, and K.M. Thomas, Methane adsorption on shale under simulated geological temperature and pressure conditions. Energy & Fuels, 2013. **27**(6): p. 3099-3109.
107. Economist, http://www.economist.com/news/business/21571171-extracting-europes-shale-gas-and-oil-will-be-slow-and-difficult-business-frack-future. 2013.
108. Weijermars, R., US shale gas production outlook based on well roll-out rate scenarios. Applied Energy,2014.**124**:p.283-297.

Chapter 6

Conclusions

The work described in this thesis deals with a variety of aspects related to the storage of carbon dioxide in geological formations. In particular we focus on the transfer between the gas phase to a fluid or solid phase. It is asserted that the transfer considerably enhances the storage capacity in geological formations. The main conclusions are first summarized before the chapter wise conclusions are repeated for the ease of reference. First, we deal with dissolution in fluid phases. A transparent Schlieren set-up was built to visualize the movement of carbon dioxide in a high pressure cell (64-84 bar) when carbon dioxide was brought above a fluid layer. This aspect is described in chapter 2. It is able to qualify, experimentally and numerically, the mass transfer rate of CO_2 to water (brine) and oil. It shows that in high salinity solution enhanced transfer due to natural convection still occurs, but is less than for less concentrated solutions. The occurrence of natural convection also occurs when the brine is replaced by an oleic phase. A qualitative comparison was made between numerical simulations and Schlieren results. We also corroborated the occurrence of enhanced transfer of carbon dioxide in porous media. A unique feature of the experimental set up is that it operates at constant pressures. Also here the salinities were varied and the same reduction with salinity as in the Schlieren set up was illustrated. Secondly we deal with the sorption mechanisms on shales. It is shown that the manometric set-up can accurately (as inferred from the Monte Carlo method) determine the sorption capacity. Our measurements indicate that shales comprise a significant sorption capacity for carbon dioxide. Indeed, the result of our measurement is used to review the potential of shales for carbon dioxide storage. Finally we review shale gas formations globally and demonstrate obstacles and opportunities for shale gas development. The thesis consists of four published/ submitted papers. Sections 6.1 to 6.4 summarize the main results of this thesis.

6.1.: VISUALIZATION AND NUMERICAL INVESTIGATION OF NATURAL CONVECTION FLOW OF CO_2 IN AQUEOUS AND OLEIC SYSTEMS

- Dissolution of CO_2 in an aqueous (or oleic) phase forms a mixture that is denser than the carbon dioxide free water or brine (oleic phase). This causes a local density increase, which induces natural convection currents (gravity fingers) when gaseous carbon dioxide is brought above the liquid phase. This enhances the rate of mixing of CO_2 in the liquid phase.
- We designed and built a cylindrical transparent high pressure cell in which gravity induced fingers (playing a major role in the enhanced mixing process) could be observed, e.g., by mounting the cylinder horizontally and filling the bottom half with liquid and the top-half with gaseous or supercritical carbon dioxide.
- We developed a Schlieren set-up that can be used to observe the gravity induced fingers based on refractive index variations. Gravity fingers have been observed in an aqueous phase with various concentrations of sodium chloride (0-25 w/w %) or with an oleic phase (n-decane). The experiments show that natural convection currents are weakest in highly concentrated brine and strongest in oil.
- The Schlieren pattern consists of a dark region near the equator and a lighter region below it. The dark region indicates a region where the refractive index increases downward, either due to the presence of a gas liquid interface, or due to the thin diffusion layer, which also appears in numerical simulations.
- It is possible to use commercial software (COMSOL Multiphysics) to simulate the natural convection process in 3-D albeit with grid cells that are too large to capture the mm-scale fine structure of the gravity fingers. As the distance between the windows is 11.6 mm it can be expected that the concentration is not uniform in the axial direction. This leads initially to a scattering region with a lighter appearance in the Schlieren pattern. For later times the erratic behavior decreases and the effect of individual gravity fingers can be observed.
- To our knowledge this is the first time that gravity fingers in the oil phase are visualized. The set-up can screen any fluid for its relative importance of natural convection flows.

6.2. EFFECT OF SALINITY AND PRESSURE ON THE RATE OF MASS TRANSFER IN AQUIFER STORAGE OF CARBON DIOXIDE

- Dissolution of CO_2 in an aqueous phase forms a mixture that is denser than the carbon dioxide free water or brine. This causes a local density increase, which induces natural convection currents (gravity fingers) when gaseous carbon dioxide is brought above the liquid phase. This enhances the rate of mixing of CO_2 in the liquid phase.
- We designed and built a cylindrical high pressure cell in which gravity induced fingers (playing a major role in the enhanced mixing process) could be occurred, e.g., by mounting the cylinder horizontally and filling the 90% with sand pack (k=59 Darcy and porosity =40%) and then saturate it with water or brine and the top with gaseous or sub-supercritical carbon dioxide at constant pressure.
- The experiments show that natural convection currents are weakest in highly concentrated brine and strongest in pure water.
- The experiments show that CO_2 consumption is bigger in subcritical than supercritical condition.
- The experimental results propose a semi linear relation between mass transfer rate and Rayleigh number.
- To our knowledge, this is the first time that such of experiments are carried out at constant pressure injection in the lab scale with considering the effect of salinities.

6.3. SORPTION OF CH_4 AND CO_2 ON BELGIUM CARBONIFEROUS SHALE USING A MANOMETRIC SET-UP

- It is possible to use the manometric set-up to accurately measure excess sorption of CO_2 and CH_4 on Belgian carboniferous black shale at temperatures of 308, 318 and 336 K and in a pressure range between 0- 105 bar.
- The CO_2 excess sorption isotherm shows an initial increase to a maximum value of 0.175 ± 0.004 mmol/gram-shale before it starts to decrease until it becomes zero at 82 bar, which can be converted using the Span-Wagner EOS to a gas-density of 255 kg/m^3. Subsequently the excess sorption becomes negative.
- The CH_4 excess sorption isotherm at 308 K shows an initial increase to a maximum value of 0.0392 ± 0.003 mmol/gram-shale. The CH_4 excess sorption isotherm at 318 K shows an initial increase to a maximum value of 0.022 ± 0.006 mmol/gram-shale before it

decreases until it becomes zero at 104 bar. Subsequently the excess sorption becomes negative. We see the same behaviour for CH_4 sorption at 336 K; however, its maximum is about 0.014±0.005 mmol/ gram-shale. As expected the CH_4 excess sorption isotherm at 308K is the largest. Indeed, the experiments on CH_4 show a decreasing sorption at increasing temperature. In comparison to the experiment that we have done for CO_2 at 318 K, the amount of excess CO_2 sorption is about 7 times higher than CH_4 sorption. It validates the idea that sorption capacity of CO_2 is much higher than of CH_4.

6.4. Shale Gas Formations and Their Potential for Carbon Storage: Opportunities and Outlook

- Carbon capture and storage to mitigate the impact of CO_2 emissions from the power and industrial sectors receives increased interest in importance, and sequestration of CO_2 in gas shale formations has significant potential. Shales are widely distributed. Fracked shales have infrastructure in place that can be used for CO_2 storage. The CO_2 storage in shale formations has reduced potential for induced seismicity relative to CO_2 storage in saline aquifers. Furthermore, EGR using CO_2 presents an interesting opportunity to produce a relatively clean burning fuel while simultaneously promoting environmental sustainability through CO_2 storage. We recognize, however, that various studies suggest that shale gas production and utilization may result in significant GHG emissions depending on the total fugitive CH_4 emissions during extraction and utilization. Additionally, extraction of shale gas may have negative impacts on water resources, public health, biodiversity, food supply and soil without adequate technical precautions and regulatory oversight. Hence, EGR and storage of CO_2 in gas shale formations must be further explored before the environmental benefits can be decisively concluded.
- As discussed, technically recoverable shale gas is abundant globally although only the United States and Canada have made substantial progress in the development and production of shale gas reservoirs. Several countries with substantial technically recoverable shale gas, such as China and countries in the MENA region, are struggling not only with technical challenges for shale gas development, but also financial and regulatory challenges. Nonetheless, there is a great global opportunity for developing large, economically recoverable shale gas resources, and so it is necessary to investigate now how such reservoirs may perform for both CO_2 storage and EGR. Our review of the literature on this topic suggests that CO_2 storage and EGR are viable, yet dependent on shale physical characteristics. Hence, knowledge of shale properties is critical to assessing the economic viability of CO_2 storage in shales.

- The literature review in this chapter indicates that shales are in fact a good medium for CO_2 storage with capacities of 5 to 10 kg/ton of formation or approximately 1 million metric tons per square kilometer. This level of storage capacity suggests a substantial opportunity for CO_2 storage in shales. The opportunity for CO_2 storage in shales via EGR becomes even more attractive as significant energy can be extracted with relatively modest energy input. As discussed in this chapter, EGR can be used to exploit the high affinity of shales for CO_2 relative to CH_4 (14:1 on a mass basis).
- Although widespread exploitation of shale gas resources and the long-term economic viability of carbon capture and storage are not certain, the state of knowledge regarding geologic storage of CO_2 and EGR in shale formations needs to be improved in order to make these processes viable as the extraction of gas from shale resources gains traction globally. Based on the studies reviewed and information presented in this chapter, we conclude that there is a very good opportunity globally regarding the future of geologic storage of CO_2 in depleted shale gas formations and as part of EGR operations.

Appendix A

Varying void volume

The purpose of this Appendix is to include the effect of a changing void volume. In practice the void volume determination is subject to uncertainties. First the void volume determined with Helium, may overestimate the void volume accessible to CO_2 and CH_4. Then the void volume can change at every time step due to the finite volume of the sorbed phase, swelling of the clays and possible reactions of the introduced gas with the minerals present in the black shale. To obtain a formulation for a changing void volume we must modify Eqs. (4. 1, 2) to

$$V_r\left(\rho_f^i-\rho_{eq}^i\right)-\left(V_v^i\rho_{eq}^i-V_v^{i-1}\rho_{eq}^{i-1}\right)=m_{ads}^i-m_{ads}^{i-1}\ , \qquad \text{(A. 1)}$$

This means that the incremental sorption requires the void volume at the previous step and at the present step. Adding the terms in Eq. 3 for *i=1...N,* where *N* are the number of steps in the experiment, leads to

$$\begin{array}{lllll}
V_r\left(\rho_f^N-\rho_{eq}^N\right) & -V_v^N\rho_{eq}^N & +V_v^{N-1}\rho_{eq}^{N-1} & = & m_{ads}^N-m_{ads}^{N-1}\\
V_r\left(\rho_f^{N-1}-\rho_{eq}^{N-1}\right) & -V_v^{N-1}\rho_{eq}^{N-1} & +V_v^{N-2}\rho_{eq}^{N-2} & = & m_{ads}^{N-1}-m_{ads}^{N-2}\\
V_r\left(\rho_f^{N-2}-\rho_{eq}^{N-2}\right) & -V_v^{N-2}\rho_{eq}^{N-2} & +V_v^{N-3}\rho_{eq}^{N-3} & = & m_{ads}^{N-2}-m_{ads}^{N-3}\\
----- & ----- & ----- & -- & -----\\
\sum_{i=1}^{N}V_r\left(\rho_f^i-\rho_{eq}^i\right) & -V_v^N\rho_{eq}^N & +0 & = & m_{ads}^N
\end{array}\ , \qquad \text{(A. 2)}$$

The final result in Eq. 4 expresses that for the computation of the cumulative sorbed mass m_{ads}^N we only need the void volume V_v^N at the present step N.

By considering the mechanisms for modifying the void volume mentioned above, we write

$$V_v^N=V_v^{N-1}-\Delta V_{sw}^N-\Delta V_{ads}^N-\Delta V_{react}^N\ , \qquad \text{(A. 3)}$$

where ΔV_{sw}^{N}, ΔV_{ads}^{N} and ΔV_{react}^{N} are the change in void volume due to swelling, sorption and reaction respectively. Using the same approach as above we can relate the void volume at the Nth step as a sum of individual void volume changes, i.e.,

$$\begin{array}{cccccc} V_v^N & = & V_v^{N-1} & -\Delta V_{sw}^{N} & -\Delta V_{ads}^{N} & -\Delta V_{react}^{N} \\ V_v^{N-1} & = & V_v^{N-2} & -\Delta V_{sw}^{N-1} & -\Delta V_{ads}^{N-1} & -\Delta V_{react}^{N-1} \\ V_v^{N-2} & = & V_v^{N-3} & -\Delta V_{sw}^{N-2} & -\Delta V_{ads}^{N-2} & -\Delta V_{react}^{N-2} \\ --- & -- & --- & --- & --- & --- \\ V_v^{N} & = & V_v^{0} & -\sum_{i=1}^{N}\Delta V_{sw}^{i} & -\sum_{i=1}^{N}\Delta V_{ads}^{i} & -\sum_{i=1}^{N}\Delta V_{reac}^{i} \end{array} , \qquad \text{(A. 4)}$$

In other words, the void volume is equal to the initial void volume corrected for all volume changes at each step, and includes volume changes due to swelling, sorption and reaction.

Summary

The work described in this thesis deals with a variety of aspects related to the storage of carbon dioxide in geological formations. In particular we focus on the transfer between the gas phase to a fluid (liquid) or solid phase. This thesis limits its interest to study the sequestration capacity of CO_2 in saline aquifers and more specifically on the mass transfer between CO_2 and the brine, show the effect of salinity and visualize the fingering of CO_2 rich brine in bulk phase outside a porous medium by applying Schlieren technique.

Furthermore, we also illustrate the importance of shale formations in the world for storing carbon dioxide and our experimental methods to measure the sorption capacity for enhanced gas recovery- EGR. To achieve our goals we designed, constructed and improved three different setups.

The main research objectives addressed in this thesis are: (1) to investigate, experimentally and numerically, the mass transfer rate of CO_2 to water (brine), oil (2) visualization of natural convection flow of CO_2 in aqueous and oleic systems, (3) to illustrate the effect of salinity on the transfer rate of CO_2 in bulk and porous media, (4) to model natural convection instability of CO_2 rich fluid flow in the bulk aqueous and oleic phase, (5) to determine the sorption capacity of shale experimentally by applying the manometric method and estimate errors based on a Monte-Carlo simulation, (6) to review shale gas formations and their potential for CO_2 storage. Each chapter is summarized as follows:

In chapter 2, we compare numerical model results with a set of high pressure visual experiments, based on the Schlieren technique, in which we observe the effect of gravity-induced fingers when sub- and super-critical CO_2 at in situ pressures and temperatures is brought above the liquid, i.e., water, brine or oil. A short description of the Schlieren set-up and the transparent pressure cell is presented. The Schlieren set-up is capable of visualizing instabilities in natural convection flows in the absence of a porous medium. The experiments illustrate that natural convection currents are weakest in the highly concentrated brine and strongest in oil. Therefore, the set-up can rank

aqueous salt solutions or oil in sequence of its relative importance of natural convection flows and the ensuing enhanced transfer. The experimental results are compared to numerical results. It is shown that natural convection effects are stronger in cases of high density differences. To our knowledge there are no visual data in the literature for natural convection flow of CO_2 in the aqueous and oleic phase in equilibrium with supercritical CO_2. Indeed, there is no available experiment for CO_2-oil. There are no data in the literature that show the presence of a diffusive boundary layer and the continuous initiation of fingers.

In chapter 3 we experimentally investigated the effect of salinity and pressure on the rate of mass transfer, for aquifer storage of carbon dioxide in porous media. There is a large body of literature that numerically and studies analytically the storage capacity and the rate of transfer between the overlying CO_2-gas layer and the aquifer below. There is, however, a lack of experimental work that address the transfer rate into a water-saturated porous medium at in-situ conditions using carbon dioxide and brine at elevated pressures. We emphasize that the experiment uses a constant gas pressure and measures the dissolution rate using a high pressure ISCO pump. It is shown that the transfer rate is much faster than predicted by Fick's law in the absence of natural convection currents.

Chapter 4 investigates the sorption of CH_4 and CO_2 in Belgian Carboniferous Shale, using a manometric set-up. Only a few measurements have been reported in the literature for high-pressure gas sorption on shales. Some recent studies illustrate that, in shale, five molecules of CO_2 can be stored for every molecule of CH_4 produced. The technical feasibility of Enhanced Gas Recovery (EGR) needs to be investigated in more detail. Globally, the amount of extracted natural gas from shale has increased rapidly over the past decade. A typical shale gas reservoir combines an organic-rich deposition with extremely low matrix permeability. One important parameter in assessing the technical viability of (enhanced) production of shale gas is the sorption capacity. Our focus is on the sorption of CH_4 and CO_2. Therefore we have chosen to use the manometric method to measure the excess sorption isotherms of CO_2 at 318 K and of CH_4 at 308, 318 and 336 K and at pressures up to 105 bar. We apply an error analysis based on Monte-Carlo simulation to establish the accuracy of our experimental data.

Chapter 5 reviews the global shale gas resources and discusses both the opportunities and challenges for their development. It then provides a review of the literature on opportunities to store CO_2 in shale, thus possibly helping to mitigate the impact of CO_2 emissions from the power and industrial sectors. The studies reviewed indicate that the opportunity for geologic storage of CO_2 in shales might be significant, but knowledge of the characteristics of the different types of

gas shales found globally is required. The potential for CO_2 sorption as part of geologic storage in depleted shale gas reservoirs must be assessed with respect to the individual geology of each formation. Likewise, the introduction of CO_2 into shale for enhanced gas recovery (EGR) operations may significantly improve both reservoir performance and economics.

In chapter 6 the main conclusions of the thesis are summarized.

Samenvatting

Het werk dat in dit proefschrift wordt beschreven gaat over verschillende aspecten die samenhangen met het opslaan van koolstofdioxide in geologische formaties. In het bijzonder richten we ons op de overdracht van gas naar vloeistof of naar een vaste fase. We beperken ons tot het bestuderen van CO_2 in reservoirs met pekel en meer specifiek tot (1) de massaoverdracht tussen CO_2 en pekel, (2) het aantonen van het effect van het zoutgehalte en (3) het visualiseren van de vorming van "vingers" van kooldioxiderijk pekel in de bulk-fase bij afwezigheid van het poreuze medium door toepassing van de Schlieren-techniek.

Bovendien, laten we ook het belang inzien van kleiformaties in de wereld voor het opslaan van kooldioxide en het belang van onze experimentele methoden om de sorptie capaciteit te meten ten behoeve van verbeterde gaswinning. Om onze doelen te bereiken, hebben wij drie verschillende opstellingen ontworpen, geconstrueerd of verbeterd.

Het voornaamste onderzoekdoelstellingen die in dit proefschrift worden nagestreefd zijn: (1) het onderzoeken, experimenteel en numeriek, van de massaoverdracht van CO_2 naar water (pekel) en olie (2) het visualiseren van natuurlijke convectiestroming van CO_2 in waterige en olieachtige systemen, (3) het illustreren van het effect van het zoutgehalte op de overdrachtssnelheid van CO_2 in de bulk-fase en poreuze media (4) het modelleren van instabiele natuurlijke convectie van kooldioxiderijke vloeistofstroming in een bulkwaterige en bulkolieachtige fase, (5) het experimenteel bepalen van de sorptiecapaciteit van schalie met de manometrische methode en het afschatten van de meetfout gebaseerd op een Monte-Carlo simulatie, (6) een overzicht te geven van schaliegas formaties en hun potentieel voor CO_2 opslag. Elk hoofdstuk wordt als volgt samengevat.

In hoofdstuk 2, vergelijken we numerieke modelresultaten met een verzameling van visuele experimenten bij hoge druk gebaseerd op de Schlieren-techniek, waarin we het effect waarnemen van door zwaartekracht veroorzaakte "vingers" indien sub-kritisch of superkritisch CO_2 bij in de ondergrond heersende drukken en temperaturen boven vloeistof, d.w.z. water, pekel of olie,

wordt gebracht. Een korte beschrijving van de Schlieren-opstelling en de doorzichtige druk-cel wordt gegeven. De Schlieren-opstelling is in staat instabiliteiten te visualiseren in natuurlijke convectiestroming in afwezigheid van een poreus medium. De experimenten tonen aan dat natuurlijke convectie het zwakste is in hoge concentratie pekel en het sterkste in olie. Daarom kan de opstelling zoutoplossingen en olie rangschikken in volgorde van het relatieve belang van natuurlijke convectiestroming en de daaruit voortvloeiende versnelde massaoverdracht. De experimentele resultaten worden vergeleken met numerieke resultaten. Het blijkt dat natuurlijke convectie-effecten sterker zijn bij hogere drukverschillen. Voor zover wij weten bestaan er geen visuele gegevens in de literatuur voor natuurlijke convectiestroming van CO_2 in de waterige of olieachtige-fase in evenwicht met superkritisch CO_2. Inderdaad bestaat er in de literatuur geen experiment dat de aanwezigheid bevestigt van een diffusieve grenslaag en de voortdurende initiatie van “vingers”.

In hoofdstuk 3 onderzochten wij experimenteel het effect van het zoutgehalte en druk op de massaoverdrachtssnelheid, ten behoeve van opslag van kooldioxide in watervoerende lagen. Er is een groot stuk literatuur dat de opslagcapaciteit en de overdrachtssnelheid tussen een CO_2 gas-laag en de watervoerende laag daaronder bestudeert. Er is, echter, een gebrek aan experimenteel werk dat gaat over de overdrachtssnelheid naar een met water verzadigd poreus medium onder veldomstandigheden bij gebruik van koolstofdioxide en pekel bij verhoogde drukken. We benadrukken dat ons experiment plaatsvindt bij constante druk en de overdrachtssnelheid meet met een hogedruk ISCO pomp. Het blijkt dat de overdrachtssnelheid veel sneller is dan voorspeld met de wet van Fick in afwezigheid van natuurlijke convectie stromingen.

In hoofdstuk 4 onderzoeken wij experimenteel, de sorptie van CH_4 en CO_2 in Belgische schalie uit het carboon met behulp van een manometrische opstelling. Er zijn slechts enkele metingen in de literatuur beschreven van hoge druk gas sorptie in schalies. Sommige recente studies laten zien dat in schalie vijf moleculen CO_2 kunnen worden opgeslagen voor elk geproduceerd CH_4 molecuul. De technische haalbaarheid van verhoogde gaswinning (EGR) moet in meer detail worden onderzocht. De hoeveelheid gas, wereldwijd onttrokken aan schalie, is de laatste tien jaar sterk gestegen. Een typisch schaliegas reservoir bestaat uit een organisch-rijke afzetting in een reservoir met een extreem lage matrix permeabiliteit. Een belangrijke parameter om de technische haalbaarheid in te schatten van verhoogde gaswinning uit schaliegas is de sorptie capaciteit. Onze belangstelling gaat uit naar de sorptie van CH_4 en CO_2. Daarom hebben we gekozen voor de manometrische methode om de “excess sorption” isothermen van CO_2 bij 318 K en van CH_4 bij 308, 318 en 336 K en bij drukken tot 105 bar te bepalen. We passen een fouten

analyse toe gebaseerd op een Monte-Carlo simulatie om de nauwkeurigheid van onze experimentele gegevens te bepalen.

Hoofdstuk 5 geeft een overzicht van de wereldwijde schaliegasvoorkomens en bespreekt zowel de mogelijkheden en uitdagingen voor schaliegaswinning. Vervolgens geeft het een literatuuroverzicht van de mogelijkheden om CO_2 in schalies op te slaan en zodoende mogelijkerwijs bij te dragen om de schade van CO_2 emissies van de energie- en industriële sectoren te verzachten. De studies waarvan een overzicht is gegeven wijzen aan dat de mogelijkheid voor geologische opslag van CO_2 in schalies significant is, maar dat kennis is vereist van de karakteristieken van de verschillende types gasschalies die wereldwijd worden gevonden. Het potentieel van CO_2 sorptie als onderdeel van geologische opslag in leeg-geproduceerde gas reservoirs moet worden geschat in vergelijking met de specifieke geologie van elke formatie. Op dezelfde manier kan de introductie van CO_2 in schalie voor verbeterde gaswinningsoperaties (EGR), zowel de winning als de economie verbeteren.

Hoofdstuk 6 geeft een samenvatting van de conclusies van het proefschrift.

Acknowledgments

I would like to express my special appreciation and thanks to my family, friends and colleagues for their love, encouragement, support and advice during PhD period. I would like to take this opportunity to express my gratitude.

First and foremost, I would like to state special thanks to my supervisors Prof. Hans Bruining and Dr. Karl- Heinz for giving me the opportunity to fulfil my PhD research at Delft University of Technology. Hans, I would like to express my sincere gratitude to you for your persistence, knowledge, guidance, dedication and support during my research. Karl- Heinz, working with you has had a benefit of not only attaining technical knowledge and being supported in the lab but also getting familiar and learning the way of dealing with different projects related to CO_2 sequestration subject. I am also very grateful to my supervisors for their scientific advice, technical suggestions and insightful discussions during our meetings.

I am thankful to Dr. Rouhi Farajzadeh for his collaboration, helpful comments and suggestions during our friendly discussions. I would like to thank to Dr. Gerrit Elsinga, Prof. Steve Griffiths and Dr. Andreas Busch for all supports, contribution and kind attention during my PhD. I would like to acknowledge the rest of the examination committee members: Prof. Pacelli Zitha, Prof. Rien Herber, and Prof. Chris Spiers for participating in my Ph.D. defence and giving valuable comments.

I would like to thank Henk Van Asten, Marc Friebel and Michiel Slob for supporting and helping me with different experimental part of my thesis. Henk, all of my experiments certainly would not have been possible without your professional help, technical expertise and guidance in Dietz lab. I truly enjoyed working with you and the chatting we had during the experiments always renewed my vigor and has challenged my ideas. I would like to appreciate Marc Friebel for being very supportive during the novel experiments in Hydro-dynamic lab in 3ME, which led to an intimate friendship. I would also like to acknowledge other technicians who helped me, "Dick, Ellen, Jan, Jolanda, Pual and Wim" in Dietz Lab. I would like to thank Karel, for all his support during my Ph.D.

My special thanks go to the secretaries and administrative side of Geoscience and Engineering department, Anke, Asha, Hannie, Lydia, Margot, Marja, Marijk, Marlijn and Ralf for their welcoming support with administrative works from the first day of my PhD. Hannie, thanks a lot for always being kind and supportive. Lydia, Margot, and Marlijn, thanks for your consideration and all kindness.

I am also thankful to Prof. Ruud Weijermars for giving me the opportunity to cooperate with him as assistant editor in Energy strategy Review Journal. I appreciate head of SPE chapter in the Netherlands, Ruud Camphuysen, for his support and consideration while I was a member of board and vice president of SPE chapter at Delft University of Technology.

I want to appreciate all my friends around the world for their time and nice chatting we had despite the distance and time difference. I would also be always grateful to my friends in the Netherlands and colleagues of Petroleum engineering section, Geoscience and Engineering department that I shared propitious and memorable moments with them. Regrettably, I cannot acknowledge them by name. I owe my gratitude to my former teachers, instructors and supervisors during wonderful years of studying back home. I would like to convey my heartfelt thanks to my home university, Amirkabir University of Technology (Tehran Polytechnic) for offering me an ideal environment.

Last but not least, I would like to express my warmest feelings and special thanks to my wife, my father, my mother, my brother and my sisters for their sincere encouragement and inspiration throughout my research work. I owe everything to them. I would like to thank my lovely wife, Negar for being there for me during all my difficult times with her abundant patience and love. Most of all, thank you for being my soulmate and best friend. Your love and support without any complaint or regret has enabled me to complete this Ph.D. thesis. I am very grateful for my great parents. Their understanding, care and love encouraged me to work hard and never bend to difficulty. Mama and PaPa, I am always proud of you. You have been a constant source of strength and inspiration, which motivates me to work harder and do my best. My great thanks are extended to my brother, Ramin and my sisters, Roya and Rana for their loving, supportive and encouraging presence in my life. I love you all so much, and I would not have made it this far without you. My lovely and cute niece, Golmehr and nephew, Radmehr have brought happiness to my life. They always knew when to call me at just the right time.

Roozbeh Khosrokhavar,

Delft, October 2014

Propositions

1. Growing concern about global warming is the main reason for increased interest in the geological storage of carbon dioxide (CO_2) (Thesis).

2. Dissolution of CO_2 in brine forms a mixture that is denser than the carbon dioxide free brine, but in the oleic phase, the mixture is only denser under favourable conditions. Even if this causes a local density increase, it induces natural convection currents (gravity fingers) when gaseous carbon dioxide is brought above the liquid phase only under favourable conditions. Consequently, the rate of mixing of CO_2 in the liquid phase is not always enhanced. (Chapter 2 and 3).

3. A Schlieren set-up can only be used to observe gravity induced "fingers" in the bulk phase. The porous media experiments in chapter 3, show that the observations in chapter 2, i.e., that natural convection currents are weakest in concentrated brine are also valid in porous media. (Chapter 2 and 3).

4. Temperature control is the key condition to use the manometric set-up to accurately measure excess sorption of CO_2 and CH_4 on Belgian carboniferous black shale at temperatures of 308, 318 and 336 K and in a pressure range between 0- 105 bar. (Chapter 4).

5. Enhanced gas recovery using CO_2 presents a viable opportunity to produce a relatively clean burning fuel from shale gas while simultaneously promoting environmental sustainability through CO_2 storage. (Chapter 5).

6. Air injection is an effective method for light oil recovery at shallow reservoirs; however gas over-ride, heterogeneity and channelling effects on the stability of the process should be considered (N. Khoshnevis Gargar).

7. Pragmatic storage of carbon dioxide (CO_2) in aquifers requires dissolution in the aqueous phase (A. A. Eftekhari).

8. A frequently ignored difference between the developed and developing countries is the way that they look to human resource. (Peter Drucker).

9. "To have a society characterized by sustainable development, proponents of this idea should be the initiators of change targeted at reaching this goal", inspired on "You must be the change you wish to see in the world (Mahatma Gandhi)".

10. A flower does not think of competing with the flower next to it. It just blooms.

Stellingen

1. De groeiende bezorgdheid over globale opwarming is de voornaamste reden voor de toegenomen belangstelling voor geologische opslag van koolstofdioxide (CO_2). (Dit proefschrift).

2. Het oplossen van CO_2 in pekel vormt een mengsel dat dichter is dan kooldioxide-vrije pekel, maar in de olieachtige fase is het mengsel alleen dichter onder gunstige omstandigheden. Zelfs indien dit een lokale dichtheidstoename veroorzaakt, leidt dit slechts onder gunstige omstandigheden tot natuurlijke convectie stromen (zwaartekrachtsvingers) wanneer gasvormig kooldioxide boven de vloeistoffase wordt gebracht. Dientengevolge wordt de mengsnelheid niet altijd versterkt. (Hoofdstuk 2 en 3).

3. De Schlieren opstelling kan slechts worden gebruikt om door zwaartekracht gedreven "vingers" in de bulk-fase te visualiseren. De poreuze media experimenten in hoofdstuk 3 tonen aan dat de waarnemingen in hoofdstuk 2, d.w.z. dat natuurlijke convectiestromen het zwakst zijn in geconcentreerde pekel, ook geldig zijn in poreuze media. (Hoofdstuk 2 en 3).

4. Temperatuur beheersing is de voornaamste voorwaarde om de manometrische opstelling te gebruiken om nauwkeurig de "excess sorption" van CO_2 en CH_4 in Belgische zwarte schalie uit het carboon bij temperaturen van 308, 318 en 336 K en in het drukgebied 0-105 bar te meten. (Hoofdstuk 4).

5. Verbeterde gaswinning met gebruik van CO_2 biedt een haalbare kans om een relatief schone brandstof te produceren uit schaliegas en tegelijkertijd milieuduurzaamheid te bevorderen door opslag van CO_2. (Hoofdstuk 5).

6. Luchtinjectie is een effectieve methode voor lichte-oliewinning in ondiepe reservoirs; echter men moet rekening houden met de effecten van het bovenlangs schieten van gas, heterogeniteit en gaskanaalvorming op de stabiliteit van het proces. (N. Khoshnevis Gargar).

7. Pragmatische opslag van kooldioxide (CO_2) in watervoerende lagen vereist oplossing in de waterachtige-fase. (A. A. Eftekhari).

8. Een vaak genegeerd verschil tussen ontwikkelde landen en ontwikkelingslanden is de manier waarop zij aankijken tegen het menselijk potentieel. (Peter Drucker).

9. Om een duurzame maatschappij te krijgen zouden de voorstanders van dit idee de initiatiefnemers moeten zijn van veranderingen die er opgericht zijn dit doel te bereiken, (geïnspireerd op "Gij moet de verandering zijn die u in de wereld wenst. (Mahatma Gandhi) ".

10. Een bloem denkt er niet aan te wedijveren met een naburige bloem. Hij bloeit alleen.

Scientific contribution

1. Khosrokhavar, R., Elsinga, G. E., Farajzadeh, R., and Bruining, H., "Visualization and Investigation of Natural Convection Flow of CO_2 in Aqueous and Oleic Systems", Journal of Petroleum Science and Engineering (2014).
2. Khosrokhavar, R., Wolf, K. H., and Bruining, H., "Sorption of CH_4 and CO_2 on a Carboniferous Shale from Belgium Using a Manometric Set-up", International Journal of Coal Geology, 128, 153-161, (2014).
3. Khosrokhavar, R., Griffiths, S., and Wolf, K. H., Shale Gas Formations and Their Potential for Carbon Storage: Opportunities and Outlook", Environmental Processes, 1-17, (2014).
4. Khosrokhavar, R., Wolf, K. H., and Bruining, H., "Sorption of CH_4 and CO_2 on a Carboniferous Shale Using a Manometric Set-up by Applying Error Analysis ", 6th International Conference on Porous Media and Annual Meeting of International society for porous media (Interpore), Milwaukee, USA (2014).
5. Khosrokhavar, R., Eftekhari, A., Farajzadeh, R., and Bruining, H., "Effect of Salinity and Pressure on the Rate of Mass Transfer in Aquifer Storage of Carbon Dioxide"', accepted to 18th European Symposium on Improved Oil Recovery conference, Dresden, Germany (2014).
6. Khosrokhavar, R., Wolf, K. H., and Bruining, H., "Sorption of CH_4 in Organic Shales Using the Manometric Set-up ", 2th International Conference on Nonlinearities and Upscaling in Porous Media (NUPUS), Bergen, Norway (2013).
7. Khosrokhavar, R., Elsinga, G., Farajzadeh, R., and Bruining, H., "Numerical and Experimental Investigation of Natural Convection Flow of (Sub-) and (Super-) Critical CO_2 in Aqueous Phase", COMSOL Conference, Milan, Italy (2012).
8. Khosrokhavar, R., Schoemaker, C., Battistutta, E., Wolf, K. H. A., and Bruining, H., Sorption of CO_2 in shales Using the Manometric Set-up, SPE Europec/EAGE Annual Conference, Copenhagen, Denmark (2012).

9. Khosrokhavar, R., Elsinga, G., Mojaddam, A., Farajzadeh, R., and Bruining, H., "Visualization of Natural Convection Flow of Super Critical CO_2 in Water by Applying Schlieren Method", SPE EUROPEC/EAGE Annual Conference and Exhibition, Vienna, Austria (2011).

10. Khosrokhavar, R., Elsinga, G., Farajzadeh, R., and Bruining, H., "Visualization of Natural convection flow of sub critical CO_2 in Oleic phase by applying Schlieren method ", 3th International Conference on Porous Media and Annual Meeting of International society for porous media (Interpore), Bordeaux, France (2011).

11. Khosrokhavar, R., Elsinga, G, Farajzadeh, R., and Bruining, J., "An Introduction to Schlieren Technique ", International Research NUPUS Meeting, Freudenstadt, Germany (2010).

About the Author

Roozbeh Khosrokhavar was born on June 16, 1979 in Tehran, Iran. Roozbeh obtained mathematics and physics diploma from Amirkabir high school, Tehran in 1997. He received his B.Sc. and M.Sc. degree in Chemical Engineering in 2001 and 2004 from Amirkabir University of Technology (Tehran Polytechnic), Tehran, Iran. From 2004 to late 2009, he worked in research institute of petroleum industry as researcher and coordinator manager. In the same period, he was member of board in NGO's and private companies. Then he moved to the Netherland. In October 2010 he started his Ph.D. of Petroleum Engineering in the department of Geoscience and Engineering at Delft University of Technology, where he conducted his research under supervision of Prof. Dr. J. Bruining and Dr. Karl-Heinz Wolf. His research includes experimental work, modeling and simulation of CO_2 sequestration in geological formations and enhanced gas recovery.